



Southwestern Regional Partnership For Carbon Sequestration (Phase 2)

*Pump Canyon CO₂- ECBM/Sequestration Demonstration,
San Juan Basin, New Mexico*

Final Report

*Submitted by:
Advanced Resources International, Inc.
Houston, TX*

January 31, 2010



ConocoPhillips

KINDER MORGAN INC.

Pinnacle



New Mexico Tech
Petroleum Recovery Research Center



THE UNIVERSITY OF UTAH

Schlumberger



Advanced Resources International, Inc.

Disclaimers

This is a preliminary version of a Final Report that will be submitted to the National Energy Technology Laboratory for publication by the U.S. Department of Energy.

U.S. Department of Energy

This report was prepared as an account of work sponsored by an agency of the United States Government. Neither the United States Government nor any agency thereof, nor any of their employees, makes any warranty, express or implied, or assumes any legal liability or responsibility for the accuracy, completeness, or usefulness of any information, apparatus, product, or process disclosed, or represents that its use would not infringe privately owned rights. Reference herein to any specific commercial product, process, or service by trade name, trademark, manufacturer, or otherwise does not necessarily constitute or imply its endorsement, recommendation, or favoring by the United States Government or any agency thereof. The views and opinions of authors expressed herein do not necessarily state or reflect those of the United States Government or any agency thereof.

Advanced Resources International, Inc.

The material in this Report is intended for general information only. Any use of this material in relation to any specific application should be based on independent examination and verification of its unrestricted applicability for such use and on a determination of suitability for the application by professionally qualified personnel. No license under any Advanced Resources International, Inc., patents or other proprietary interest is implied by the publication of this Report. Those making use of or relying upon the material assume all risks and liability arising from such use or reliance.

Executive Summary

The Southwest Regional Partnership on Carbon Sequestration (SWP) is one of seven regional partnerships sponsored by the U.S. Department of Energy (USDOE).

Within the SWP, three demonstrations of geologic CO₂ sequestration are being performed – one in an oilfield (the SACROC Unit in the Permian basin of west Texas), one in a deep, unmineable coalbed (the Pump Canyon site in the San Juan basin of northern New Mexico), and one in a deep, saline reservoir (underlying the Aneth oilfield in the Paradox basin of southeast Utah). The Pump Canyon CO₂-enhanced coalbed methane (CO₂/ECBM) sequestration demonstration project plans to demonstrate the effectiveness of CO₂ sequestration in deep, unmineable coal seams via a small-scale geologic sequestration project. The site is located in San Juan County, northern New Mexico, just within the limits of the high-permeability fairway of prolific coalbed methane production. The study area for the SWP project consists of 31 coalbed methane production wells located in a nine section area.

CO₂ was injected continuously for a year and different monitoring, verification and accounting (MVA) techniques were implemented to track the CO₂ movement inside and outside the reservoir. A total of 256 MMscf of CO₂ (or 14,885 tons) were injected over a 12-month period (July 30st, 2008 to August 12th, 2009); primarily due to highly permeable coal. However, as expected, the CO₂ injectivity dramatically decreased over the injection period. This was mainly due to matrix swelling and permeability reduction, as a result of the CO₂ being adsorbed onto the coal, while displacing methane, as well as increasing reservoir pressure. It was also determined that injection was predominately into the basal coal, reducing injectivity by 20%.

The CO₂ sensors installed at the three immediate offset wells, as well as the gas sampling from neighboring CBM wells (three immediate offset wells and an additional ring of immediately surrounding wells), suggest that no CO₂ breakthrough has occurred at the site. However, a steady increase in the CO₂ content at one of the offset wells, the FC State Com 1, might be a sign of breakthrough. The CO₂ monitoring system has been left in place and the data will be regularly updated to verify whether this is the case.

Perfluorocarbon tracers injected in the CO₂ stream showed up a few months later at the two closest offset wells, the FC State Com 1, followed by the EPNG Com A 300 (where breakthrough is expected to occur first due to its alignment with the face cleats, if it does occur). This may also could be an early sign of breakthrough.

In addition to monitoring for breakthrough, the project also adopted several ground monitoring techniques to observe any ground deformation. The different ground monitoring techniques used (Tiltmeters, GPS and InSar) all converge to the same conclusion, that no ground deformation is seen even though their effectiveness was probably limited due to the small amount of CO₂ injected.

In order to assess the integrity of the site, the project conducted a thorough seismic interpretation of about nine square miles of 3D seismic data centered around the injection well. The seismic interpretation reveals considerable stratigraphic complexity in the Fruitland formation depositional system. Post-stack processing of the 3D seismic suggests the presence of fracturing and minor faulting within the Kirtland Shale caprock, whereas indicators for extensive fracturing and faulting within the Fruitland sequence are much less apparent. However, interpreted faults and fracture zones, with limited vertical extent and major penetrative faults, have not been observed at the site reinforcing the fact that no leakage is expected. Baseline and post injection vertical seismic profiles (VSP) were collected at zero offset and three non-zero offsets, but the preliminary processing is still in progress. A detailed study of the integrity of the Kirtland Shale caprock is provided in an independent report.

The simulation work was able to adequately replicate the production/injection profile of the injector and the three immediate offset wells. The model is also showing that methane production was enhanced due to the CO₂ injection. While the match is not perfect and predicts breakthrough perhaps a bit too early, the model was successful in tying the results from the field, such as the gas samples (CO₂ content and nitrogen content), to the well performance, lending confidence in the accuracy of the match.

Table of Contents

Disclaimers	i
Executive Summary.....	ii
List of Tables	vi
List of Figures.....	vii
1.0 Introduction	1
2.0 Permitting and Regulatory.....	4
2.1 Injection Well.....	5
2.2 Pipeline.....	5
2.3 Access to the Site	6
2.4 National Environmental Policy Act (NEPA)	6
2.5 National Historic Preservation Act (Section 106).....	6
3.0 Site Preparation.....	7
3.1 Pipeline Construction	7
3.2 Surface Deformation Measurements	7
3.3 Well Drilling	11
3.4 Logging and VSP	13
3.5 Coring.....	13
3.6 CO ₂ Sensors at Offset Production Wells.....	14
3.7 Baseline Water Sampling	17
3.8 Soil Gas	20
3.8.1 Pre-Injection, Background Surveys.....	20
3.8.2 Perfluorocarbon (PFC) Tracer Injections	24
3.8.3 Monitoring Procedures	25
3.8.4 Grid.....	27
4.0 Field Operations	31
5.0 Monitoring, Verification and Accounting	34
5.1 Offset Production Wells	34
5.1.1 CO ₂ Sensors.....	34
5.1.2 Gas Samples	36
5.2 Geophysical Interpretation	37
5.2.1 3D Seismic.....	38
5.2.2 Attribute Analysis.....	45
5.2.3 Surface EM Characterization	48
5.2.4 Logging.....	50
5.2.5 Vertical Seismic Profile (Pre-Injection)	57
5.2.6 Conclusions	59
5.3 Tiltmeters, GPS and InSar.....	62
5.3.1 Surface Deformation	62
5.3.2 GPS Elevation Profile.....	73
5.3.3 Reservoir Strain Computation	75
5.3.4 Conclusions	78
5.4 Soil Gas and Tracers	79
5.5 Water Analysis	85

5.5.1	Analysis Methods and Produced Water Chemistry.....	85
5.5.1.1	Ion Concentration.....	85
5.5.1.2	Trace Metal Ion Analysis.....	85
5.5.1.3	Carbon Isotope Analysis.....	86
5.5.1.4	Dissolved Organics.....	86
5.5.2	Results and Discussion.....	87
5.5.2.1	Baseline Measurement of Chemical Composition of Produced Water.....	87
5.5.2.2	Water Chemistry after Injection.....	88
5.5.3	Conclusions and Recommendations.....	97
6.0	Reservoir Characterization.....	99
6.1	Database Development.....	99
6.2	Core Analysis.....	102
6.3	Analysis of Bottomhold Pressure Data.....	102
7.0	Reservoir Modeling.....	112
7.1	Reservoir Description.....	112
7.1.1	Structure and Isopach.....	112
7.1.2	Isotherms.....	113
7.1.3	Pressure Data.....	115
7.1.4	Cleat Orientation.....	115
7.1.5	Permeability and Porosity.....	116
7.2	Model Construction.....	117
7.3	History Matching.....	118
7.3.1	Procedure.....	118
7.3.2	History-Match.....	120
7.3.3	Discussion.....	129
7.3.4	Enhanced Coalbed Methane.....	129
7.3.5	What-if Scenarios.....	131
8.0	Conclusions.....	137
9.0	References.....	139

List of Tables

Table 1: Gas Sampling Results for Well EPNG COM A 300S.....	37
Table 2: Gas Sampling Results for Well EPNG COM A 300.....	37
Table 3: Gas Sampling Results for Well FC STATE COM 1	37
Table 4: Summary of the Composition of Formation Water from the Nearby Offset Wells	88
Table 5: Well Tests Primary Input Parameters.....	104
Table 6: Analysis Results	109
Table 7: Langmuir Isotherm Constants	114
Table 8: Langmuir Isotherm Constants at In-Situ Conditions.....	114
Table 9: Model Isotherms Inputs	115
Table 10: Reservoir Pressure Measurements.....	115
Table 11: History-Match Fixed Parameters.....	121
Table 12: History-Match Variables and Ranges.....	122
Table 13: History-Match Optimized Parameters	128
Table 14: Cumulative Methane Recovery Comparison.....	129

List of Figures

Figure 1: U.S. DOE Regional Partnerships Map	1
Figure 2: Location of the Pump Canyon Unit, San Juan Basin	2
Figure 3: Pump Canyon Demonstration Area Base Map	2
Figure 4: Land Ownership Map.....	4
Figure 5: Layout of Tiltmeter Array Showing the 36 Sites and GPS System Showing the Remote and Base Stations (Red Squares). Well EPNG Com A.	9
Figure 6: Raw Tiltmeter Data Curve Showing the Initial Settling Period.....	10
Figure 7: Injection Well Schematics.....	12
Figure 8: (A) Base Map Showing Location of Cross-Section (B) Cross-Section through Demonstration Site	12
Figure 9: Diagram of the CO ₂ Sensor Installation and Data Transmission.....	15
Figure 10: Site Map of Injection and Monitoring Wells in the San Juan Basin.....	16
Figure 11: The CO ₂ Sensor Installed at the FC STATE COM Well.....	16
Figure 12: Map of Well Locations for Water Sampling.....	19
Figure 13: Typical Examples of Produced Water Samples Obtained from Offset Wells of the Injection Site	20
Figure 14: Soil-Gas Summary at the San Juan Basin Site.....	21
Figure 15: Methane Depth Profiles at the San Juan Basin Site	23
Figure 16: Soil-Gas Hydrocarbon Summary at the San Juan Basin Site.....	23
Figure 17: Hydrocarbon Anomaly Example at Location 24 – San Juan Basin Site.....	24
Figure 18: Tracer Soil-Gas Monitoring Penetrometers	25
Figure 19: Direct Soil-Gas Monitoring Methods Used at the San Juan Basin Site.....	27
Figure 20: PFC Tracer Monitoring Grid at the San Juan Basin	28
Figure 21: Conductivity Survey and Lineament Evaluation at the San Juan Basin Site.....	30
Figure 22: CO ₂ Rate and Wellhead Pressure.....	32
Figure 23: Well Abandonment Schematics	33
Figure 24: CO ₂ Concentration Change in Well EPNG COM A 300S.....	35
Figure 25: CO ₂ Concentration Change in Well EPNG COM A 300.....	36
Figure 26: CO ₂ Concentration Change in Well FC STATE COM 1.....	36
Figure 27: Schematic of Coalbed Methane Reservoir Cross Section (taken from Wray, 2000).....	39

Figure 28: In this 2D Seismic Display, Locally Steepened Dips are Evident across the Area. This Line Trends Northeast-Southwest Considerable Internal Discontinuity of Reflection Events is Evident Throughout40

Figure 29: This Northwest-Southeast Line Illustrates a Similar Level of Reflection Discontinuity along the Axis of the Basin. Local Structural Features are also Evident in the Display.40

Figure 30: Shallower Reflection Events Associated with the Upper Kirtland Shale, the Ojo Alamo Sandstone and Nacimiento Fm.42

Figure 31: Isochore Map of the Interpreted Fruitland Formation Seismic Sequence.....44

Figure 32: Isochore Map of the Interpreted Lower Fruitland Coal Zone44

Figure 33: A Detailed View of Reflection Events Associated with the Lower Fruitland Coal.....45

Figure 34: Gain Adjusted Absolute Value of the Finite Seismic Amplitude Difference Reveals Vertically Continuous Amplitude Disruptions that Cut through Laterally Coherent Reflection Events.....46

Figure 35: Close Up View of Finite Difference Attribute Along the Dip Line Shown in Figure 34. This Line Passes through the COM A 300 Well about 1200 Ft Southwest of the Injection Well. Local Structure in the Fruitland Coal, Stratigraphic Pinchouts and Amplitude Disruptions are Present in the Vicinity of the Injection Well.47

Figure 36: Rose Diagrams of Ant Tracks Mapped At A) 570 ms within the Fruitland Sequence and B) 480ms within the Middle Kirtland Shale Sequence.....48

Figure 37: Locations of Conductivity Profiles are also Shown (Red Lines).....50

Figure 38: Layered Inverse Models Developed Along the North-South Cross Section.....50

Figure 39: A) The Fast Shear Direction Determined from the Schlumberger Sonic Scanner Over the Entire Length of the Hole (275 To 3132 Ft) is Dominated by a Cluster in the Northeast Quadrant with Mean Orientation of N43E Degrees (N=4567). Smaller Peaks are Observed at Approximately N14E (N=1061) and N57W (N=500). B) Within the Upper Part of the Fruitland Formation, Peaks are Observed at N64W (N=115) and N08E (N=118); C) in the Coal Bearing Section the Average Fast Shear Direction is N14E (N=379).....52

Figure 40: Drilling Induced Breakouts Observed in the FMI Logged Interval (324 to 2,943 Ft) Have Mean Trend of N57W (N=97). Those within the Upper Part of the Fruitland (2,826 to 2,943 Ft) also Have Mean Trend of N57W (N=553

Figure 41: A) Open Fracture Trends Interpreted in the FMI Log from 1,000 To 2,905 ft in The Borehole (N= 48); B) Open Fractures in the Kirtland Shale Primary Seal (N=21); C) A Limited Number of Open Fractures (N=5) in the Upper Fruitland (2830 To 2905) have Mean Orientation of About N11E.54

Figure 42: Equal Area (Schmidt Net) Projections of Poles to Open Fracture Planes. A) All Open Fractures; B) open Fractures Observed in the Kirtland Shale; and C) Open Fractures Observed in the Upper Fruitland Formation.55

Figure 43: Hydraulic Electrical Fracture Aperture Distribution. N=4856

Figure 44: A) Healed Fracture Trends Interpreted in the FMI Log from 370 to 2,925 ft in the Borehole (N=57); B) Healed Fractures Observed in the Kirtland Shale (N=17); C) Healed Fractures (N=14) in the Upper Fruitland Formation.57

Figure 45: Base Map Showing Locations of Various Experiments on the Site. VSP Offset Source Locations are Shown as Bright Green Squares58

Figure 46: A) Baseline and B) Post Injection Monitor Survey59

Figure 47: Cumulative Surface Deformation for August 01, 2008 to November 17,63

Figure 48: Wells Layout Showing Producers from Section 32 and Surrounding Sections.....64

Figure 49: Cumulative Surface Deformation for Period August 01, 2008 to November 17, 2009 on a Smaller Deformation Scale65

Figure 50: Injection Rate65

Figure 51: Production Rate from the Three Producers, EPNG Com A 300, 300S and FC State Com 1, Surrounding the Injector Well.....66

Figure 52: Comparison of Cumulative Injected and Produced Volumes (Standard Volume) from Section 32 Including 3 COP Producers, EPNG Com A 300, 300S and FC State Com 168

Figure 53: Comparison of Cumulative Injected and Produced Volumes (Standard Volume) from Section 32 COP Producers and the Howell Wells Immediately Surrounding Section 3269

Figure 54: Cumulative Surface Deformation for Period August 01, 2008 to March 01, 200970

Figure 55: Cumulative Surface Deformation for Period March 01, 2009 to August 15, 200970

Figure 56: Cumulative Surface Deformation for Period August 15, 2009 to November 17, 2009.....71

Figure 57: Cumulative Surface Deformation for Period August 15, 2009 to October 01, 2009. Period for Approximately 1.5 Months Post-Injection.....73

Figure 58: Array and Well Layout Showing the Location of the Remote GPS Station74

Figure 59: GPS elevation Profile for Period from August 01, 2008 through November 17, 2009. Data Processed Using a 240 hr Filter, Both Pre and Post Data Point.....74

Figure 60: GPS Elevation Profile from Early June 2008 to July 31, 2008. Data Discarded Due to Initial Settling and Insufficient Data.75

Figure 61: Reservoir Strain Computation Results for Period January 06, 2009 to February 03, 2009 Performed Using Volumetrically Unconstrained Inversion. Volumetric Strain at Reservoir

Depth (Dimensionless) is shown in the Image at the Left while Theoretical Deformation at Surface (Inches) is shown in the Image to the Right.76

Figure 62: Reservoir Strain Computation Results from August 25, 2009 to September 22, 2009 Performed using Volumetrically Negatively Constrained Inversion. Volumetric Strain at Reservoir Depth (Dimensionless) is shown in the Image at the Left While Theoretical Deformation at Surface (Inches) is shown in the Image to the Right.....78

Figure 63: Breakthrough of Tracers at the Offset Well Split Stream Gas Vents80

Figure 64: PMCH Tracer Signal from the Offset Wells – San Juan Basin Site80

Figure 65: PMCH Soil-Gas Depth Profile at Site 36, San Juan Basin Site82

Figure 66: PDCH Soil-Gas Depth Profile at Site 36, San Juan Basin Site.....82

Figure 67: PDCH Soil-Gas Depth Profile at Site 51, San Juan Basin Site.....83

Figure 68: Atmospheric Tracer Plumes Monitored at the San Juan Basin Site.....83

Figure 69: Conductivity Survey and Lineament Evaluation at the San Juan Basin Site84

Figure 70: PMCH Tracer in Soil-Gas at the San Juan Basin Site84

Figure 71: Water Chemistry of Well FC State COM #190

Figure 72: Water Chemistry of Well Howell A #300.....90

Figure 73: Water Chemistry of Well Howell D350S92

Figure 74: Water Chemistry of Well Howell D351.....92

Figure 75: Water Chemistry of Well Howell G300.....93

Figure 76: Water Cchemistry ofW EPNG COM A300s93

Figure 77: Water Chemistry of Well EPNG COM A300.....94

Figure 78: Water Chemistry of Well Howell D353.....94

Figure 79: Water Chemistry of Well Howell D352S95

Figure 80: pH of Produced Water from Offset Wells.....95

Figure 81: Concentration of Bicarbonate Ion Species in the Produced Fluid from Offset Wells96

Figure 82: Strontium Ion Concentration in the Produced Water from Offset Wells.....96

Figure 83: Concentration of Barium Ion in the Produced Water from Offset Wells97

Figure 84: Top and Isopach of the Fruitland Formation.....101

Figure 85: Top and Isopach of the Kirtland Shale.....102

Figure 86: Raw Pressure and Temperature Gauge Data.....103

Figure 87: Pressure and Injection Rate.....104

Figure 88: PFOs Overlay105

Figure 89: PFO1 Log-Log Plot.....106

Figure 90: PFO2 Log-Log Plot.....107

Figure 91: PFO3 Log-Log Plot.....	107
Figure 92: PFO4 Log-Log Plot.....	108
Figure 93: PFO5 Log-Log Plot.....	108
Figure 94: PFO6 Log-Log Plot.....	109
Figure 95: Near-Well Permeability and Radius of Influence Versus Cumulative Injected CO ₂	110
Figure 96: Near-well Permeability and Radius of Influence Versus Cumulative Injected CO ₂ (without PFO4 and PFO5).....	111
Figure 97: Structure Map, Upper Coal (Units in Feet Above Sea Level)	112
Figure 98: Total Net Coal Isopach (units in feet).....	113
Figure 99: Isotherm Data	114
Figure 100: Cleat Orientation	116
Figure 101: Simulation Model Base Map.....	117
Figure 102: Model 3D View.....	118
Figure 103: Optimization Workflow	119
Figure 104: Error Function Reduction.....	122
Figure 105: Permeability Optimization	123
Figure 106: Well EPNG Com A 300 History-Match Results.....	124
Figure 107: Well EPNG Com A 300S History-Match Results	125
Figure 108: Well FC State Com 1 History-Match Results	126
Figure 109: Injector History-Match Results	127
Figure 110: Well EPNG Com A 300 Methane Production Rate – Injection Versus No Injection Comparison	130
Figure 111: Well EPNG Com A 300S Methane Production Rate – Injection versus No Injection Comparison	130
Figure 112: Well FC State Com 1 Methane Production Rate – Injection versus No Injection Comparison	131
Figure 113: Cumulative CO ₂ Injection	132
Figure 114: EPNG Com A 300 Total and CO ₂ Rate	132
Figure 115: EPNG Com A 300S Total and CO ₂ Rate	133
Figure 116: FC State Com 1 Total and CO ₂ Rate.....	133
Figure 117: EPNG Com A 300 Cumulative CH ₄ Production.....	134
Figure 118: EPNG Com A 300S Cumulative CH ₄ Production	134
Figure 119: FC State Com 1 Cumulative CH ₄ Production	136

1.0 Introduction

The Southwest Regional Partnership on Carbon Sequestration (SWP) is one of seven regional partnerships sponsored by the U.S. Department of Energy (USDOE), as outlined on **Figure 1**.

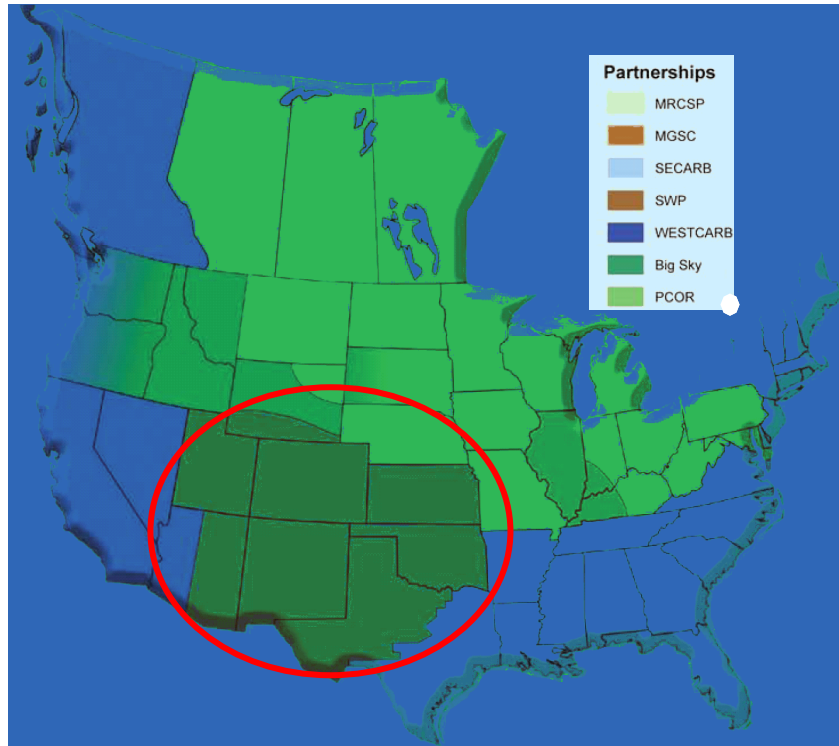


Figure 1: U.S. DOE Regional Partnerships Map

Within the SWP, three demonstrations of geologic CO₂ sequestration are being performed – one in an oilfield (the SACROC Unit in the Permian basin of west Texas), one in a deep, unmineable coalbed (the Pump Canyon site in the San Juan basin of northern New Mexico), and one in a deep, saline reservoir (underlying the Aneth oilfield in the Paradox basin of southeast Utah). The Pump Canyon CO₂-enhanced coalbed methane (CO₂/ECBM) sequestration demonstration project plans to demonstrate the effectiveness of CO₂ sequestration in deep, unmineable coal seams via a small-scale geologic sequestration project. The site is located in San Juan County, northern New Mexico, just within the limits of the high-permeability

fairway of prolific coalbed methane production (**Figure 2**). The study area for the SWP project consists of 31 coalbed methane production wells located in a nine section area, **Figure 3**.

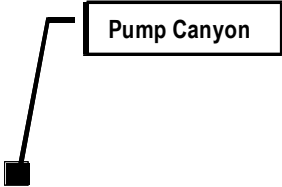


Figure 2: Location of the Pump Canyon Unit, San Juan Basin

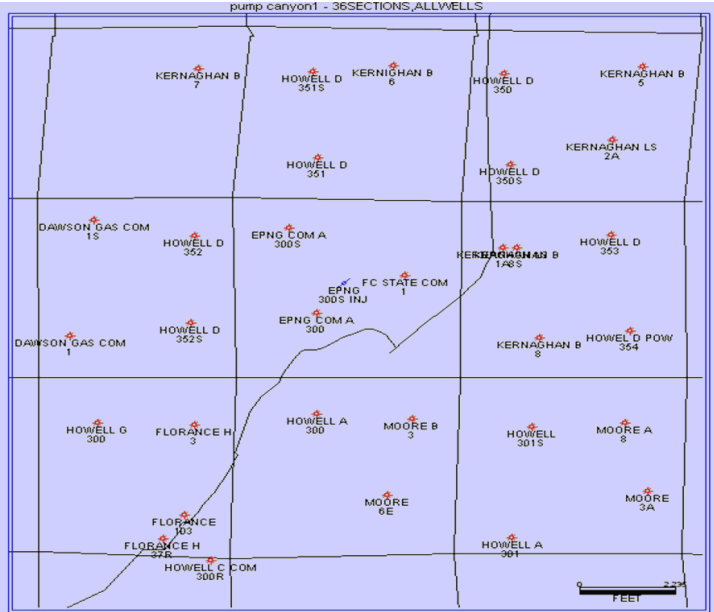


Figure 3: Pump Canyon Demonstration Area Base Map

Figure 3 also shows the injection well location at the center of section 32, T31N, R8W.

CO₂ was injected continuously for a year and different monitoring, verification and accounting (MVA) techniques were implemented to track the CO₂ movement inside and outside the reservoir. Some of the MVA methods include continuous measurement of injection volumes, pressures and temperatures within the injection well, coalbed methane production rates, pressures and gas compositions collected at the offset production wells, and tracers in the injected CO₂. In addition, time-lapse vertical seismic profiling (VSP), surface tiltmeter arrays, a series of shallow monitoring wells with a regular fluid sampling program, surface measurements of soil composition, CO₂ fluxes, and tracers were used to help in tracking the injected CO₂. Finally, a detailed reservoir model was constructed to help reproduce and understand the behavior of the reservoir under production and injection operation. This report summarizes the different phases of the project, from permitting through site closure, and gives the results of the different MVA techniques.

2.0 Permitting and Regulatory

A variety of permitting and other regulatory requirements were necessary to implement the project, including permits for drilling the new CO₂ injection well, installing the pipeline, gaining access to section 32 for the purposes of performing the various proposed MVA activities, and passing a National Environmental Policy October (NEPA) review by the DOE. For reference purposes, **Figure 4** provides a land ownership map for the demonstration area. Section 32, in which the new injection well was drilled, is on lands administered by the State Land Office (New Mexico). The U.S. Bureau of Land Management (BLM) administers the surrounding land. Note that the Simon Canyon Area of Critical Environmental Concern (ACEC) is due east of the demonstration site and that no activity should be performed in this area associated with the demonstration.

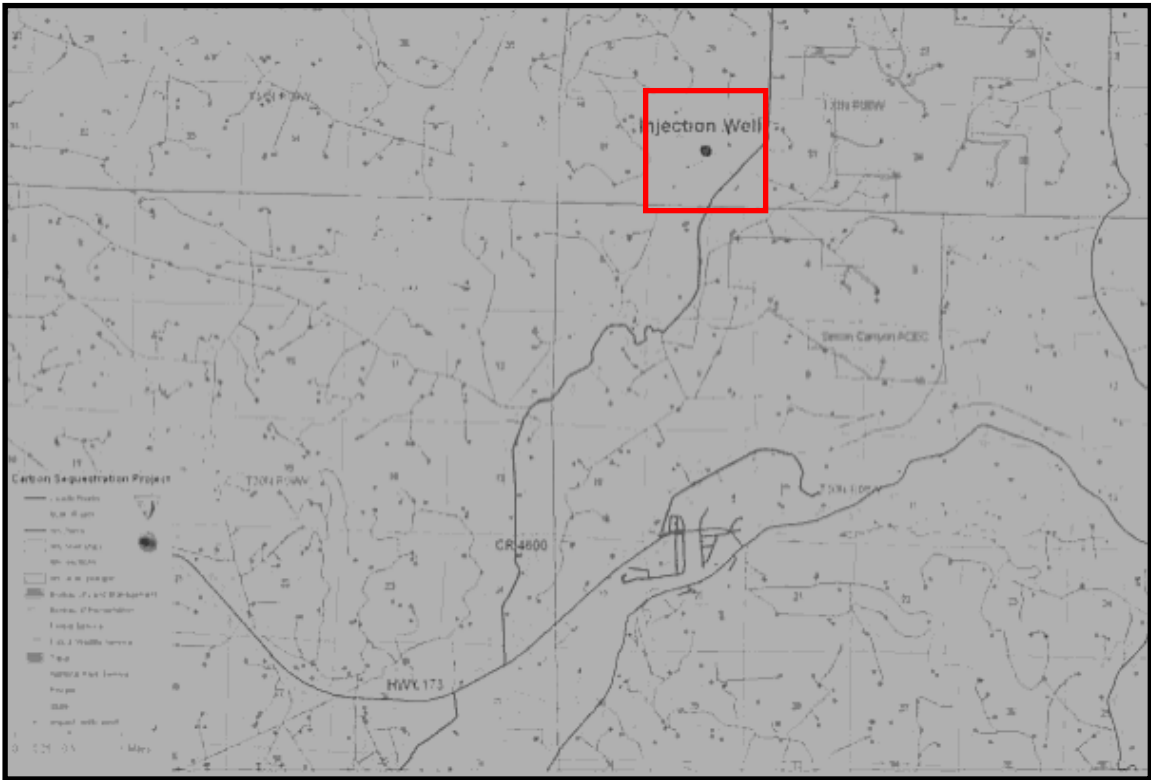


Figure 4: Land Ownership Map

2.1 Injection Well

The New Mexico Oil and Gas Conservation Division (NMOCD) is the primary permitting entity for this project and must approve the Application for a Permit to Drill (APD). The State of New Mexico retains primacy over the Federal government for regulating injection operations pursuant to the Safe Drinking Water Act; therefore, the EPA is not required to issue Underground Injection Control (UIC) permits under the Safe Drinking Water Act.

Three specific applications were required to obtain permits to drill the new well and inject CO₂ into the Fruitland coal reservoir.

- **Application for Permit to Drill (C-101)**. This is an administrative application submitted to the New Mexico Oil Conservation Division (NMOCD) that describes the well location, construction details, target formation, etc.
- **Location and Acreage Dedication Plat (C-102)**. This provides precise well location information.
- **Application for Authorization to Inject (C-108)**. The State of New Mexico retains primacy over the Federal government for regulating injection operations pursuant to the Safe Drinking Water Act. An application was thus submitted to the State for a Class 1 Underground Injection Control (UIC) permit. This is a standard form that includes information regarding fluids to be injected, into which formation, for what purpose, etc. In addition to this information, all wells and freshwater sources within a 2-mile radius of the injection were identified, and all surface owners and operators within a ½-mile of the well were notified.

These documents were presented to the NMOCD at a hearing on June 21, 2007 in Albuquerque, NM and the permit was subsequently issued.

2.2 Pipeline

In order to construct the 2.6-mile pipeline extension, a surface right-of-way had to be obtained. This required both an archeological survey to avoid surface disturbance of sensitive

sites, as well as an environmental assessment (EA) study, for traversing both Bureau of Land Management (BLM) and State Trust (State Lands Office - SLO) lands. After all the necessary studies were performed, a finding of no significant impact (FONSI) was received.

2.3 Access to the Site

In order for the various project researchers to conduct any activity on the site, primarily in State-held Section 32, permission for site access was required. A Work Authorization Agreement (WAA) between the individual SWP contractors and ConocoPhillips was completed and submitted to the State as evidence of a contractual relationship between the two parties.

2.4 National Environmental Policy Act (NEPA)

An environmental questionnaire was completed for the project and submitted to the USDOE environmental compliance officer to ensure NEPA compliance. This was completed and the USDOE provided a categorical exclusion, thus fulfilling this requirement.

2.5 National Historic Preservation Act (Section 106)

When federal funds are involved in a project, proposed surface disturbances must be reviewed by the State Historic Preservation Office (SHPO) and Native American tribes in the area. In this particular area, there are seven tribes with cultural heritage that need to be consulted. Consultation involves preparing detailed descriptions of any proposed disturbances, and their location, providing this information to the SHPO and the Tribes, with sufficient time allowed for any concerns to be raised. The consultation process was initiated in December 2007 and the Tribal approval process took several months to complete. Finally, Section 106 was approved at the beginning of April 2008, which allowed field operations to start.

3.0 Site Preparation

This section describes the different steps that were taken to prepare the injection site. This included construction of the pipeline, the drilling of the injection well (including logging and coring) and the installation of the different MVA systems (tiltmeters, CO₂ sensors, etc.) necessary to track the CO₂ plume extension.

3.1 Pipeline Construction

The new pipeline section required to reach the injection site was tied to the existing Kinder Morgan-operated Cortez pipeline, which transports CO₂ from the McElmo Dome source in Colorado (one of the world's largest known natural accumulation of nearly pure CO₂) to the Permian Basin in West Texas. Based on a maximum allowable injection rate from the UIC permit and an operating line pressure of 2,000 psig, a 2-inch pipeline diameter was deemed sufficient. However, ConocoPhillips elected to upgrade the line to a 4-inch diameter for future service.

The trenching of the pipeline started in January 2008, but had to be halted prior to entering State lands and waiting for the Section 106 consultation process to be completed. The trenching was restarted in mid-April 2008 and the pipeline was completed by the end the month. By mid-May, all sections of the pipeline were hydro-tested to operating pressure and deemed for service.

3.2 Surface Deformation Measurements

One of the primary concerns for this project was the possibility of surface deformation due to coal swelling in the presence of CO₂. To monitor and measure any deformation, a unique system of tiltmeters and GPS stations were designed and installed. Pinnacle Technologies installed a total of 36 surface tiltmeters in shallow, 40 ft deep boreholes as well as a data

collection enclosure with a satellite link to remotely collect data. All field installation work was completed by April 19, 2008.

As part of their installation, tiltmeters go through a settling process, which typically lasts approximately 2 weeks. Once settled, the instruments are able to provide more reliable data. Due to the coalbed methane (CBM) production in the area, the tiltmeter array was installed approximately eight weeks prior to the proposed injection date in order to collect six weeks of baseline data. Identifying the regional baseline trend for the CBM production area was critical in this project because the information was used to decouple the background data from the CO₂ induced inflation and swelling.

In addition to the tiltmeters, two differential GPS stations were integrated into the surface tiltmeter monitoring (STM) array in order to determine *absolute* changes in elevation and to help constrain the deformation measurements over long periods of time. A high-precision GPS system, with an absolute vertical resolution of less than 2 mm and lateral resolution of less than 1 mm, was employed. While the STM array observes relative changes in elevation with sub-millimeter precision over the array area, integrating the GPS component is one way to obtain absolute elevation measurements for the region of interest while limiting the size, and associated expense, of the tiltmeter array. The layout of the tiltmeter array and GPS stations is shown in **Figure 5**.

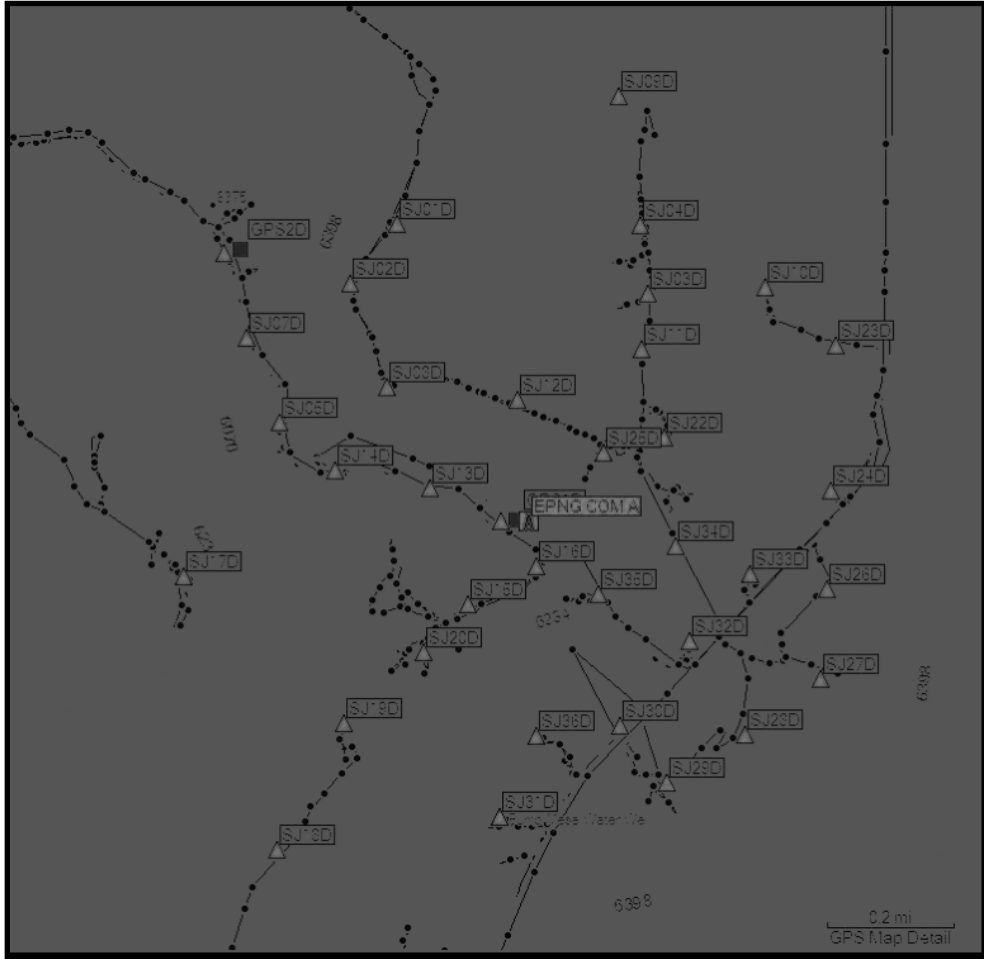


Figure 5: Layout of Tiltmeter Array Showing the 36 Sites and GPS System Showing the Remote and Base Stations (Red Squares). Well EPNG Com A.

Surface tilt measurements collected data at 4 minute intervals. This data was then transferred via radio to a central computer (data collection station) at 24-hr intervals. The central computer also recorded GPS information from remote and base stations. A processing computer then dialed into the central collection computer shortly after the daily tiltmeter download and transferred the tiltmeter and continuously recorded GPS data to servers that were designed to automatically process the collected tilt and GPS data.

Surface tilt measurements can be used primarily in three ways:

- 1) It can be integrated using a minimum curvature rule to obtain surface deformation.

- 2) It can be inverted using a poro-elastic model (Segal, Du) to compute reservoir level volumetric strain.
- 3) It can be inverted using a dislocation model (October) to obtain “fracture” parameters provided there is reasonable likelihood of fractures being formed.

For this project, the surface tilt measurements were used primarily to obtain surface deformation by integration. Computation of reservoir strain was also performed for some time-periods when tilt signals were a little more coherent than at other time periods. There were no indications of fracturing from the tilt signals and hence inversion to obtain fracture parameters was not performed.

The tiltmeters were installed in late April 2008; however, initial settling period of approximately 2 months for this field caused usable tiltmeter data to be available only after late July 2008. CO₂ injection was initiated on July 30, 2008 and surface deformation was computed from August 01, 2008 onwards.

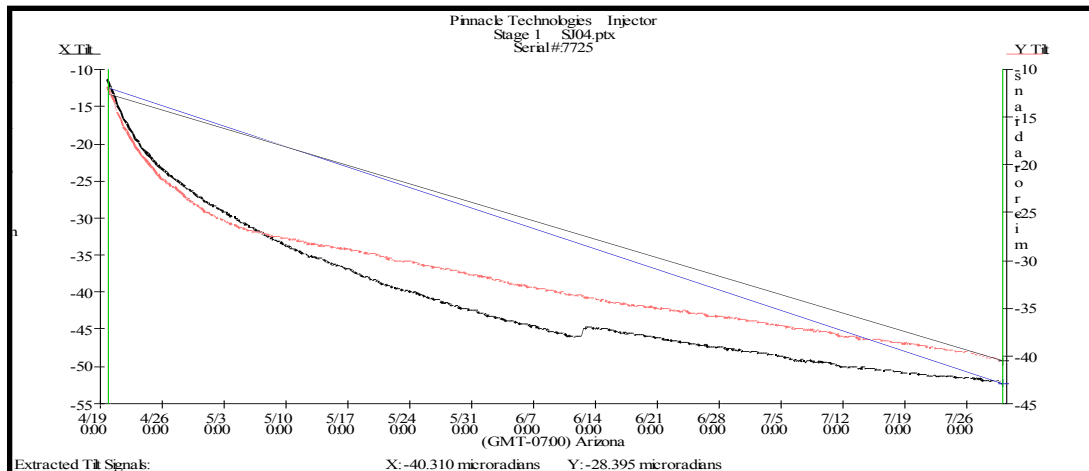


Figure 6: Raw Tiltmeter Data Curve Showing the Initial Settling Period

In addition to the 36 Tiltmeters and the 2 GPS stations, InSar (Interferometric Synthetic Aperture Radar), a satellite based mapping technique with millimeter accuracy, was used to detect any ground movement away from the immediate project area. Injection was planned to

keep CO₂ migration within the 640-acre project; InSAR allows confirmation of the deformation by imaging well beyond the area covered by the array.

3.3 Well Drilling

The drilling of the well started mid-May, 2008 and was completed by the end of June, 2008. The well was drilled to a point just above the Fruitland Coal to a depth of about 3,000 ft, and cored in the overlying Kirtland shale. The first logging suite was then conducted. Casing the well above the coal was done to protect the low pressure (~200 psig) Fruitland formation from the heavier drilling fluids needed to drill the intervals above it.

After casing was set, a smaller hole was drilled through the Fruitland using mist. The coal interval in the wellbore below the casing was then expanded to 9 in. by under-reaming. A perforated liner was placed across the Fruitland formation and attached to the casing above. Coal cuttings were collected through each coal (upper, middle and basal) for gas content analysis, isotherm measurements, proximate and ultimate analysis and vitrinite reflectance. The second logging suite was then run.

A flow computer was set up at the well to limit the injection rate to 1,110 psig, a conservative 25 psig below the 1,135 psig permit limit. A schematic of the injection well is shown on **Figure 7**. In addition, a cross-section through the demonstration site constructed by ConocoPhillips shows the location of the injector. The location of the cross-section, as well as the cross-section itself is provided in **Figures 8(A)** and **8(B)**.

The low pressure of the formation prevented from using the cavitation process to surge and expand the hole by breaking chunks of the inside of the formation. The high permeability of the coal also made fracturing unattractive.

3.4 Logging and VSP

Logging operations were conducted by Schlumberger logging services and the upper part of the well was logged on May 10, 2008. Logging depths for the different tools varied but extended roughly from 224 ft to 2,933 ft, subsurface. Logs in the upper part of the hole included the Platform Express, Formation Micro Imager (FMI) log and the Sonic Scanner for anisotropy and mechanical properties. FMI log observations provided information on fracturing to within a few feet of the Upper Fruitland Coal, which was encountered at a depth of 2,963 ft, subsurface.

The baseline VSP survey was run on June 3 and 4, 2008. Following the survey, the borehole was then extended through the Fruitland section. Two additional logging runs were made to provide observations from the Fruitland formation. The second logging run extended roughly from 2,846 ft to 3,158 ft and included gamma ray, density, Photo Electric (PEF) and Sonic Scanner runs.

3.5 Coring

The success of geologic CO₂ storage depends upon the integrity of the caprock. The Cretaceous Kirtland formation is a regional seal and aquitard, which overlies the Fruitland formation. The Kirtland was cored during the drilling of the injection well in May 2008, and a total of approximately 60 ft of core was collected from the upper and lower members of the Kirtland. Initially, 120 ft of core was planned to be collected; however, the shales proved difficult to core. A variety of analyses to assess seal integrity were conducted on the cores, which included:

- 1) Mercury injection capillary pressure used to determine seal capacity
- 2) Petrographic, petrophysical and geologic characterization through X-ray diffraction, total organic carbon content analysis, thin sections, scanning electron microscopy as well as laser scanning confocal microscopy, porosity, permeability, density and fluid saturation measurements

- 3) Analysis of noble gases to determine the natural helium concentrations, helium gradients, and $^3\text{He}/^4\text{He}$ ratios, which are being used to determine transport properties of the Kirtland and concomitant sealing behavior
- 4) Geomechanical analysis
- 5) CO_2 sorption tests.

3.6 CO_2 Sensors at Offset Production Wells

CO_2 concentration change in the produced gas stream is an important tracking mechanism and was used to determine the subsurface CO_2 movement and the CO_2 breakthrough point. Three CO_2 gas sensors were installed at the three immediate offset production wells. Each sensor, operating at control voltage of 12-24V DC, can measure CO_2 concentrations from 0% to 100%.

Figure 9 shows the diagram of the sensor installation. Gas produced from the well flowed out the separator and entered the gas compressor. A pressure regulator was used to adjust the gas pressure to encourage gas to pass through the sensor chamber. A needle valve was deployed to control the gas flow rate to less than 1 ft³/day. The CO_2 concentration of the produced gas stream was measured by CO_2 gas sensors at thirty minute intervals and the data was then transmitted via satellite to a server.

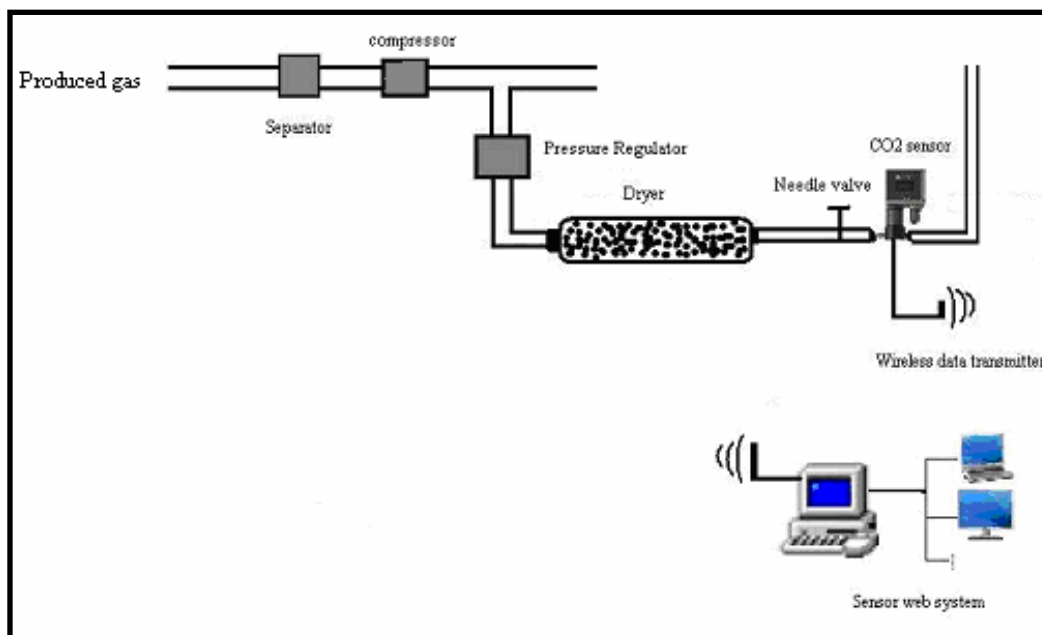


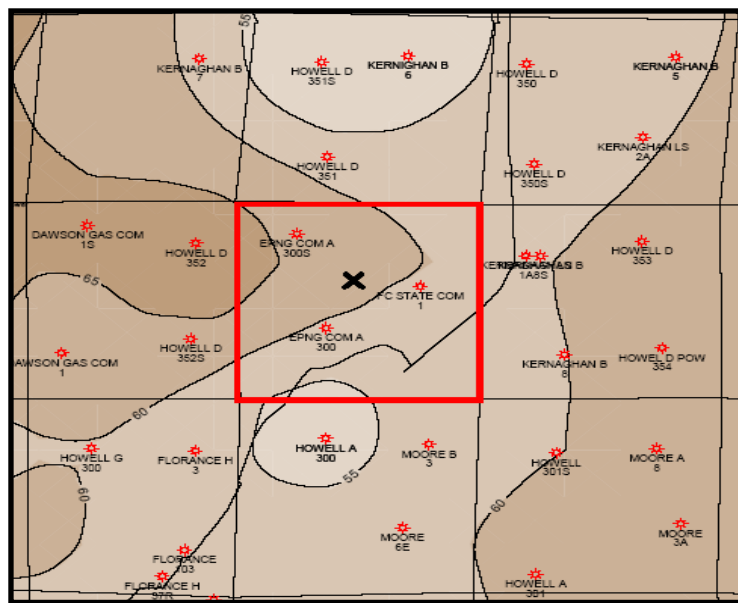
Figure 9: Diagram of the CO₂ Sensor Installation and Data Transmission

Three monitoring wells, EPNG COM A 300S, EPNG COM A 300, and FC STATE COM 1, which surround the injection well, were selected to monitor changes in CO₂ concentration during the injection process. **Figure 10** shows the location of the three monitoring wells and injection well. The distance of the monitoring well to the injectors is:

EPNG COM A 300S: 547m northwest of the injection well

EPNG COM A 300: 499 m southwest of the injection well

FC STATE COM: 386 m almost directly east of the injection well



×: Injection well

Figure 10: Site Map of Injection and Monitoring Wells in the San Juan Basin

Figure 11 shows a sensor installation and the data transmission at production well FC STATE COM 1. A modified, CO₂ sensor was installed of the wellhead and 0.125 in. stainless steel tubing was used to connect the sensor chamber with the gas separator. A solar panel supplied the power for the CO₂ sensor and data logging box. CO₂ data was collected at 30-minute intervals and transmitted to the data-shock house (**Figure 11**) via antenna.

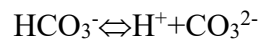
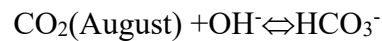
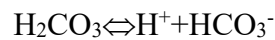
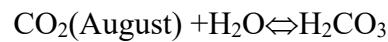


Figure 11: The CO₂ Sensor Installed at the FC STATE COM Well

All the CO₂ sensors were calibrated in the lab and tested for reliability in the field before installation.

3.7 *Baseline Water Sampling*

As CO₂ is injected into a reservoir, CO₂ will come in contact with formation fluid and rocks followed by a comprehensive chemical reaction and movement, which gives crucial indications of the CO₂ movement and its ultimate fate. Potential chemical reactions between injected CO₂ and formation fluid include [Druckenmiller et al., 2005; Raistrick, et al., 2006]:



These reactions lead to dissolution of CO₂ and dissociation of H₂CO₃ into formation water. As a result, the pH of formation water and solution alkalinity will decrease. In addition, due to the effects of leaching, ion concentrations of trace metals and isotope contents will vary correspondingly. Many experimental, modeling, and field studies have been conducted to evaluate the implications of fluid chemistry on geological carbon sequestration [Druckenmiller et al., 2005; Johnson et al., 2008]. From the chemical composition studies, the following key issues can be identified, each of which play crucial roles in quantification of carbon storage mechanisms and tracking the ultimate fate of injected CO₂:

- 1) Ultimate fate of CO₂ and long-term storage mechanisms: several mechanisms are involved in long-term CO₂ storage such as dissolution of CO₂ in H₂O followed by dissociation of H₂CO₃ (ionic trapping) and mineral storage of CO₂ through the formation of calcite, magnesite, or dolomite (mineral trapping).

- 2) Reactions induced by CO₂ in rocks that were saturated with saline waters include acid hydrolysis of rock-forming minerals and precipitation.
- 3) CO₂ movement vertically and spatially.
- 4) Potential impact on receiving environment and/or shallow water systems.

This research focuses on the investigation of the chemical composition of produced water from offset producing wells and identification of the sources of the CO₂ and its movement in the geologic framework. The information derived from this study will be an important indicator of CO₂ migration, accumulation, and leakage in heterogeneous coalbed methane formations.

Produced water samples were collected from the nearby producing wells of the CO₂ injection site. Water sampling for this project followed this procedure:

- 1) Select a faucet and run the water to drain the dead volume out to make sure the water sample is a representative sample of in-time reservoir fluid. Clean and leak-proof plastic bottles are used for water sampling. Be careful not to touch the inside of the cap and faucet when handling the water sample bottle. An attached sample information sheet must be filled out before sampling.
- 2) Fill the bottle completely and cap the sample.
- 3) Label the bottle clearly with the date, and the well name. Fold and wrap the sample information sheet around the bottle, and put them both into a waterproof plastic bag.
- 4) Keep the sample refrigerated at 5°C and ship to the recipient.
- 5) Chemical composition of produced water samples will be analyzed in two weeks.

Figure 12 shows the map of CO₂ injection and water sampling sites. The starting time for water sampling was August 08, 2007.

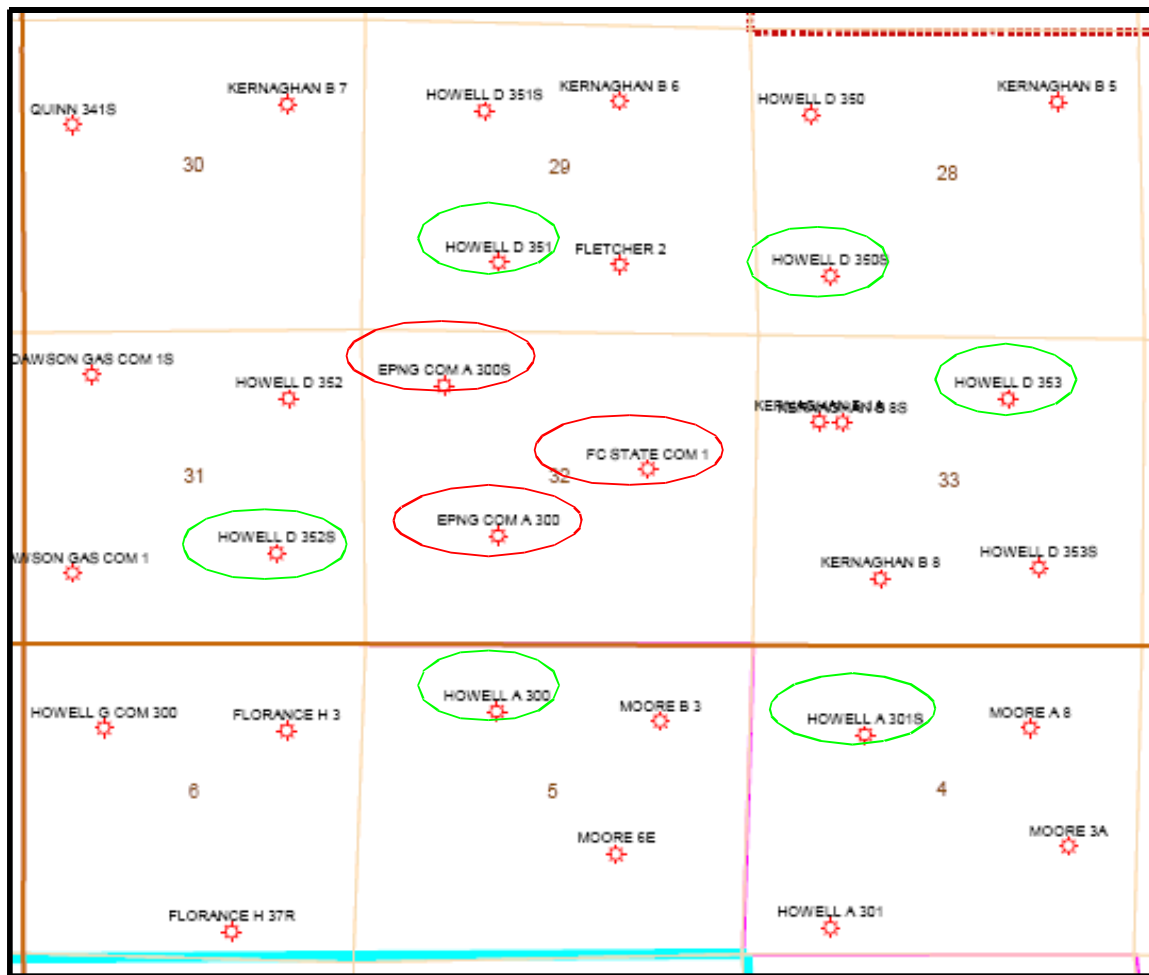


Figure 12: Map of Well Locations for Water Sampling

Most of water samples collected before CO₂ injection contained suspended solid and oil droplets. Physical and chemical properties of the produced water before CO₂ injection were tested as baseline. Dramatic differences in water chemistry from nearby wells, or at different time intervals, have been observed. **Figure 13** shows typical produced water samples collected in April 2008.



Figure 13: Typical Examples of Produced Water Samples Obtained from Offset Wells of the Injection Site

3.8 Soil Gas

3.8.1 Pre-Injection, Background Surveys

In order to detect an eventual CO₂ leak, surface and near-surface monitoring techniques were employed. These techniques included tracer additions to the injected CO₂ with soil-gas monitoring for the presence of tracers, and direct CO₂ flux monitoring at the surface.

Between April 2006 and August 2006, four background sets of sorbent packets were placed and removed from grids set up at two locations further south-west on the injection site; one in Pump Canyon, and another one on an adjacent mesa top. An additional two sets of background tracer sorbent packets were taken prior to injection at the final location. Average background perfluorodimethylcyclohexane (PMCH) tracer concentrations from these sets were compatible with worldwide distribution concentrations, with soil-gas concentrations about 50% lower than atmospheric background concentrations. Three background sets of CO₂ surface flux and soil-gas hydrocarbons (methane and ethane) and CO₂ concentrations were taken from the sampling locations. Four background sets were also taken at the test site between March 2007 and April 2008 (**Figures 14 to 17**). The CO₂ soil-gas concentration increased nearly linearly with depth, but showed no clear seasonal trend (**Figure 14**). The magnitude of carbon isotope shifts correlated to CO₂ concentrations (**Figure 14**). Hydrocarbon concentrations revealed nine

“anomalies” pictured in **Figures 15 and 16**, where hydrocarbons increase with depth, indicating the potential for seepage from depth. An example is shown in **Figure 17**. The magnitude of seepage signatures for the March 2007 survey was much higher than for previous surveys.

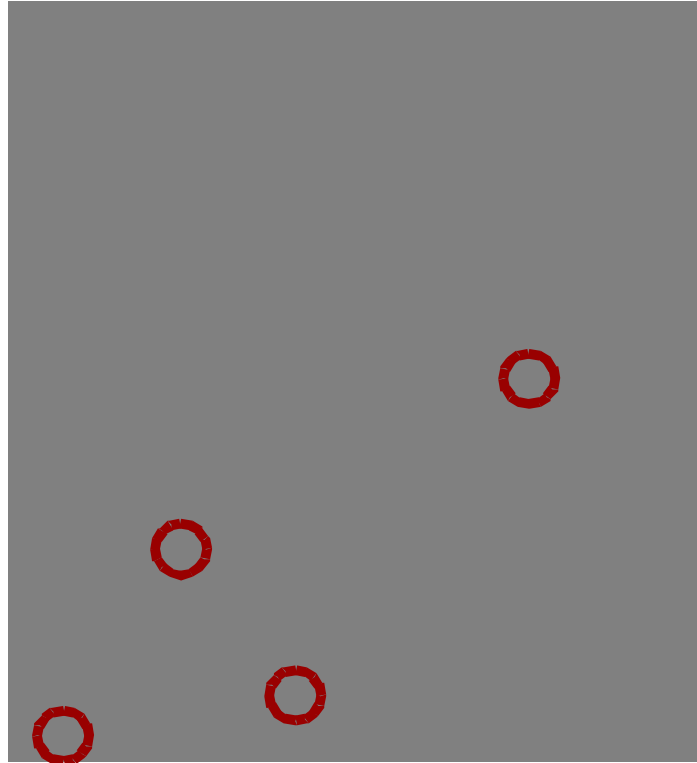


Figure 14: Soil-Gas Summary at the San Juan Basin Site

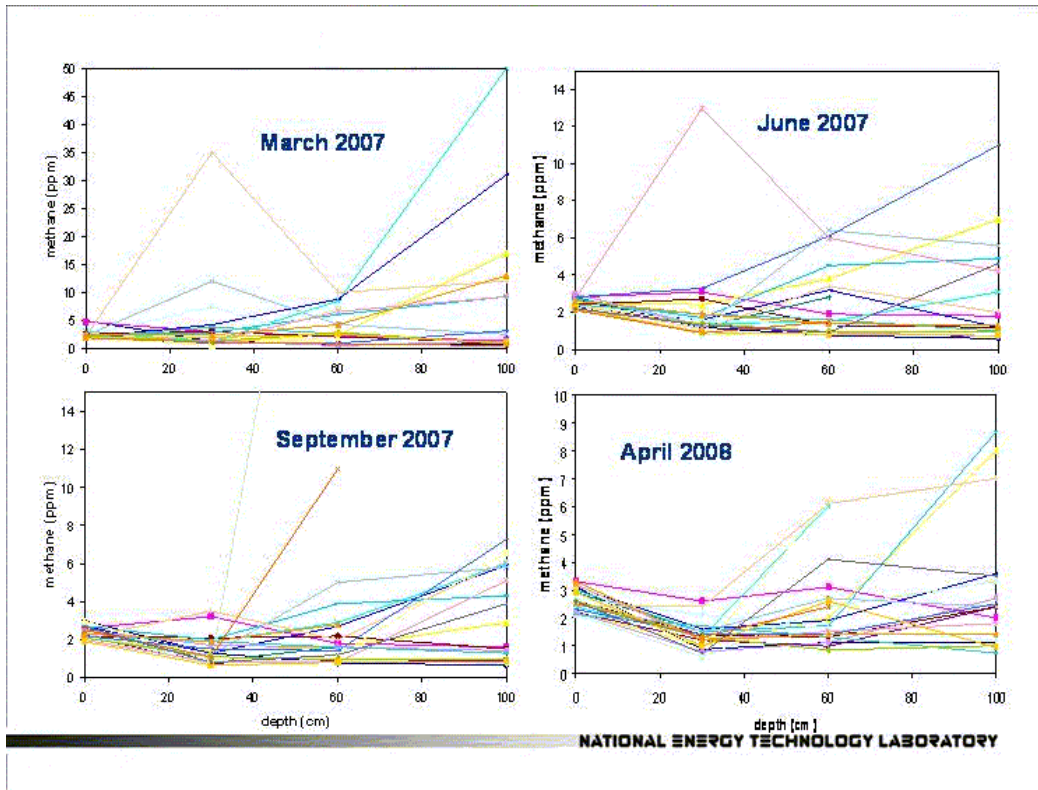


Figure 15: Methane Depth Profiles at the San Juan Basin Site

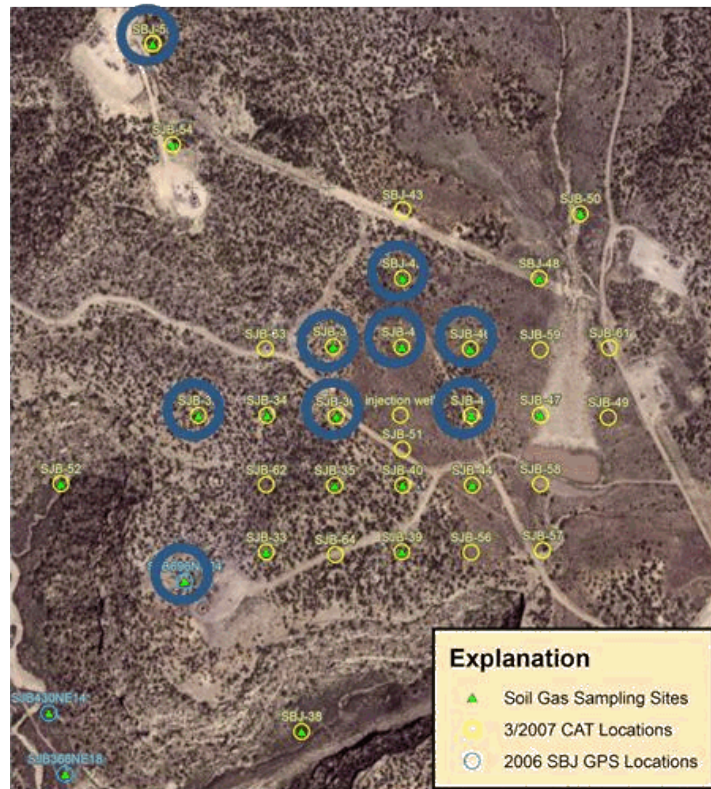


Figure 16: Soil-Gas Hydrocarbon Summary at the San Juan Basin Site

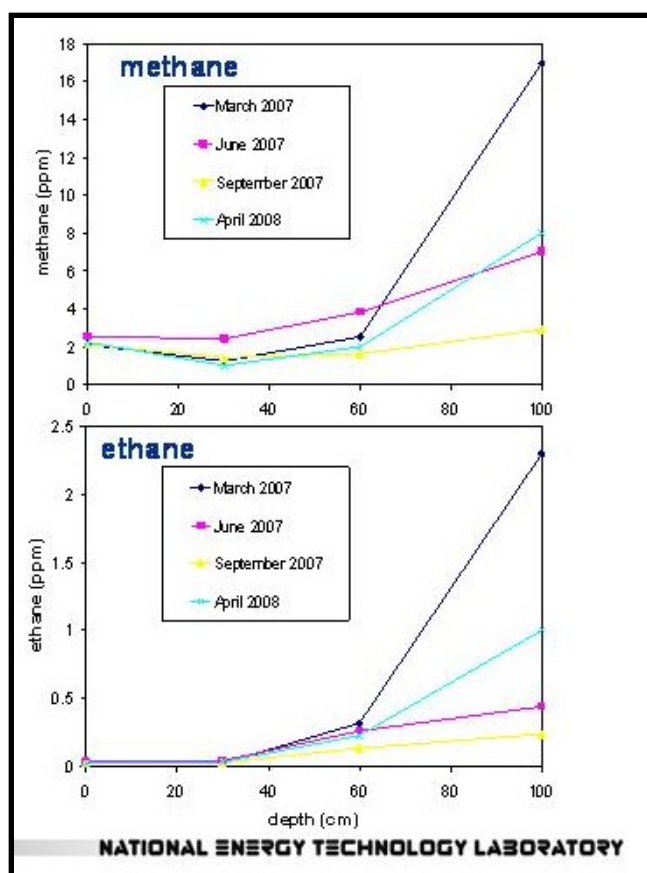


Figure 17: Hydrocarbon Anomaly Example at Location 24 – San Juan Basin Site

3.8.2 Perfluorocarbon (PFC) Tracer Injections

Two separate, three week-long, sequential tracer injections were conducted shortly after the start of CO₂ injection. The tracers were added directly to the CO₂ from a syringe pump and tracer reservoirs in a van positioned near the injection wellhead. The tracer injections consisted of 20 liters injected continuously at a uniform mixing rate adjusted to the CO₂ flow rate as measured at the wellhead. The first tracer was a mixture of 90% PMCH and 10% ortho-perfluorodimethylcyclohexane (o-PDMCH), with injection beginning on September 18, 2008. The second tracer was 100% perfluorotrimethylcyclohexane (PTCH), with injection beginning on October 9, 2008. Due to the ultra-low detection levels for PFC tracers, rigorous field protocols were observed to prevent cross contamination of samples, and to minimize tracer release to the atmosphere during the injection of tracers.

3.8.3 Monitoring Procedures

The tracer-in-soil-gas monitors were $\frac{3}{4}$ inch steel pipes driven 1 meter into the soil, and into which vials containing sorbent material were placed to collect any tracer contained in the soil-gas exposed by removing the penetrometer head. The tops of the pipes were sealed to prevent entry of atmosphere and ground water. The sorbent vials were exchanged as sets. The quantity of air or soil-gas sampled by passive diffusion into the sorbent vials has been determined to be equivalent to 200 ml/day. A brief summary of the monitoring methods and equipment is given in **Figures 18 and 19**.

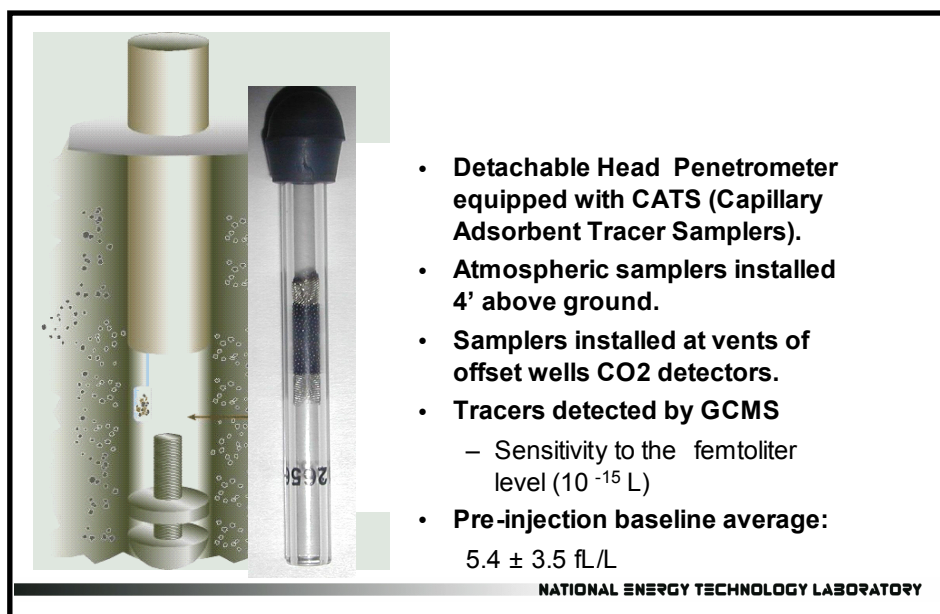


Figure 18: Tracer Soil-Gas Monitoring Penetrometers



- **CO₂ Soil flux measurements**
- **Soil gas depth profiles up to 1 meter**
 - GC determination of CO₂ and light hydrocarbons
 - $\delta^{13}\text{C}$ of CO₂ (stable isotope ratios)
- **Radon and Thoron concentrations in soil gas.**
 - Only performed on two of the four baseline surveys



NATIONAL ENERGY TECHNOLOGY LABORATORY

Figure 19: Direct Soil-Gas Monitoring Methods Used at the San Juan Basin Site

3.8.4 Grid

The PFC tracer monitoring grid at the San Juan Basin site is shown in **Figure 20**. There are a total of 46 permanent installations, and 36 sampling cages to monitor tracer in the atmosphere. All but four of the atmospheric monitors are mounted 4 feet up on steel pipes containing tracer in soil-gas monitors. Of these four, three are mounted 3 inches away from vents to CO₂ sensors that sample a split stream of production gas for monitoring CO₂ concentrations at the three off-set wells (sites 65, 66 and 67). These three locations are distinct from all other sites in that their purpose is not to detect near-surface leakage. Tracer detection at these locations is an indication of breakthrough of injected gas to the offset wells *at depth*. It is expected that tracer breakthrough would precede CO₂ breakthrough due to the adsorption of CO₂ on coal. One atmospheric sampling cage (site 68) is not associated with soil-gas monitors or the three off-set wells. A subset of 23 of the tracer monitoring locations were also selected for CO₂ surface flux monitoring, hydrocarbon and CO₂ soil-gas depth profiling, and radon/thoron monitoring.



Figure 20: PFC Tracer Monitoring Grid at the San Juan Basin

A rectangular grid was employed with spacing between monitors of 100 meters (**Figure 20**). In addition, monitors were placed adjacent to six near-by wells to evaluate potential leakage associated with wellbores. Other monitors lying off the main grid were placed to evaluate areas of increased leakage potential based upon the geological assessment conducted by West Virginia University (WVU), **Figure 21**. This assessment combined a conductivity survey and lineament analysis, both shown in **Figure 21**.

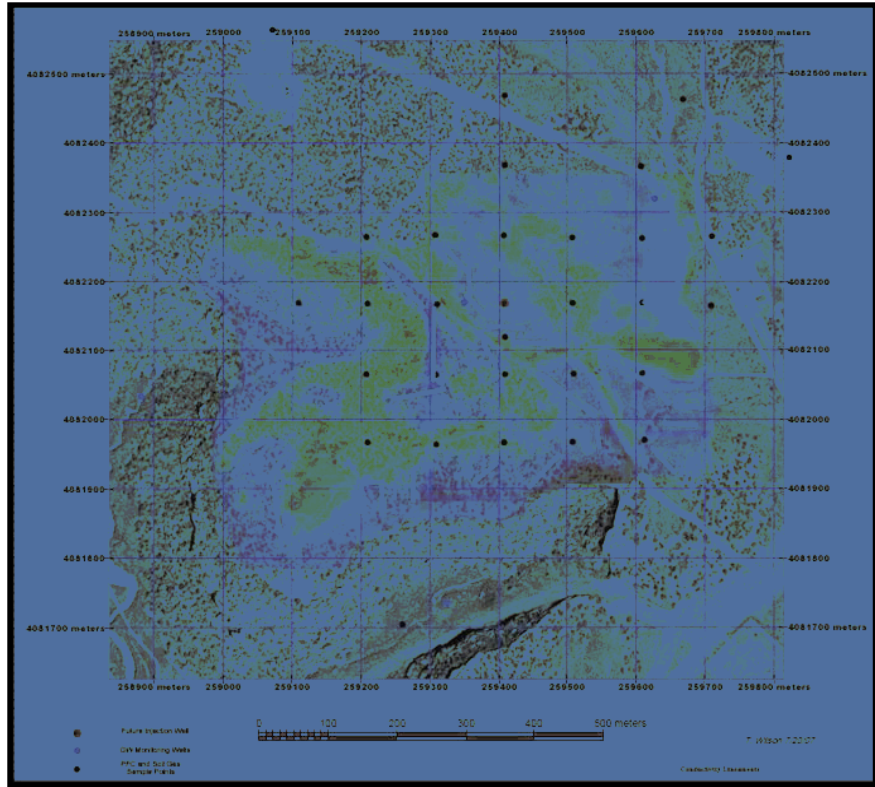


Figure 21: Conductivity Survey and Lineament Evaluation at the San Juan Basin Site

4.0 Field Operations

An important operating fact for the demonstration is that, since ConocoPhillips has the duty to act in the best economic interests of its' financial partners in the offset producer wells, should CO₂ breakthrough occur in one or more production wells, CO₂ injection into the injection zone should stop. At least two potential events could lead to or otherwise accelerate CO₂ breakthrough at an offset well.

- First, the coal face cleat orientation (N35E) is almost precisely aligned in the direction of the offset well directly to the southwest of the injector, the EPNG Com A 300. This well is also the closest offset well, located only 1,100 ft from the injector. These factors represent significant risk of early CO₂ breakthrough in the EPNG Com A 300 well.
- Secondly, due to extremely low reservoir pressures that appear to exist in the area (about 75-100 psig), fracturing pressures are also expected to be quite low. Since hydraulic fractures in coal also tend to align themselves with the face cleat, this further exacerbates the risk of early CO₂ breakthrough, and again also in the southwest direction towards the EPNG Com A 300 well.

To mitigate the potential for early CO₂ breakthrough due to these risks, CO₂ injection was initially proposed to occur in stages, starting with the basal coal. Should CO₂ breakthrough occur in any of the offset producer wells (breakthrough being defined as an increase in CO₂ content of the produced gas by over 10% (mole fraction) of the baseline trend, CO₂ injection into the basal coal will be terminated. The basal coal would be sealed off and injection would resume in the middle coal. Similarly, if CO₂ breakthrough occurs when injecting into the middle coal, it too will be sealed and the upper coal perforated and used for injection.

Unfortunately, due to delays in permitting during the Section 106 process, it was decided to inject CO₂ into the 3 layers simultaneously to be able to inject the volumes the demonstration had been designed for.

The injection started on July 30th, 2008 and ended on August 12th, 2009. **Figure 22** shows the injection rate and wellhead pressure over the course of the injection period. A total volume of 14,885 tons of CO₂ was injected. A loss of injectivity is clearly noticeable as the rate drops from 3,500 Mscfd to 250 Mscfd over the year of injection and is probably due to pressurization of the system and matrix swelling and permeability reduction as CO₂ is being adsorbed onto the coal around the injector.

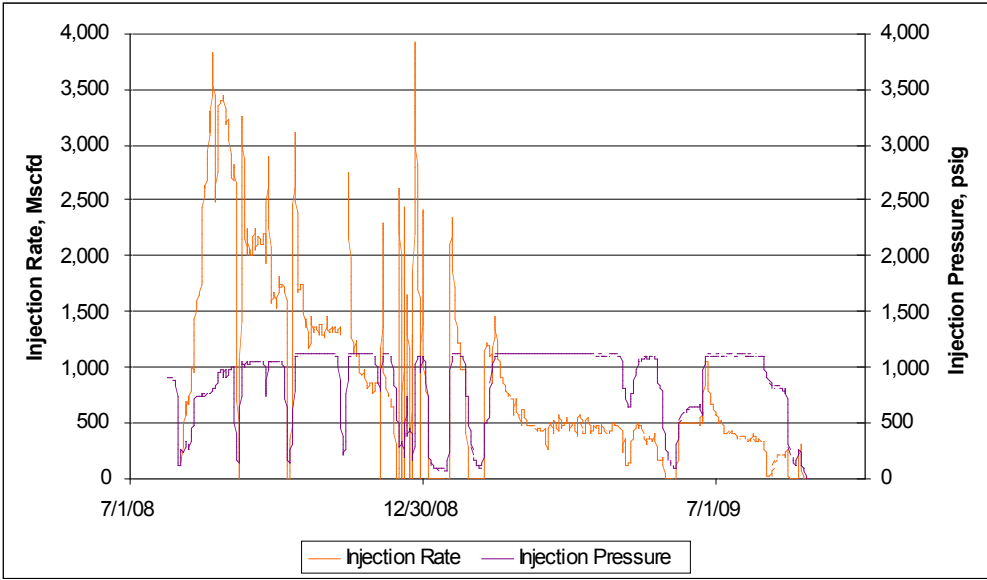


Figure 22:CO₂ Rate and Wellhead Pressure

The injection well was plugged and abandoned using the procedure described below. A schematic of the abandoned well is shown in **Figure 23**.

1. Move in & rig up
2. Pressure test blowout preventer equipment
3. Fill hole with 2% KCL and check injection ability at a low pump rate
4. Release packer
5. Trip out of hole with tubing and packer
6. Run in hole with cement retainer and set retainer at 2,900'
7. Trip in hole with workstring and sting into retainer and establish injection
8. Squeeze 5-1/2 inch liner with 35 bbl cement.

9. Sting out of retainer & circulate tubing and casing clean
10. Pressure test casing and retainer to 500 psig.
11. Trip out of hole with work string and lay down pipe
12. Rig down and move off

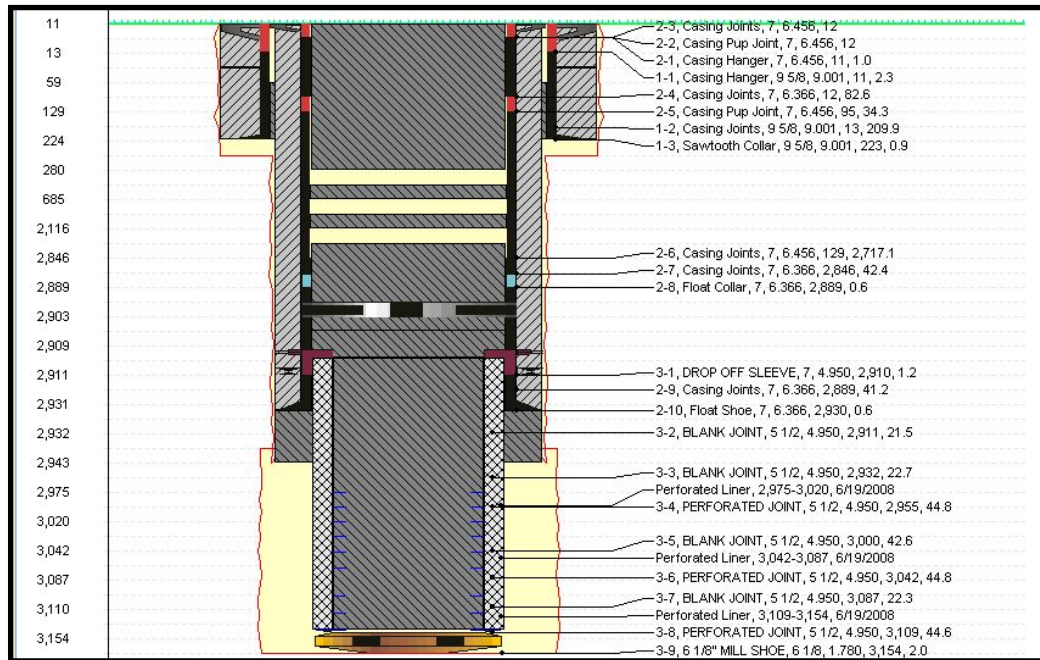


Figure 23: Well Abandonment Schematics

5.0 Monitoring, Verification and Accounting

This section describes the results from the various monitoring techniques deployed at the site.

5.1 Offset Production Wells

5.1.1 CO₂ Sensors

As mentioned previously, CO₂ sensors were deployed at the three immediate offset wells to track the produced CO₂ concentration. This section describes the results from the data collected through the sensors.

Figure 24 shows the CO₂ concentration data collected from EPNG COM A 300S, 547 meters northwest of the injection well. The data from July 1 to July 30, 2008 was regarded as the background data for each well. Data from well EPNG COM A 300S was around 30% during the injection period. A very low CO₂ concentration was observed around August 20, 2008. These low values occurred because the needle valve to control the gas flow rate through the sensor chamber was shut off. Thus, no gas passed through the sensor during that time.

Figure 24 also shows the high CO₂ content fluctuating between November 2008 and March 2009. A desiccant was added during this time to remove water from the gas stream. It was determined that the desiccant also adsorbed CO₂ and was sensitive to temperature. Therefore, it would absorb and desorb CO₂ on about a 24 hour cycle in conjunction with daily temperature fluctuations. On March 11, 2009, the desiccant was removed and the dryer container repositioned to serve as a water drip pod. From that time forward, the CO₂ concentration values were much more stable. Compared with the background CO₂ data in well EPNG COM A 300S (29%), no breakthrough has been observed as of November 19, 2009.

Figure 25 shows the CO₂ data for well EPNG COM A 300, 499 meters southwest of the injection well. Again, CO₂ content was observed to fluctuate before March 2009. After March

11, 2009, CO₂ concentration has again been quite stable. The average CO₂ concentration in well EPNG COM A 300 was around 20%. Some spikes were occasionally observed (**Figure 25**) between March and November 2009. After discussion with ConocoPhillips, it is believed that those CO₂ peaks were due to the well operation problem and not due to breakthrough.

Figure 26 shows the CO₂ data of FC STATE COM 1, 386 meters east of the injection well. The average CO₂ concentration in well FC STATE COM 1 is 22% before July 2009. CO₂ concentration has been observed to slowly increase from 22% to 25% from July to November 2009.

Based on the observations from **Figures 24 to 26**, it is concluded that CO₂ concentrations in the monitoring (production) wells did not change during the period from July 2008 to November 2009. CO₂ concentration in well FC STATE COM 1 increased slowly from 22% to 25% after July 2009. However, more CO₂ data is required to confirm whether or not CO₂ breakthrough is occurring in this well. The CO₂ monitoring system has been left in place, but the continuous uplink has been removed, so the data will be physically retrieved every few months.

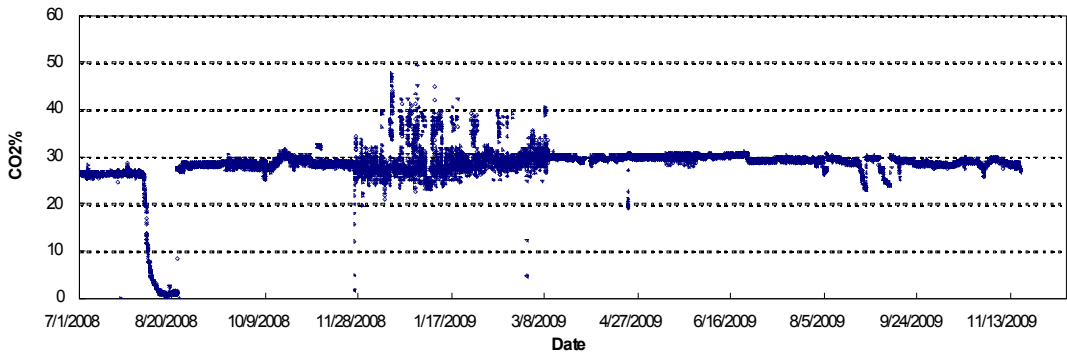


Figure 24: CO₂ Concentration Change in Well EPNG COM A 300S

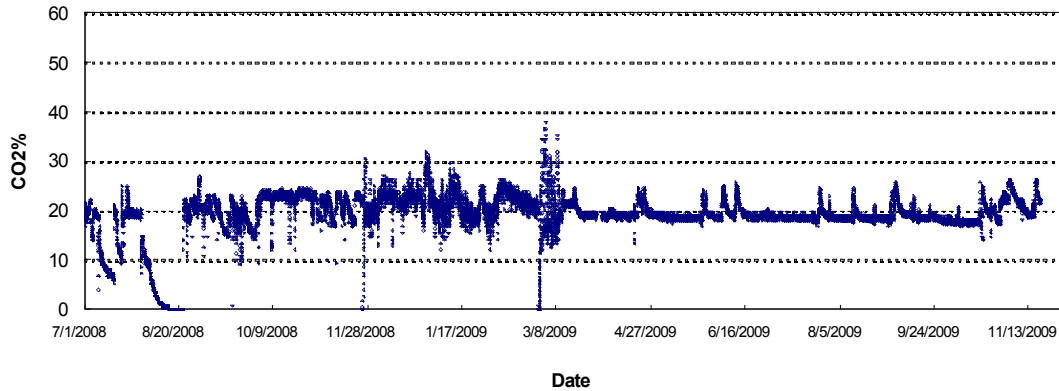


Figure 25: CO₂ Concentration Change in Well EPNG COM A 300

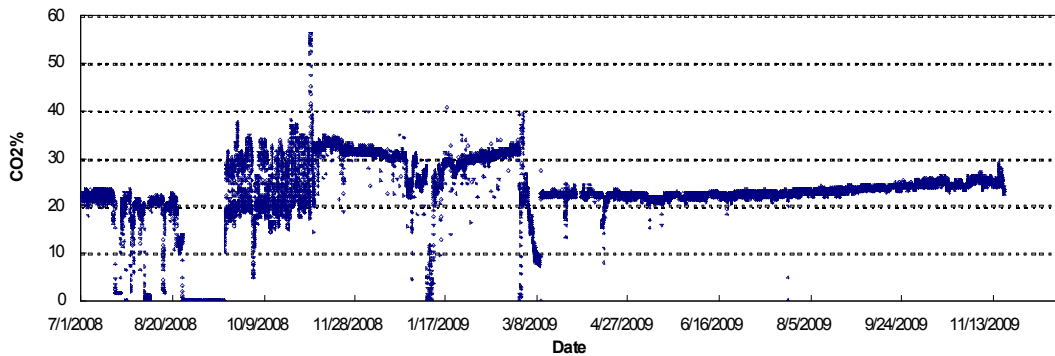


Figure 26: CO₂ Concentration Change in Well FC STATE COM 1

5.1.2 Gas Samples

Gas samples were collected periodically at up to fourteen production wells that surround the injection well. **Tables 1 to 3** show the gas sampling results for each of the three monitoring wells. The results are consistent with the CO₂ sensors and confirm that CO₂ concentration did not change for well EPNG COM A 300S and EPNG COM A 300 and increased 3% (from 25.4% to 28.5%) for well FC STATE COM 1 between May and October of 2009. Of interest is the nitrogen concentration for well EPNG COM A 300, which increased from <0.1% to 0.4% from July to September, and has remained above 1.5% since November 2008. A similar increase from about 0.5% or less to above 1.3% has occurred for FC STATE COM 1 (**Tables 2, 3**). Nitrogen may be starting to increase in EPNG COM A 300S as of October 2009. Here the concentration has increased from $\leq 0.1\%$ to 0.476%. The nitrogen concentration increase in those two wells was due traces of N₂ present in the injected CO₂ stream. Since CO₂ is

preferentially adsorbed onto the coal as compared to N₂, the nitrogen is being reproduced much faster. This phenomenon was also noticed at the Allison Unit CO₂-EOR site where N₂ concentration increased before CO₂ breakthrough occurred.

Table 1: Gas Sampling Results for Well EPNG COM A 300S

Composition	10/24/2007	1/4/2008	4/30/2008	7/26/2008	9/11/2008	11/13/2008	2/25/2009	5/20/2009	10/20/2009
N2	0.032	0.048	0.043	0.033	0.063	0.056	0.042	0.11	0.476
CO2	28.5	20.3	20.8	28.3	28.5	28.7	27.6	28.5	28.6
Methane	70	74.7	75.8	70	69.6	69.4	70.2	69.5	69.1
Ethane	1.068	2.897	2.143	1.173	1.203	1.226	1.409	1.281	1.245
Propane	0.387	1.662	0.987	0.391	0.447	0.473	0.602	0.506	0.474
1-Butane	0.047	0.199	0.11	0.05	0.054	0.055	0.07	0.059	0.055
n-Butane	0.037	0.158	0.083	0.04	0.04	0.043	0.055	0.046	0.043
1-Pentane	0.007	0.033	0.016	0.008	0.008	0.008	0.01	0.009	0.008
n-Pentane	0.003	0.013	0.007	0.004	0.003	0.003	0.004	0.004	0.003
Hexane	0.005	0.013	0.019	0.011	0.014	0.023	0.013	0.015	0.018

Table 2: Gas Sampling Results for Well EPNG COM A 300

Composition	10/24/2007	1/4/2008	4/30/2008	7/26/2008	9/11/2008	11/13/2008	2/25/2009	5/20/2009	10/20/2009
N2	0.051	0.039	0.147	0.078	0.448	2.02	1.724	1.512	1.55
CO2	19.8	19.4	19.7	20.6	19.4	23.7	21.4	20	23.3
Methane	75.9	78.9	76.3	78	76.7	72.1	73.7	74.8	71.9
Ethane	2.375	1.099	2.202	0.969	1.999	1.354	1.838	2.125	1.931
Propane	1.454	0.418	1.309	0.27	1.142	0.671	1.026	1.238	0.988
1-Butane	0.182	0.055	0.16	0.038	0.146	0.082	0.125	0.15	0.115
n-Butane	0.147	0.041	0.126	0.03	0.11	0.066	0.102	0.123	0.126
1-Pentane	0.028	0.008	0.025	0.007	0.022	0.013	0.02	0.025	0.03
n-Pentane	0.013	0.004	0.011	0.004	0.01	0.006	0.009	0.011	0.021
Hexane	0.014	0.007	0.014	0.018	0.017	0	0.032	0.03	0.114

Table 3: Gas Sampling Results for Well FC STATE COM 1

Composition	10/24/2007	1/4/2008	4/30/2008	7/26/2008	9/11/2008	11/13/2008	2/25/2009	5/20/2009	10/20/2009
N2	0.238	0.036	0.438	0.352	0.509	1.786	1.482	1.433	1.339
CO2	28.5	25.4	25.9	24.8	22.5	24	24.7	20.2	20.2
Methane	77.4	79.1	73.1	73.9	74.6	71.8	71.1	71.2	68.4
Ethane	1.326	0.529	1.161	1.173	1.466	1.098	1.09	1.264	1.219
Propane	0.652	0.059	0.47	0.433	0.683	0.412	0.391	0.524	0.475
1-Butane	0.082	0.009	0.058	0.056	0.083	0.051	0.049	0.062	0.056
n-Butane	0.065	0.007	0.046	0.048	0.075	0.041	0.04	0.052	0.047
1-Pentane	0.013	0.001	0.009	0.01	0.018	0.008	0.008	0.01	0.009
n-Pentane	0.007	0	0.004	0.005	0.012	0.005	0.003	0.005	0.004
Hexane	0.014	0.014	0.005	0.007	0.044	0.012	0.009	0.003	0.01

5.2 Geophysical Interpretation

Geophysical and geological characterization at the site was undertaken by West Virginia University in support of NETL's tracer and soil gas measurement efforts. Research incorporated

independent subsurface mapping, acquisition, processing and interpretation of satellite imagery data (QuickBird, INSAR, and radar), field mapping of surface fracture systems, acquisition, processing and modeling of terrain conductivity data, acquisition and interpretation of comprehensive well logs from the injection well, FMI log analysis of subsurface fracture data, design and specialized processing of the time lapse VSP monitoring survey and 3D seismic interpretation.

5.2.1 3D Seismic

Seismic analysis incorporated synthetic seismic ties, horizon interpretation and mapping of a 9 square mile area surrounding the site. Post-stack processing incorporated a variety of edge and discontinuity enhancement algorithms to extract and enhance seismic features that might represent potential fracture zones and faults; structural features that could facilitate migration of injected CO₂ into overlying strata.

Post stack processing incorporated edge enhancement and event similarity prediction algorithms, along with calculation and evaluation of tuning cubes and Ant Tracking. The analysis reveals internal compartmentalization of the Fruitland coals through this area, accompanied by a fairly extensive system of interpreted fracture networks concentrated in the primary seal (the Kirtland Shale).

Seismic analysis reveals complex subsurface geology at the scale of the pilot site. Amplitude anomalies are numerous in the vicinity of the injection well in addition to kilometer wavelength structures. Regional studies by Fassett (1997), Wray (2000), reveal the presence of considerable heterogeneity within the Fruitland formation and individual seams. The detailed study of Ayers and Zellers (1994) conducted near the pilot site reveals considerable complexity in the Fruitland depositional systems. In a schematic sense, Wray (2000) represents the variety of heterogeneity that can be encountered in the Fruitland coals (**Figure 27**). Fassett (1997) indicates that continuity of subsurface coals over distances of a mile is speculative, at best. Pinchouts, local fault truncations, channel scour and facies changes are all encountered in the Fruitland coals. Seismic analysis provides a glimpse of some of this heterogeneity.

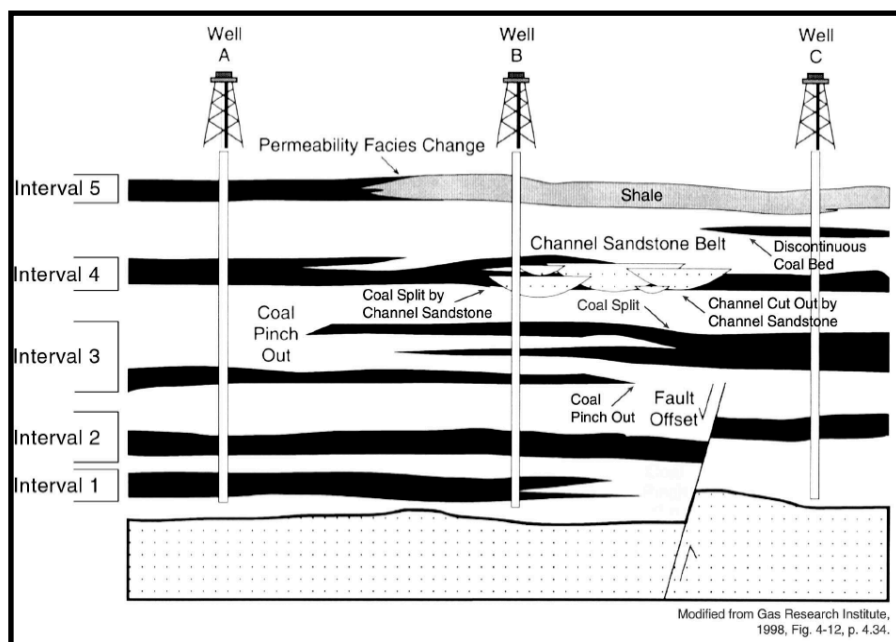


Figure 27: Schematic of Coalbed Methane Reservoir Cross Section (taken from Wray, 2000)

The black and white variable area wiggly trace display (**Figure 28**) illustrates basic features associated with the seismic response of the Fruitland sequence.

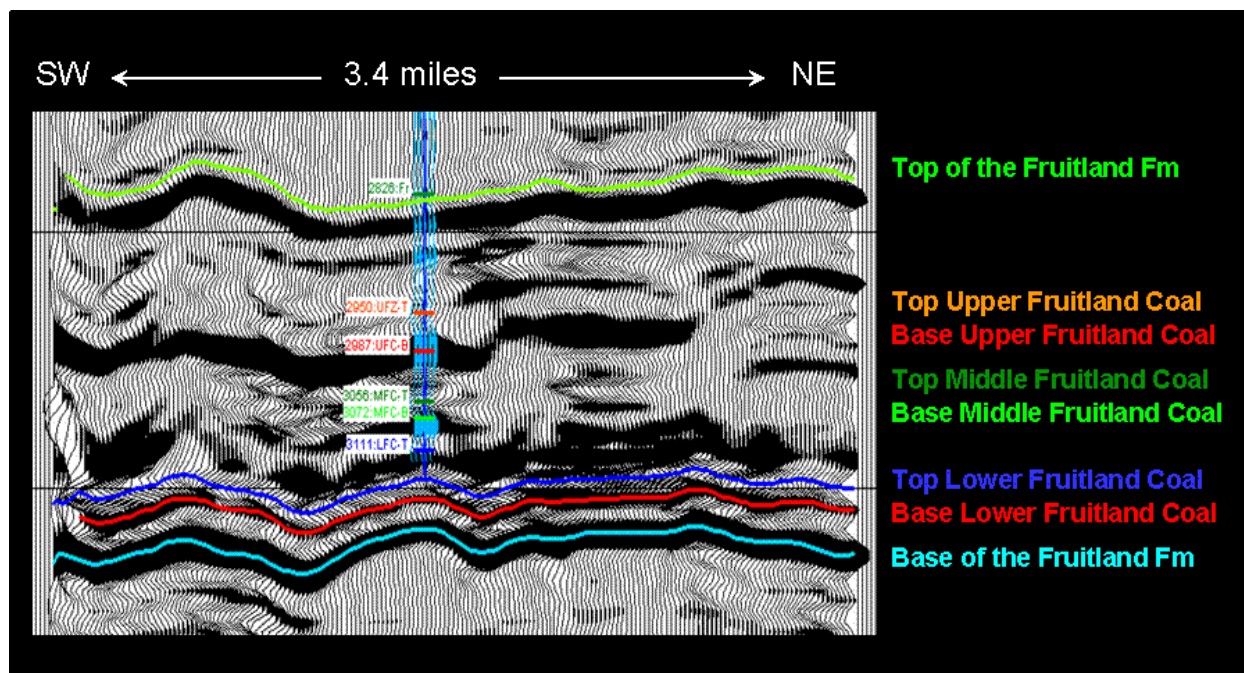


Figure 28: In this 2D Seismic Display, Locally Steepened Dips are Evident across the Area. This Line Trends Northeast-Southwest Considerable Internal Discontinuity of Reflection Events is Evident Throughout

3D seismic interpretation reveals that the Late Cretaceous Fruitland formation forms a well defined seismic sequence with high amplitude reflection events marking the top and base of the sequence. The pattern of internal reflection events is generally parallel and conformable near the top and base of the sequence. However, considerable internal reflection discontinuity is present. This discontinuity appears to be associated primarily with the upper and middle Fruitland coals. The 3D seismic view of the Fruitland formation is considerably different than that inferred from well log cross sections. The seismic reveals significant discontinuity as noted, whereas the coal intervals shown in well log cross sections often suggest continuity which may, in fact, not be the case. These are problems related to sparse sampling. Seismic interpretation also reveals the presence of local fold-like structures (Figures 28 and 29) with wavelengths ranging from 1 km to 3.5km accompanied by relief of 6 ft to 60 ft.

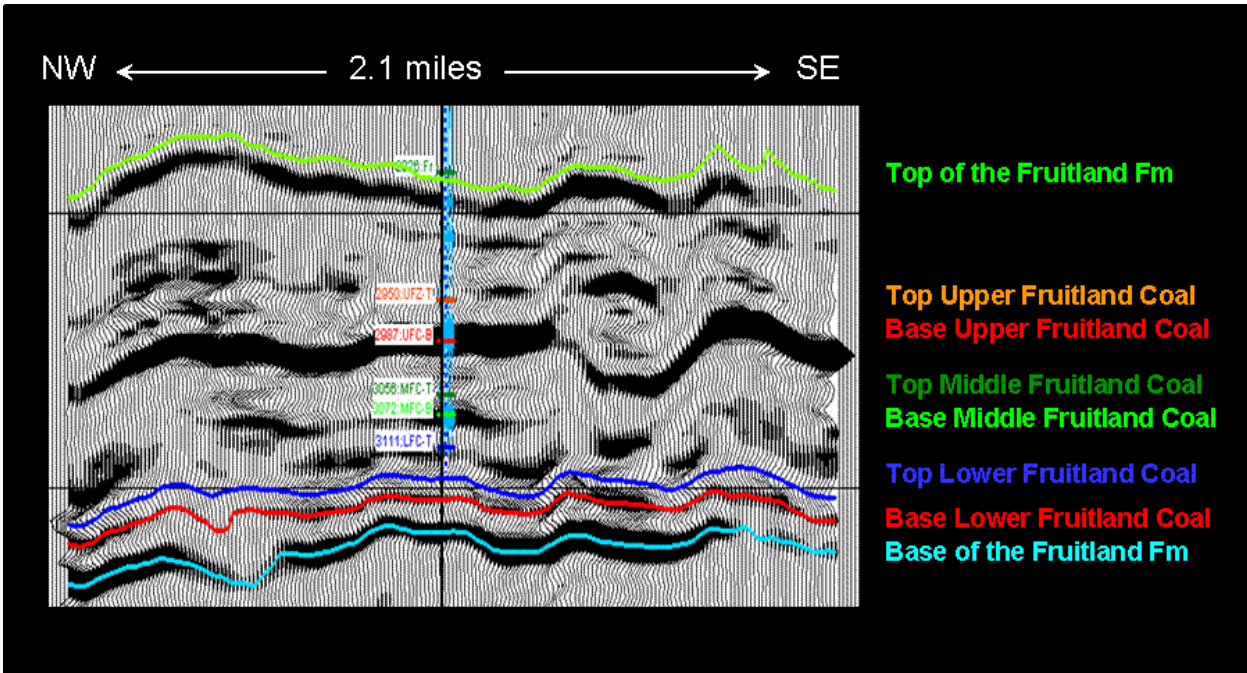


Figure 29: This Northwest-Southeast Line Illustrates a Similar Level of Reflection Discontinuity along the Axis of the Basin. Local Structural Features are also Evident in the Display.

The origin(s) of these structures is uncertain. In some cases, time-structural rise across the top of the Fruitland is accompanied by a drop across the base. This could, for example, represent time-sag associated with increased travel time through relatively low velocity intervals within the Fruitland sequence. Other time structures observed in the Fruitland carry upwards through overlying Paleocene and Late Cretaceous intervals. For example, to the northwest, (Figure 30) there is a gentle structural rise in both the upper Fruitland and the Kirtland and adjacent reflection events. On the southeast end of this line small folds in the upper and middle Fruitland appear to have some hint of continuation into intervals overlying the Kirtland.

Geologic controls to consider include detachment within the coals and differential compaction associated with lateral variations of net compressibility associated with variations in depositional environments and lithologic heterogeneity within the Fruitland sequence. Although regional face cleat trend in the area has NE-SW trend, Ayers and Zellers (1994) note that compaction folding of coals above and below channel sandstones could produce localized areas of enhanced fracture density. Their cross sections reveal coal splitting associated with fluvial channel systems within the Fruitland formation. Compaction induced coal fracture systems are discussed by Donaldson (1979) and Tyler et al. (1991). Internal reflection patterns observed in the 3D seismic from the area (Figures 28 and 29) suggest the presence of some channeling.

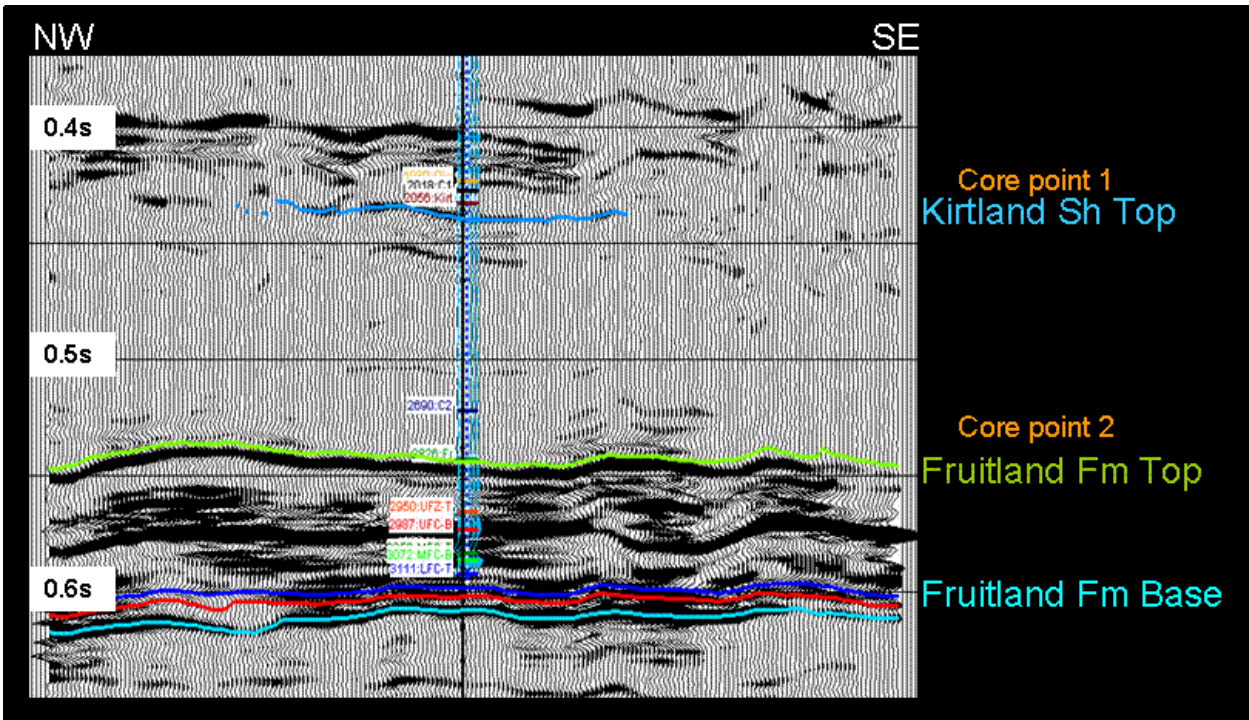


Figure 30: Shallower Reflection Events Associated with the Upper Kirtland Shale, the Ojo Alamo Sandstone and Nacimiento Fm.

Seismic displays (**Figures 29 and 30**) suggest thinning to the southeast. The isochore map (**Figure 31**) shows areas of thinning (orange and red areas) that stretch to the southeast along the axis of the basin. The morphology of these patterns is not clearly associated with specific depositional environments. Sandstone deposits in the Fruitland formation generally flowed northeastward onto coastal areas of the Western Interior Seaway. While there appear to be channel like features in some vertical displays, we do not see the dip-elongate (northeast oriented) pattern of sandstone bodies expected in the Fruitland (Ayers and Zellers, 1994). The isochore might reveal depositional patterns if they are accompanied by differential compaction. The change in travel time through the Fruitland sequence encountered in the vicinity of the injection and production wells is at most 8 milliseconds. Using an average interval velocity of 10,600 ft per second for the Fruitland, this corresponds approximately to thickness changes on the order of 42 ft.

Reflection events arising from the lower Fruitland coal are continuous and well defined throughout the area. Travel time changes from these continuous internal reflections in the vicinity of the injection well and surrounding production wells correspond to thickness variations on the order of 2 to 3 ft, or so (**Figure 32**). This estimate assumes a constant velocity of about 7,700 ft/second in this coal interval. The reflection event from the top of the coal appears to be closer to the overlying zero crossing (**Figure 33**). The following negative cycle was used due to its continuity. While the events interpreted to be associated with the lower Fruitland coal do not coincide with the actual top and base of the lower Fruitland seam, they do provide a measure of the internal thickness variations and structure of this lower coal zone.

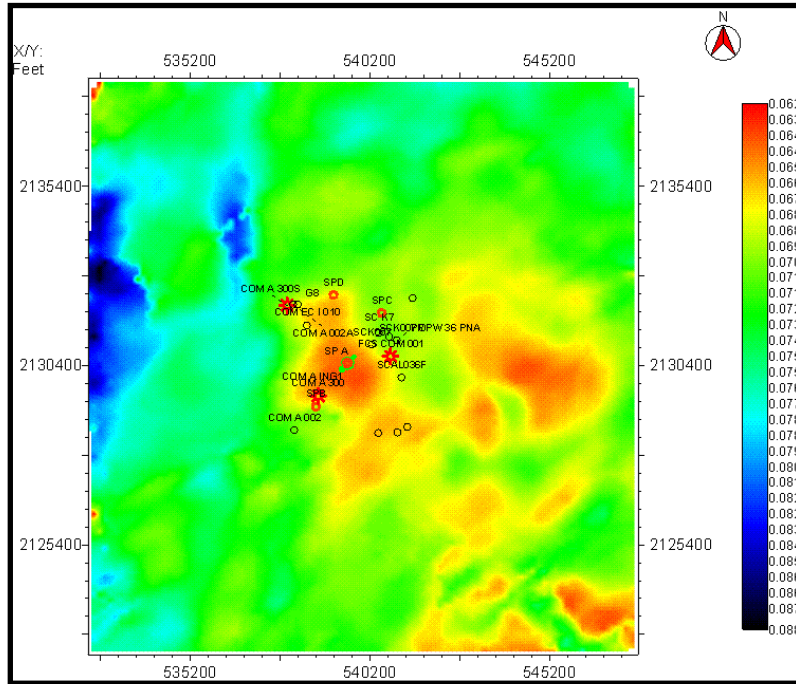


Figure 31: Isochore Map of the Interpreted Fruitland Formation Seismic Sequence

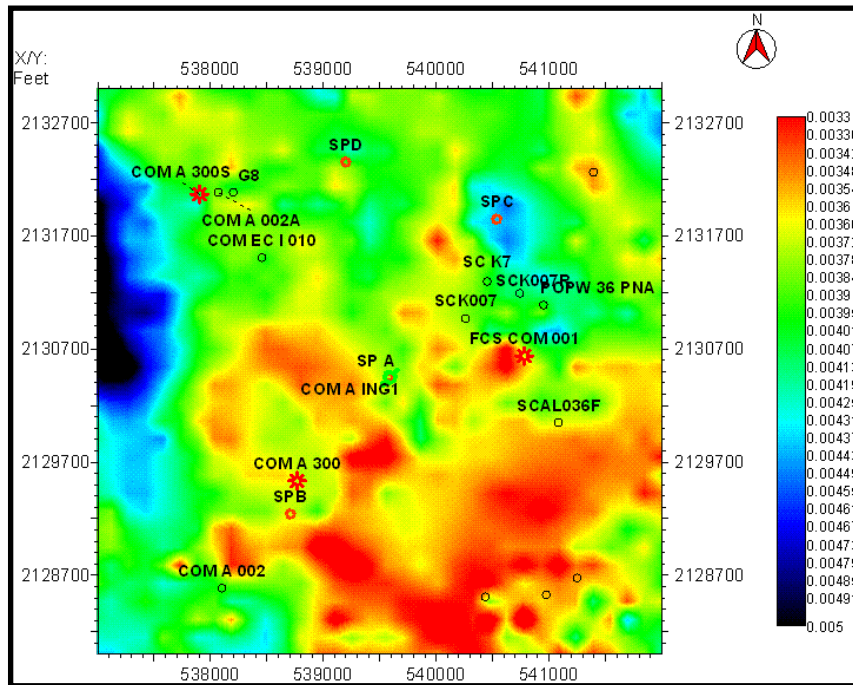


Figure 32: Isochore Map of the Interpreted Lower Fruitland Coal Zone

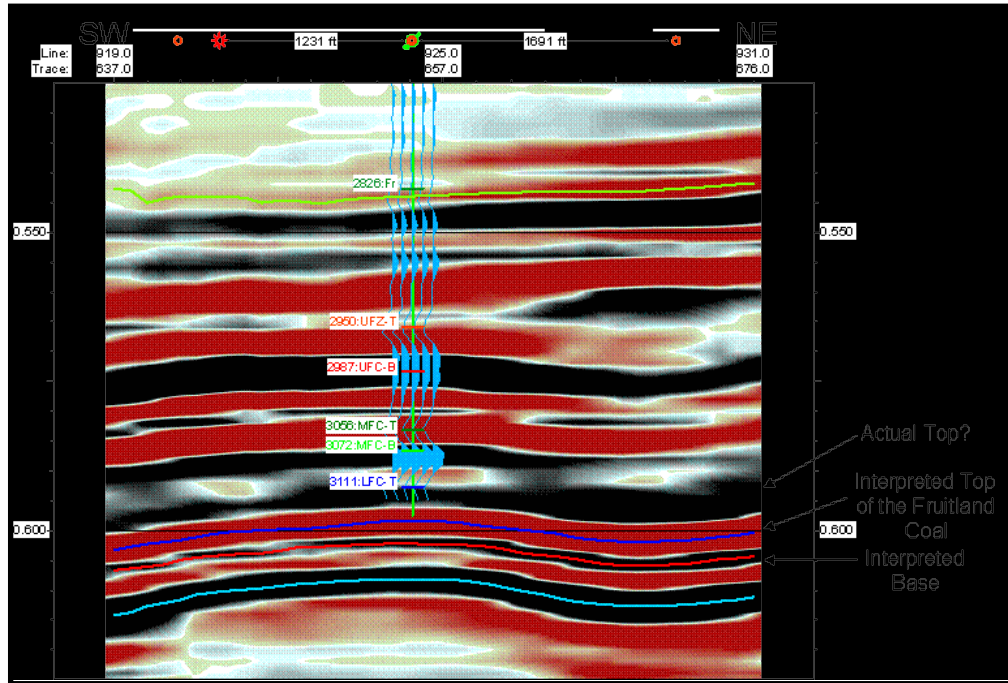


Figure 33: A Detailed View of Reflection Events Associated with the Lower Fruitland Coal

5.2.2 Attribute Analysis

Several seismic attributes have been calculated and examined to determine if additional insights can be gained from the seismic data regarding the structural and stratigraphic integrity of the reservoir and overlying strata. Our main objective is to assess the potential for vertical leakage of injected CO₂. Thus, we are interested in identifying possible fracture zones and faults that might facilitate the escape of injected CO₂ into overlying formations and possibly to the surface.

An example of this analysis (**Figure 34**) illustrates how additional information can be extracted regarding the presence of possible fracture zones and fault systems. The absolute value of the derivative of seismic amplitude was calculated. An Automatic Gain Control (AGC) was applied to the derivative to normalize amplitude variations. Between the Fruitland top and base (**Figure 34**) there are some subtle features that may be associated with vertically juxtaposed stratigraphic pinchouts or internal faults. Some of these occur near the periphery of the pilot area as defined by the production wells. Considerable evidence of fracturing and minor faulting is

observed in the Kirtland Shale. While large penetrative faults are not present in the strata overlying the Fruitland Formation, considerable fracturing of overlying intervals is suggested by the data. If the integrity of the reservoir is compromised, eventual escape to the surface might be facilitated by these fracture systems.

A close-up view (**Figure 35**) along this same dip line reveals some subtle disruptions of amplitude within the Kirtland Shale to the southwest near one of the producing wells (COM A 300). The injection well sits on top of a subtle structure in the lower Fruitland. Stratigraphic pinchouts coincident with this high are observed in the underlying Pictured Cliffs Sandstone. The Fruitland isochore (**Figure 31**) reveals a northwest trending zone of thinning in the Fruitland sequence. Thinning correlates to the presence of reflection terminations against the lower Fruitland sequence boundary. These reflection patterns are interpreted to be associated with northwest trending shoreline sands in the Pictured Cliffs Sandstone. We speculate that sequence thinning is related to differential compaction over a shoreline sand body. We also speculate that differential compaction could enhance fracture intensity along this northwest trend, particularly in the lower part of the sequence where interpreted differential compaction is more pronounced.

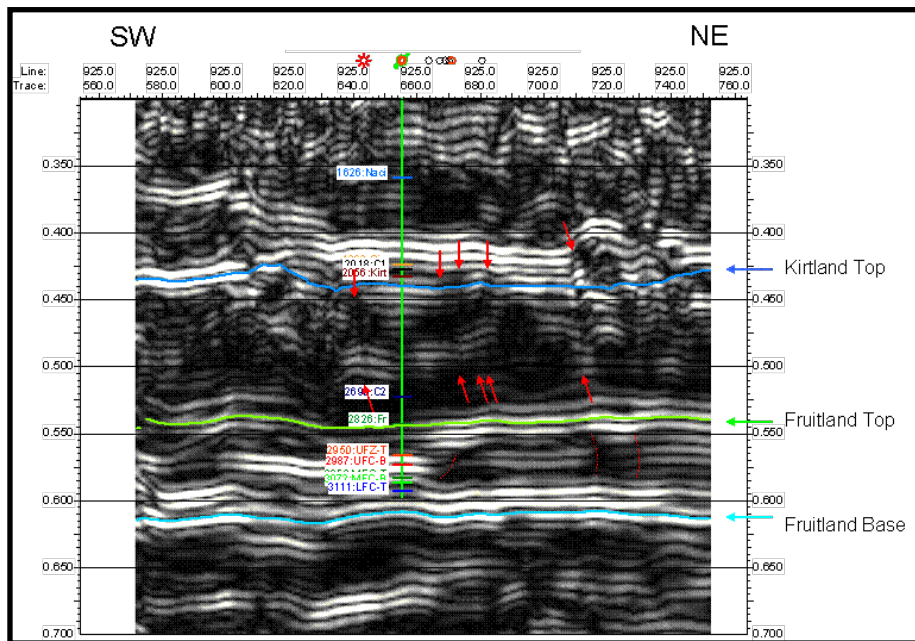


Figure 34: Gain Adjusted Absolute Value of the Finite Seismic Amplitude Difference Reveals Vertically Continuous Amplitude Disruptions that Cut through Laterally Coherent Reflection Events

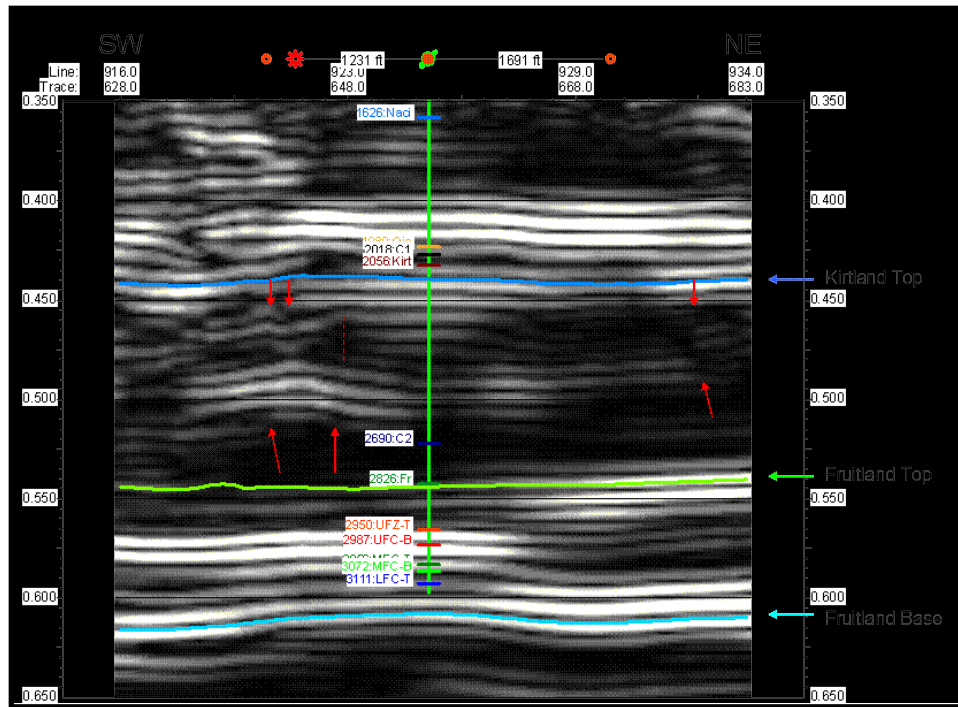


Figure 35: Close Up View of Finite Difference Attribute Along the Dip Line Shown in Figure 34. This Line Passes through the COM A 300 Well about 1200 Ft Southwest of the Injection Well. Local Structure in the Fruitland Coal, Stratigraphic Pinchouts and Amplitude Disruptions are Present in the Vicinity of the Injection Well.

Subtle seismic indications of fracturing within the Fruitland sequence are present in places (e.g. **Figure 34**), however, the finite difference computations do not provide clear evidence of local faults within the Fruitland formation. The results obtained from analysis of additional seismic attributes will be presented at the meeting. One of these attributes (Ant Tracking) reveals a regular system of discontinuities interpreted to be fracture zones or small faults within the Fruitland formation. Rose diagrams of Ant Tracks reveal pronounced clusters with N50-55E trend throughout the Fruitland (e.g. **Figure 36A**). Less pronounced NW trending clusters are infrequently observed. The NE trend is also very pronounced in the overlying Kirtland Shale (e.g. **Figure 36B**), Ojo Alamo Sandstone and Nacimiento formation.

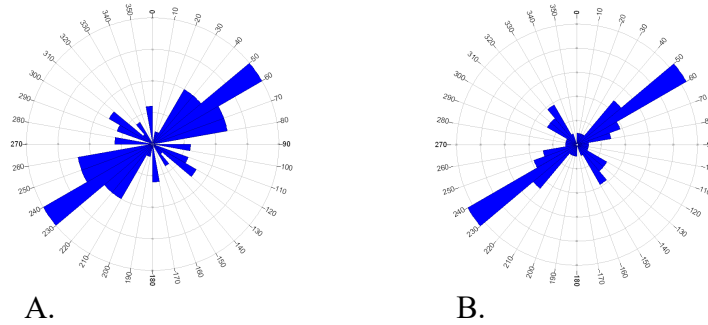


Figure 36: Rose Diagrams of Ant Tracks Mapped At A) 570 ms within the Fruitland Sequence and B) 480ms within the Middle Kirtland Shale Sequence

5.2.3 Surface EM Characterization

Approximately 70 line kilometers of EM data were collected over the site to locate flow paths in the near-surface sandstone that caps the site mesa. In some cases, surveys were repeated using only two transmission frequencies to gain to improve transmission power and signal-to-noise ratio. The high frequency response (47,000 Hz) over the site reveals complex conductivity variations across the site associated with soil distribution, site infrastructure and varying water saturation in the near surface (upper 10 meters) at the site.

Conductivity inversions reveal continuous resistivity layering down to depths of about 8 meters beneath the surface. The low conductivity area that opens like a fan to the west (see map view **Figure 37**) appears to consist of a headward conduit that extends from the surface down into higher resistivity less conductive areas of the sandstone that caps the mesa. This reveals a layered subsurface consisting of three layers that become increasingly resistive with depth (**Figure 38**).

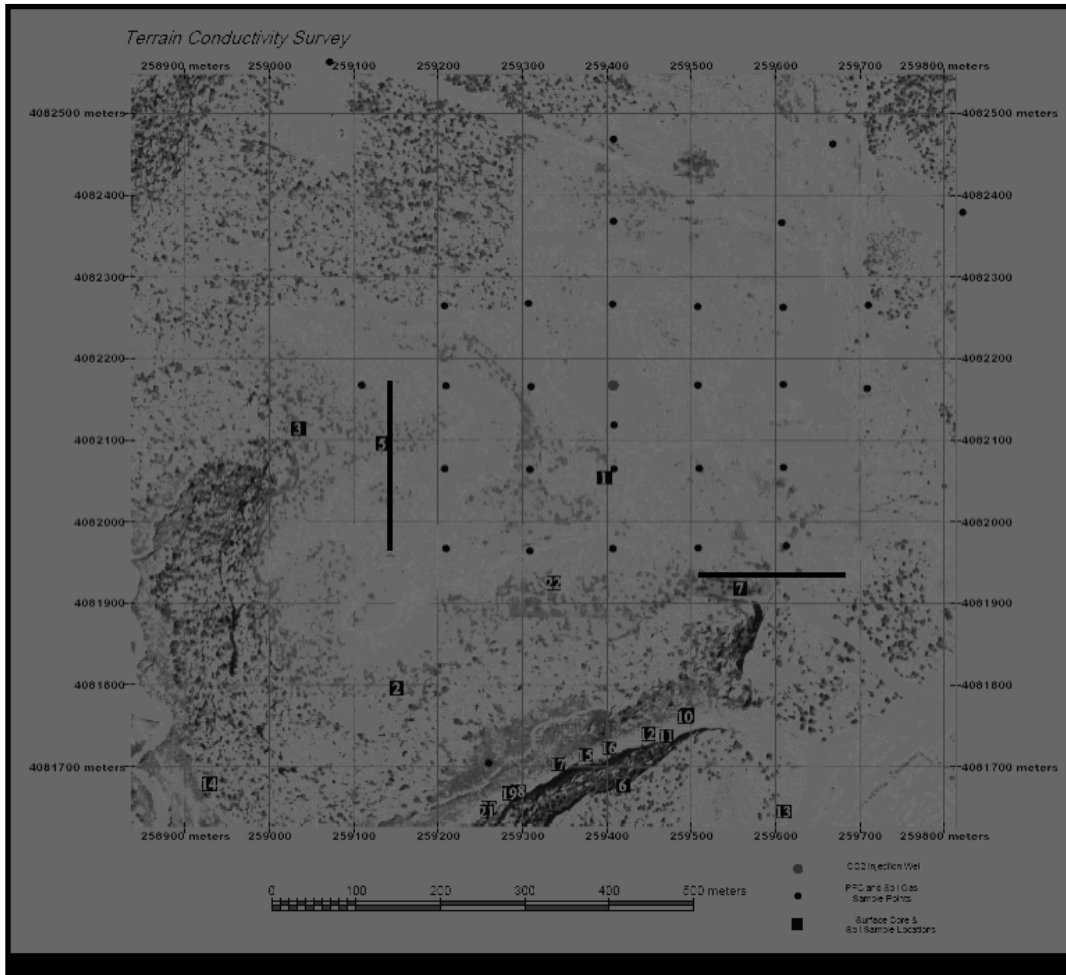


Figure 37: Locations of Conductivity Profiles are also Shown (Red Lines)

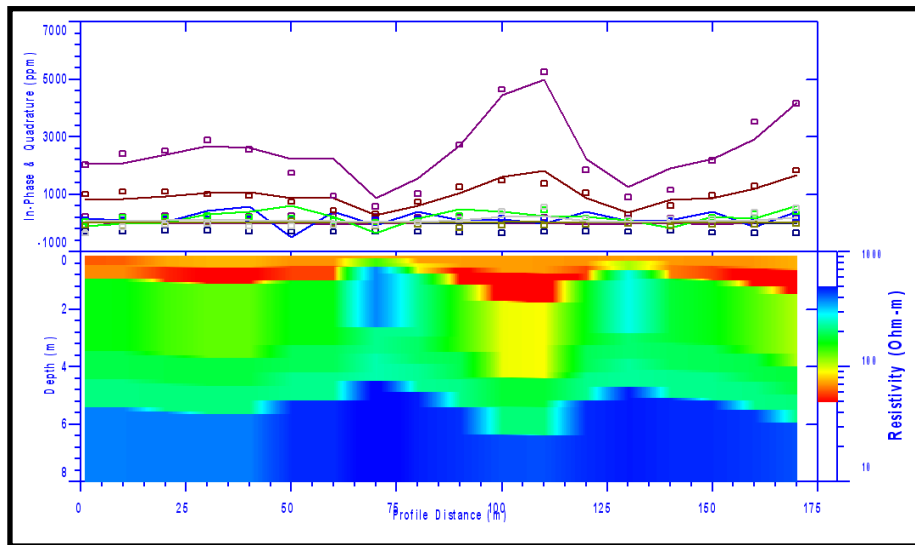


Figure 38: Layered Inverse Models Developed Along the North-South Cross Section

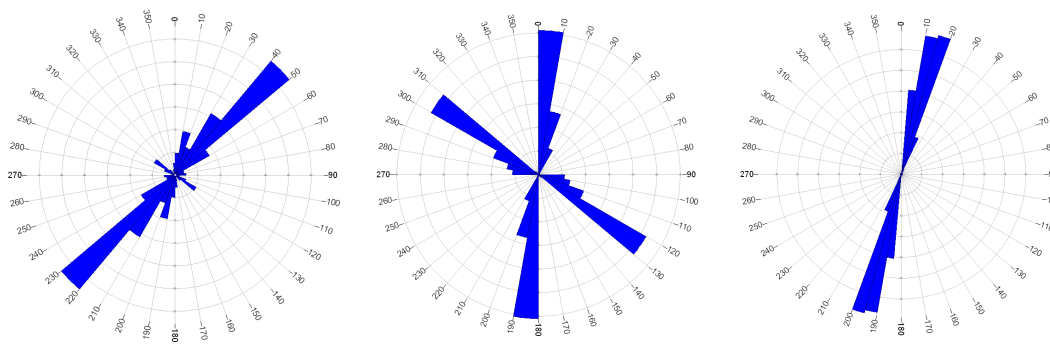
Low conductivity channels (high resistivity or blue areas in **Figures 37 & 38**) are interpreted to represent high permeability well drained areas in the sandstone that caps the site mesa. The low resistivity (red) areas are probably controlled by variable soil thickness across the surface of the mesa.

The area in the vicinity of the injection well consists of a patchy distribution of low conductivity areas that are the most likely conduits for near-surface migration of CO₂ into the atmosphere.

5.2.4 Logging

Fast Shear Azimuth - Fast shear directions measured by the sonic scanner along the entire length of the borehole reveal a major peak in the northeast quadrant with a vector mean orientation of N37E (**Figure 39A**). The 95% confidence limit about the mean is approximately 1

degree. Secondary peaks in the northwest and northeast quadrants have vector mean orientation of N57W and N14E, respectively (**Figure 39A**). Within the upper part of the Fruitland formation logged in the first drilling run (2,826 to 2,943 ft) the fast shear directions form two clusters (**Figure 39B**) with mean trends of N64W and N08E. In the lower coal bearing Fruitland formation (2,943 to 3,132 ft) logged in the second run, the fast shear direction has little variability about a mean orientation of N14E (**Figure 39C**). The fast shear direction appears to be fairly weak and variable through the upper Fruitland where it drifts from NW to N and then NE directions down the hole. All distributions are significantly non-random at an α -level of 0.001. The 95% confidence limit on the mean fast-shear azimuth in the lower Fruitland coal section is less than 1 degree.



A)

B)

C)

Figure 39: A) The Fast Shear Direction Determined from the Schlumberger Sonic Scanner Over the Entire Length of the Hole (275 To 3132 Ft) is Dominated by a Cluster in the Northeast Quadrant with Mean Orientation of N43E Degrees (N=4567). Smaller Peaks are Observed at Approximately N14E (N=1061) and N57W (N=500). B) Within the Upper Part of the Fruitland Formation, Peaks are Observed at N64W (N=115) and N08E (N=118); C) in the Coal Bearing Section the Average Fast Shear Direction is N14E (N=379).

Drilling induced breakouts - Drilling induced breakouts observed in the FMI log through the upper Fruitland from 2,826 to 2,943 ft (N=5) have a vector mean orientation of N57W (**Figure 40**) and 95% confidence limit of 10 degrees. The vector mean orientation of all breakouts identified in the FMI log (N=97) is also N57W (95% confidence limit of 3.6 degrees). Breakout orientation is generally consistent along the entire length of the borehole. The shallowest breakout was interpreted at 329 ft and the deepest observation made at 2,936 ft. The drilling induced breakouts, and fast shear direction, provide independent measures of the maximum compressive stresses in the rock. The breakouts form normal to the present-day in-situ maximum compressive stress. The N57W breakout trend implies a maximum compressive stress (σ_H) of N33E. The fast-shear azimuth generally lies parallel to the present day maximum compressive stress and its value of N37E (95% confidence limits of ± 1 degree) is similar to the N33E (95% confidence limits of ± 3.6 degrees) value inferred from the breakout orientations.



A)

B)

Figure 40: Drilling Induced Breakouts Observed in the FMI Logged Interval (324 to 2,943 Ft) Have Mean Trend of N57W (N=97). Those within the Upper Part of the Fruitland (2,826 to 2,943 Ft) also Have Mean Trend of N57W (N=5).

In contrast, the fast-shear direction observed in the Fruitland coal section, taken by itself, has a more northerly (N14E) trend. The orientations of coal face cleats observed in the GRI NEBU well about 7 miles east of the injection well have approximately N35E trend (Mavor and Close, 1989). The breakout orientations and fast shear directions in the strata overlying the Fruitland formation are consistent with that trend; however, the rotation of the fast-shear direction to the NE within the lower coal bearing section suggests some possibility that the face cleats may have more northerly trend at the pilot site.

Open fractures – A total of 48 open fractures were interpreted in the FMI log (**Figure 41A**). Although three clusters appear in the open fracture trends: N63W, N01E and N67E; the low value of \bar{R} suggests randomness in distribution. From an interpretive perspective, preferred orientations appear to be forming in the distribution, but the number of observations is too low to suggest definitive geological relationships.

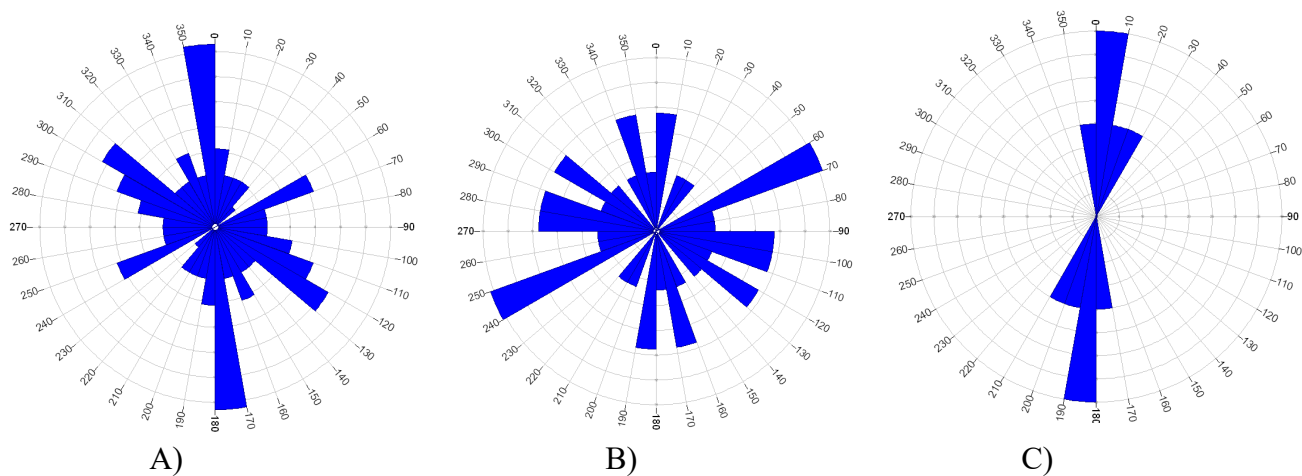


Figure 41: A) Open Fracture Trends Interpreted in the FMI Log from 1,000 To 2,905 ft in The Borehole (N= 48); B) Open Fractures in the Kirtland Shale Primary Seal (N=21); C) A Limited Number of Open Fractures (N=5) in the Upper Fruitland (2830 To 2905) have Mean Orientation of About N11E.

The orientations of open fractures in the Kirtland Shale are not statistically different from a random distribution; however, a mode appears to begin taking form with approximate N65E trend. A limited number of open fractures (N=5) observed in the FMI log in the upper Fruitland formation have vector mean strike of N11E similar to the fast shear orientation inferred from the sonic scanner in the Fruitland formation. Taken separately from the total, this subdivision of fractures is significantly non-random with α level of 0.01 and a 95% confidence interval of 19 degrees. The top of the Upper Fruitland Coal is reported at 2,963 ft; however, a significant coal fraction is encountered at approximately 2,948 ft where the density drops to about 1.8 gm/cm³. The FMI log provides fracture interpretations only down to about 2,943 ft, 20 ft above the Upper Fruitland Coal. The fast-shear direction rotates to N14E in the Fruitland coal section and suggests possibility of a rotation in the residual stress field within the Fruitland Formation. Instability in the fast-shear measurements in the upper 100 ft of the Fruitland formation suggests transition in residual stress from N37E to the N14E. We speculate that the open fractures observed in the well may have formed in response to late-stage Laramide compression. The late-stage compression may have produced some detachment in the coal section.

Equal area projections of open fractures observed in the injection well reveal almost random distribution of poles as suggested in the analysis of fracture strike (**Figure 42**) particularly for the total set of open fractures and those observed in the Kirtland Shale (**Figures 42 A and B**). The set of open fractures observed in the upper Fruitland is small and in this case also supportive of a northeasterly preferred trend (**Figure 42**).

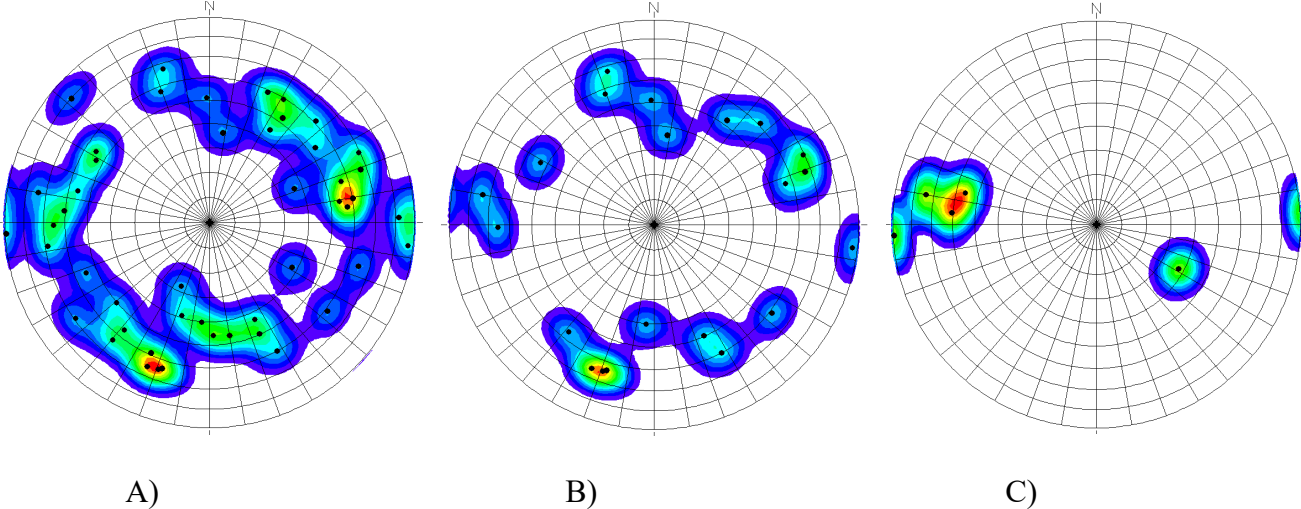


Figure 42: Equal Area (Schmidt Net) Projections of Poles to Open Fracture Planes. A) All Open Fractures; B) open Fractures Observed in the Kirtland Shale; and C) Open Fractures Observed in the Upper Fruitland Formation.

Schlumberger’s FMI log analysis includes computation of the hydraulic electrical apertures. Fracture aperture distribution is an important fracture property critical to flow simulation. The open fractures penetrated in this well provide a general view of aperture distribution in the cover strata at the site (**Figure 43**). The frequency distribution is positively skewed with mode of 0.08 inches.

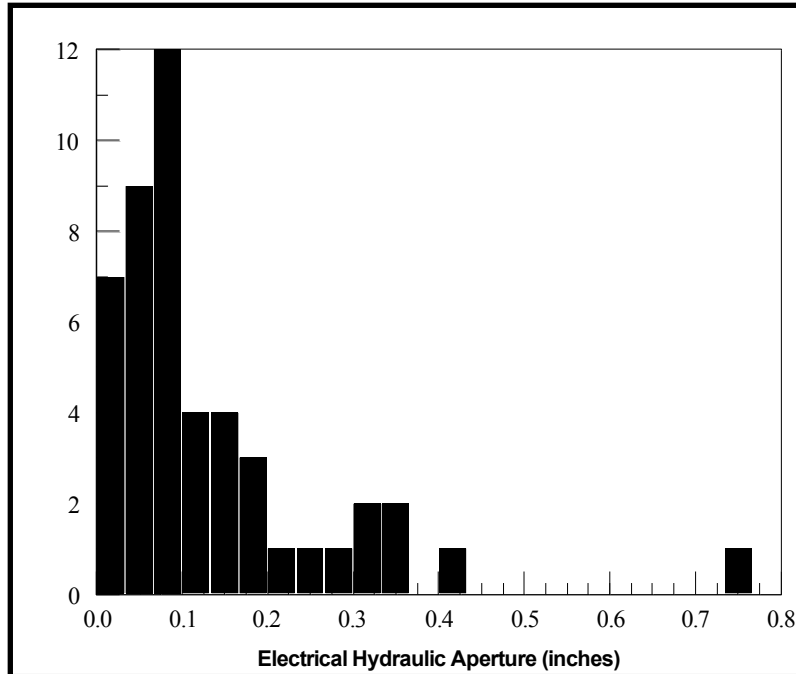


Figure 43: Hydraulic Electrical Fracture Aperture Distribution. N=48

Healed Fractures - The orientations of healed fractures appear to be more widely scattered (**Figure 44A**) than the open fractures (**Figure 44B**) penetrated by the wellbore. However, as with the open fractures, the \bar{R} -value is low these differences are attributed to random scatter. A total of 57 healed fractures were mapped in the FMI log interpretation. The orientations of healed fractures in the Kirtland Shale show some tendency for preferred orientation at $\alpha = 0.1$. A mode with approximate N45W trend emerges from the background. Healed fractures along the length of the borehole were distributed with similar frequency from depths of 370 ft to the top of the Fruitland formation at 2,826 ft subsurface. A relatively large number of healed fractures (14 or about 25%) were observed in the upper 100 ft of the Fruitland formation (**Figure 44C**). The \bar{R} -value for these fractures taken separately is also quite low, suggesting the orientations are effectively random in distribution. However, modes appear to emerge along trends consistent with tectonic in-situ strains inferred from the drilling induced breakouts and fast-shear directions. Mean azimuths of the three modes observed in the full sample (**Figure 44A**) occur at N53W, N14E and N59E. The confidence limits on the mean orientations of each cluster are 13 degrees, 13 degrees and 9 degrees, respectively. Peaks in the

rose diagram of healed fractures in the upper Fruitland occur at N66W, N03W, and N50E, with confidence limits of 11 degrees, 14 degrees and 21 degrees, respectively.

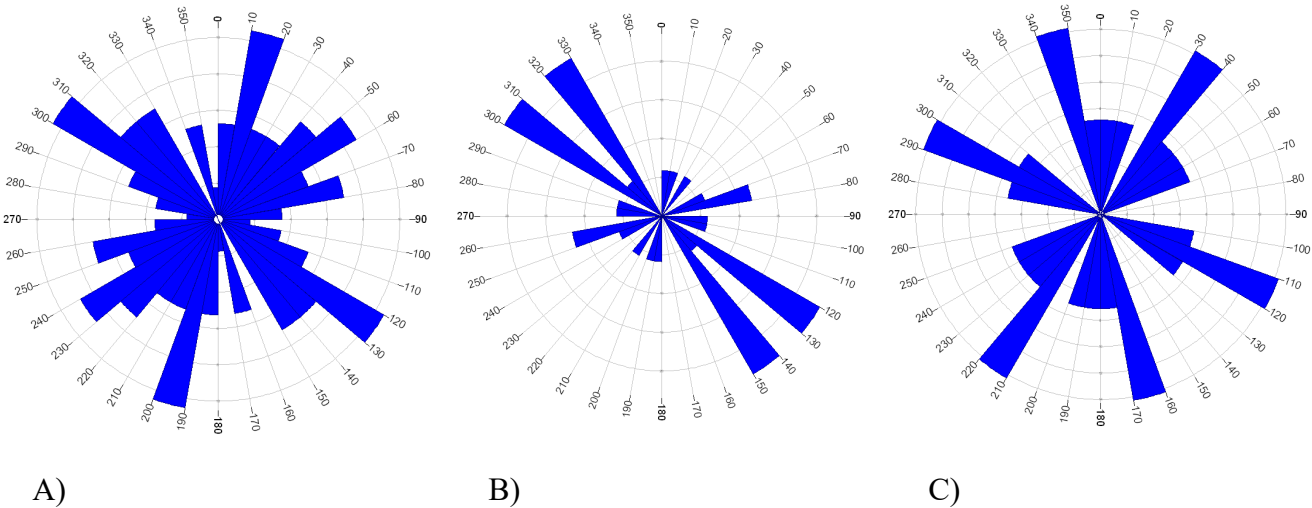


Figure 44: A) Healed Fracture Trends Interpreted in the FMI Log from 370 to 2,925 ft in the Borehole (N=57); B) Healed Fractures Observed in the Kirtland Shale (N=17); C) Healed Fractures (N=14) in the Upper Fruitland Formation.

5.2.5 Vertical Seismic Profile (Pre-Injection)

The VSP surveys were completed on June 3 and 4, 2010. The pre-injection surveys included a zero offset survey acquired on June 3, and three offset VSPs acquired the following day. The sources have the following locations relative to the injection well.

- A Elevation 0 ft Offset 114 ft Azimuth 245 Deg.
- B Elevation 47 ft Offset 1,498 ft Azimuth 216 Deg.
- C Elevation -27 ft Offset 1,693 ft Azimuth 34 Deg.
- D Elevation -62 ft Offset 1,942 ft Azimuth 349 Deg.

The locations of VSP sources A through D are shown on **Figure 45**.

The monitor surveys were acquired in mid September 2009 after CO₂ injection ceased.

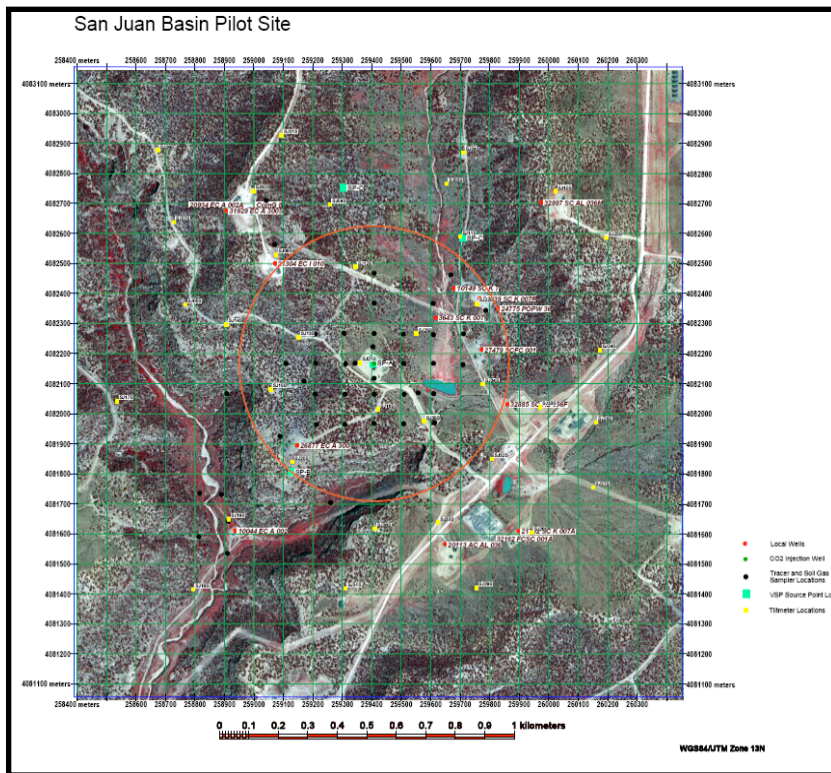


Figure 45: Base Map Showing Locations of Various Experiments on the Site. VSP Offset Source Locations are Shown as Bright Green Squares

A comparison of the baseline and monitor VSP ongoing wavefield with NMO correction is shown in **Figure 46**.

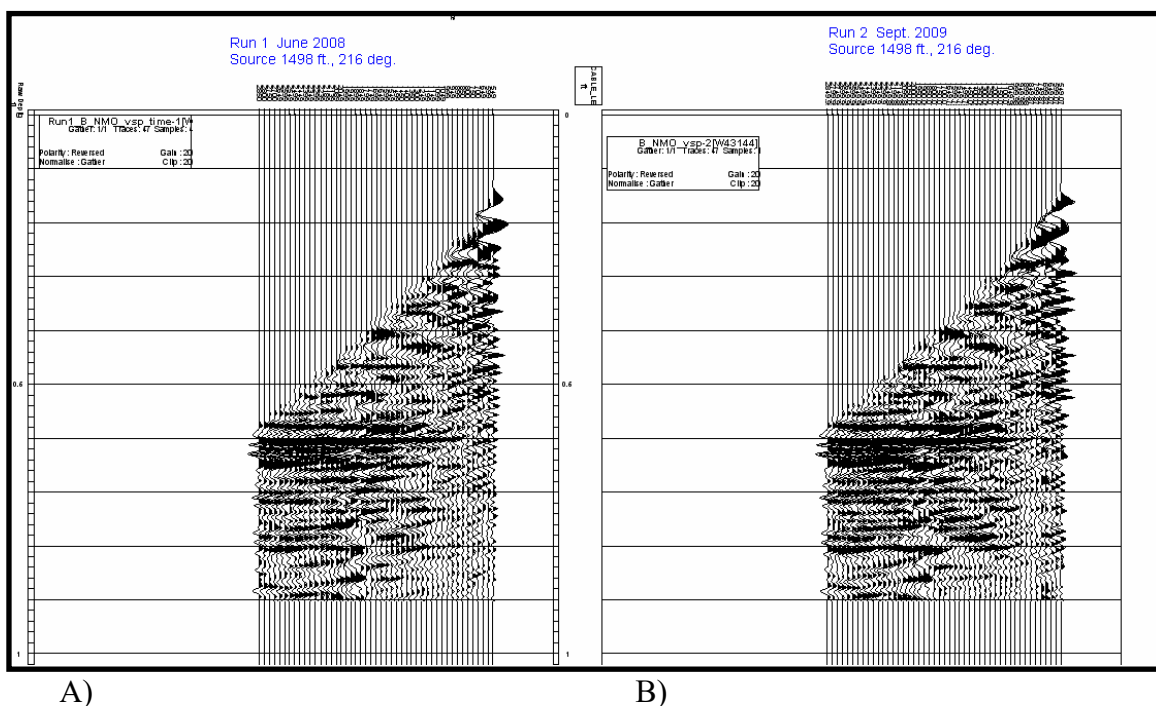


Figure 46: A) Baseline and B) Post Injection Monitor Survey

5.2.6 Conclusions

3D Seismic study: Seismic interpretation of about 9 square miles of 3D seismic data centered around the injection well reveals that the late Cretaceous Fruitland formation forms a well defined seismic sequence with high amplitude reflections marking the top and base of the sequence. Internal reflection patterns suggest considerable stratigraphic complexity in the Fruitland formation depositional systems. The lower Fruitland coal reflection events are fairly continuous across the site, whereas the middle and upper Fruitland coal events are fairly discontinuous and difficult to correlate through the surrounding area. The detailed seismic view also reveals considerable local structural complexity not generally observed in well log-derived cross-sections. The overlying Kirtland Shale is considered to represent the effective caprock for Fruitland Formation reservoirs. Variable area wiggly trace displays illustrate the stratigraphic and structural complexity of the Fruitland sequence. Isochore (travel time difference) maps of the Fruitland sequence and lower Fruitland coal intervals reveal considerable variability of thickness throughout the area. Thinning of the Fruitland sequence occurs along a NW-SE trend

through the pilot site that coincides with a high in the base of the sequence. Stratigraphic buildup and pinchout are observed in the upper Pictured Cliffs seismic sequence. We speculate that thinning of the Fruitland sequence observed along the NW-SE trend is associated with differential compaction over northwest trending shoreline sand bodies in the upper Pictured Cliffs Sandstone and that differential compaction of the Fruitland may enhance local fracture intensity along this NW-SE trend.

Post-stack processing of the 3D seismic was undertaken to help enhance seismic indicators of fracturing and faulting. The output from specific post stack processing steps is generally defined as a seismic attribute. There are a multitude of seismic attributes including instantaneous phase, instantaneous frequency, envelope, energy, etc. In this study we explored the potential use of a less common attribute consisting of the absolute value of the derivative of the seismic amplitudes. An automatic gain control (AGC) was applied to the output to help equalize attribute amplitude over short time windows. The result of this simple process suggests the presence of considerable fracturing and minor faulting within the Kirtland Shale caprock. Indicators for extensive fracturing and faulting within the Fruitland sequence are much less apparent. The Schlumberger Ant Tracking process however does delineate subtle zones of reflection discontinuity that form clusters with approximate N50-55E trend. Similar patterns of discontinuity are observed in the Kirtland and overlying Tertiary intervals (interpreted Ojo Alamo and Nacimiento seismic sequences).

3D seismic coverage is critical to the assessment of site integrity. In this study, 3D seismic analysis reveals numerous details about internal reservoir stratigraphic and structural framework that we are unable to infer from limited borehole correlations. Seismic attribute analysis can be used effectively to enhance subtle features in the seismic response that may be indicative of fracture zones and faults that could jeopardize reservoir integrity. The results of the analysis suggest that several small faults and fracture zones disrupt overlying intervals and to less extent, the reservoir interval. However, interpreted faults and fracture zones have limited vertical extent and major penetrative faults have not been observed at the site.

EM surveys and model study: Approximately 70 line-kilometers of EM data were collected across the site. Inverse models suggest the presence of a network of low permeability (low conductivity) pathways in the near-surface sandstone at the site that would facilitate atmospheric return of CO₂ should leakage occur.

Injection well logging: Fracture detection and mechanical properties logs helped us extend our understanding of residual stress and fracture distribution from the near surface down through strata overlying the Fruitland coal injection zone. Sonic Scanner observations, unlike those from the FMI log, were available through the injection zone. Drilling induced breakout orientations of N57W along the length of the borehole suggest invariant in-situ principal compressive stress direction of N33E. The average fast-shear direction obtained from Sonic Scanner measurements over the entire length of the borehole is N43E. The fast-shear direction is associated with stress induced or fracture induced stress anisotropy. The fast-shear direction refers to the shear wave vibration direction. Fracture induced intrinsic anisotropy arises through birefringence of the shear wave into a fast-shear vibration component that parallels the maximum principal compressive stress direction (or the dominant fracture trend) in strata surrounding the borehole; the slow-shear direction is orthogonal to the fast-shear direction. Stress induced anisotropy results from in-situ stress. When the fast-shear direction is evaluated over local intervals above and within the Fruitland coal section, a transition occurs from the average N43E trend to a N14E trend within the coal section. We speculate that this N14E trend observed through the coal bearing intervals may be related to fracture induced anisotropy and also imply a face cleat orientation of N14E.

A variety of open and healed fracture trends are penetrated between subsurface depths of 370 ft to 2,925 ft within the upper Fruitland formation. The distributions are marginally non-random at best. A small set of open fractures in the upper Fruitland (N=5) are significantly non-random with mean trend of N11E with 95% confidence interval of 19 degrees. The occurrence of these open fractures in the transition zone observed in the fast-shear orientations within the upper Fruitland supports speculation that open fractures and face cleats in the underlying Fruitland coal section may have more northerly trend.

VSP time-lapse survey: Baseline and post injection monitor vertical seismic profiles (VSP) were collected at zero offset and 3 non-zero offsets. The monitor survey was not acquired until September 17, 2009. Preliminary processing with Schlumberger is still in progress. Interpretation and modeling of this data will be continued at West Virginia University as part of continued collaborative efforts with NETL's MMV team lead by Art Wells.

5.3 Tiltmeters, GPS and InSar

The following section gives the results from the tiltmeters and GPS installed at the site to monitor the ground deformation.

5.3.1 Surface Deformation

CO₂ injection was terminated on August 12, 2009. Tilt measurements continued for approximately 3 months after cessation of injection.

The cumulative surface deformation map generated from the tiltmeters' data for the period of August 01, 2008 to November 17, 2008 is presented in **Figure 47**.

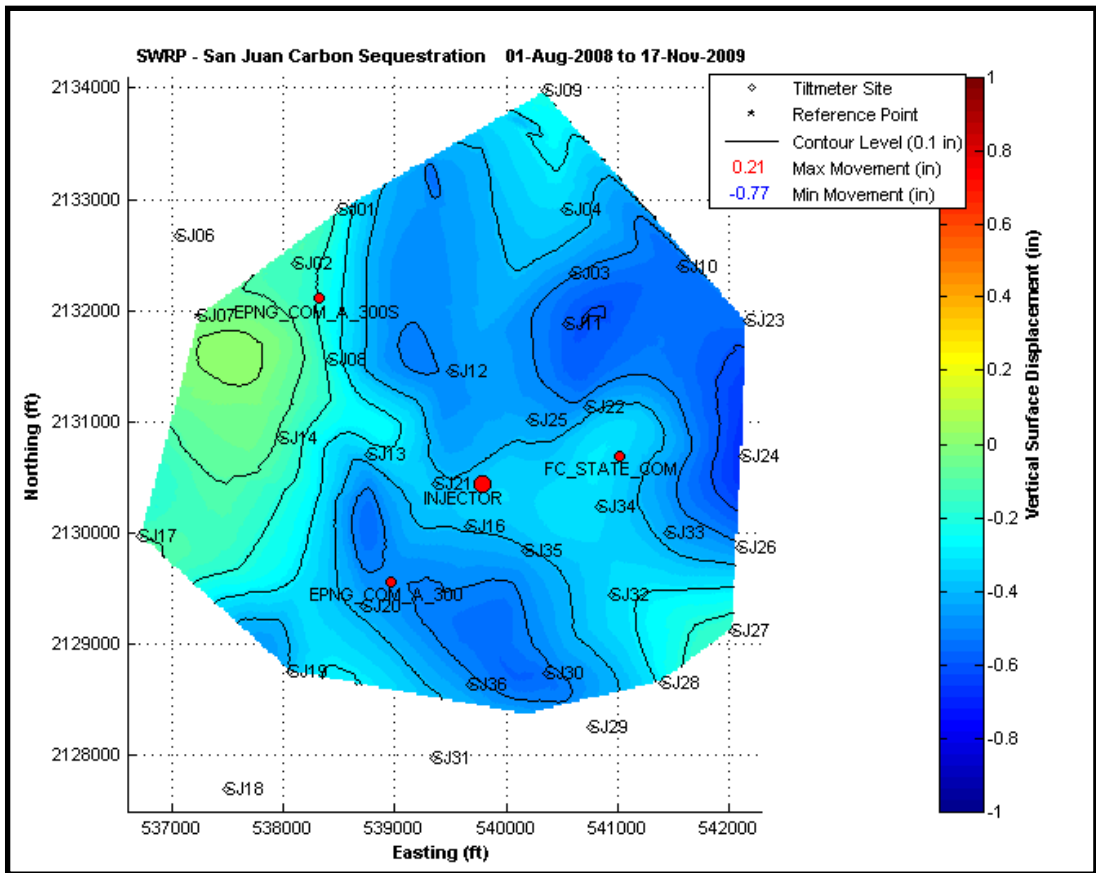


Figure 47: Cumulative Surface Deformation for August 01, 2008 to November 17, 2009

From the cumulative surface deformation it is seen that there is an overall subsidence in the field. The subsidence is spread out primarily around the periphery of the tiltmeter array. There is some minimal uplift to the immediate SW of well EPNG Com A 300S but that could be due to the reference tiltmeter(s) (SJ06/SJ07) being located in that region. (Note: All surface deformation is computed with reference to a tiltmeter site, which is assumed to be at constant elevation. For this project, sites 06 and 07 were chosen as the primary and secondary reference sites).

In addition to the production from the three wells producing from the Fruitland coal in Section 32, there are numerous wells producing from the periphery of Section 32 (**Figure 48**).

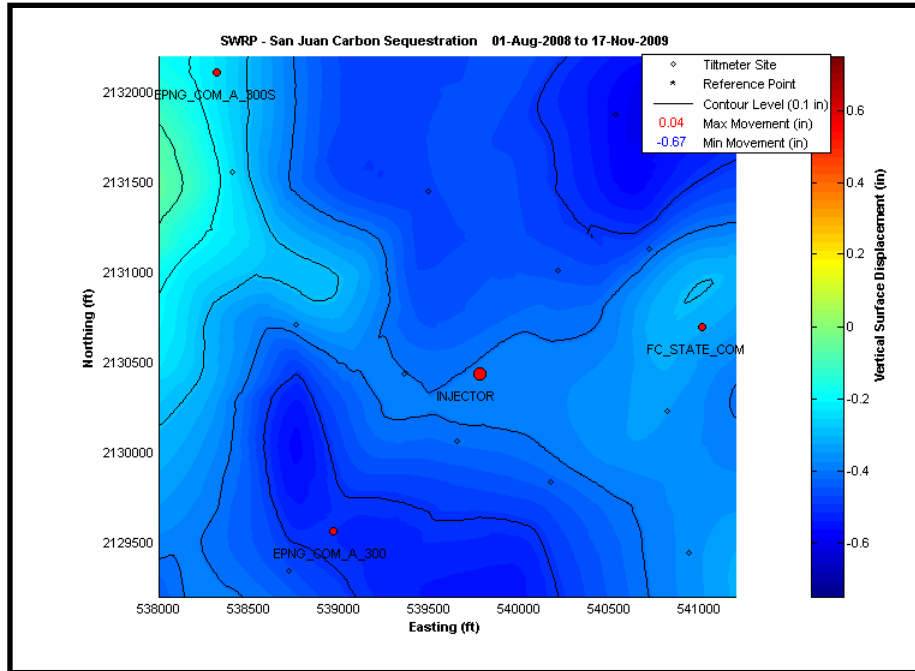


Figure 49: Cumulative Surface Deformation for Period August 01, 2008 to November 17, 2009 on a Smaller Deformation Scale

Injection and production rate information are presented in **Figures 50 and 51** below.

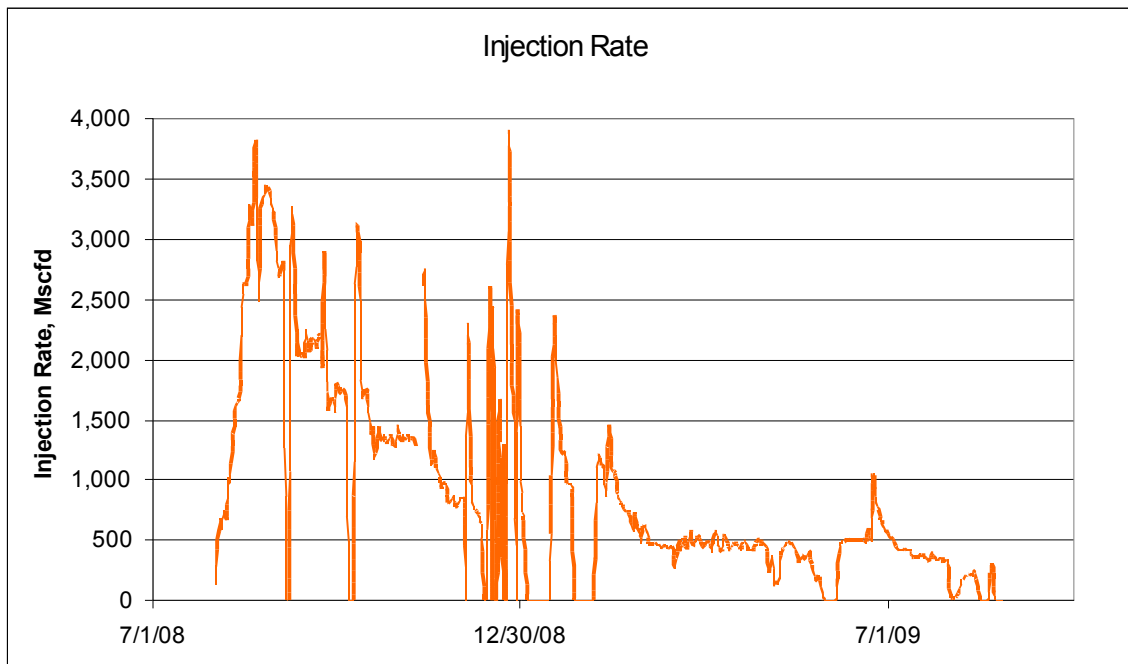


Figure 50: Injection Rate

From **Figure 50** above it is clear that the injection rate of CO₂ has not been continuous. Initially, the target rate of 3,800 Mscf/day was reached, however it was unsustainable for any length of time. Apart from the occasional instantaneous spikes at restart, following a period of shut-in, the average instantaneous injection rate has been around 1,000 Mscf/day, with additional periods of shut-in. Injection was terminated on August 12, 2009.

The production rate from the three producers surrounding the injector has been fairly constant (**Figure 51**). Although initially there was fluctuation in the production rate, since March 01, 2009 the production rate has been constant. Individual wells may have exhibited rate fluctuation but the sum of the three remained fairly constant.

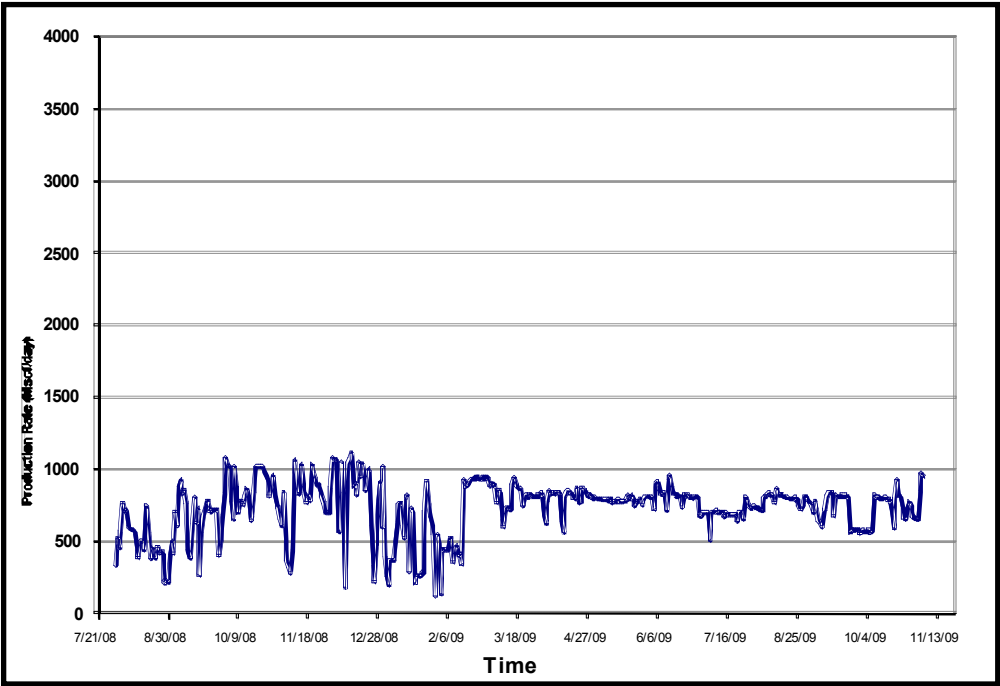


Figure 51: Production Rate from the Three Producers, EPNG Com A 300, 300S and FC State Com 1, Surrounding the Injector Well

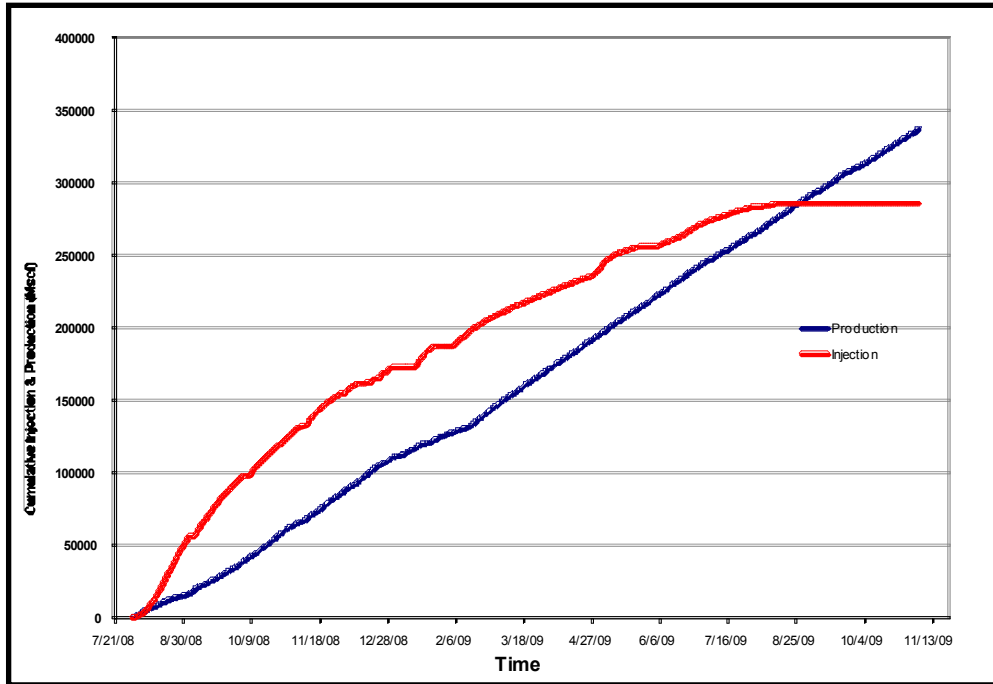


Figure 52: Comparison of Cumulative Injected and Produced Volumes (Standard Volume) from Section 32 Including 3 COP Producers, EPNG Com A 300, 300S and FC State Com 1

A comparison of the cumulative injected and produced volumes is presented in **Figure 52**, above. Although the cumulative injected volume was initially larger than the produced volume, the injection tapered off significantly and the cumulative volumes were almost equal at time of injection cessation (i.e. August 12, 2009). The actual production from Section 32 and surrounding wells should include production from the first ring of producers surrounding the three producers in Section 32. These wells are Howell A 300, Moore B3, Howell 301S, Kernaghan BS, Kernaghan B8S, Kernaghan SA, Howell D350S, Howell D351, Howell D352, Howell D352S and Florence H3. However, the only production information available is from the Howell wells. **Figure 53** is generated using production figures from the three Section 32 producers and the Howell wells.

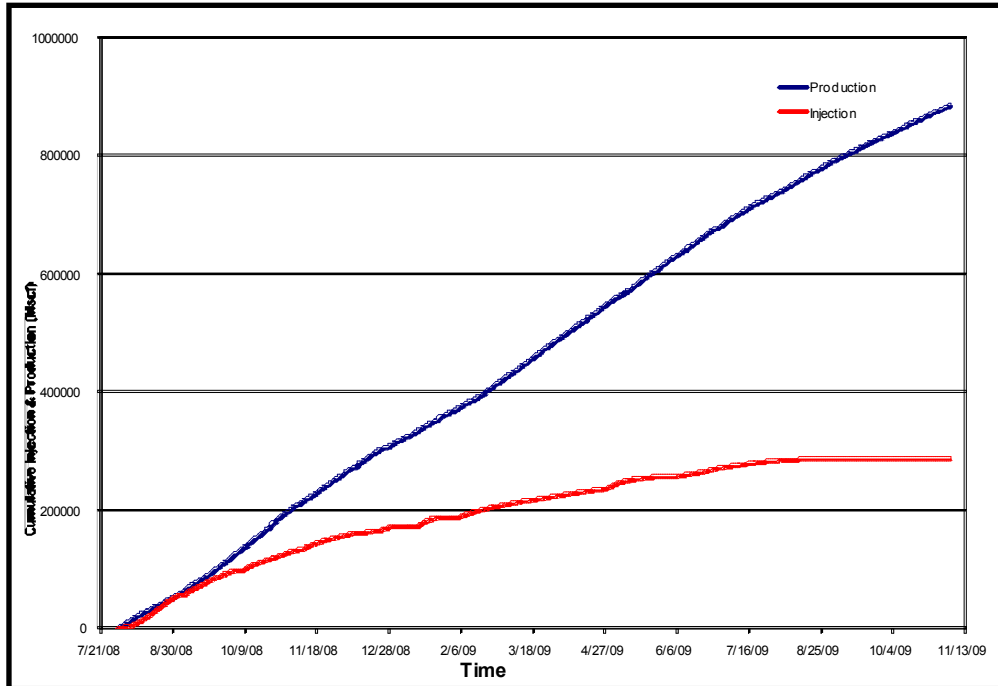


Figure 53: Comparison of Cumulative Injected and Produced Volumes (Standard Volume) from Section 32 COP Producers and the Howell Wells Immediately Surrounding Section 32

From **Figure 53** it is evident that the cumulative produced volumes (not accounting for all relevant production) is three times that of the cumulative injection.

From the injection behavior we can identify three periods of change in injection rate behavior:

1. pre-March 01, 2009 when average injection rate was larger
2. post-March 01, 2009 when average injection rate was lower
3. post August 12, 2009 when injection rate was zero. Surface deformation images for these three periods are presented in **Figures 54 to 56**.

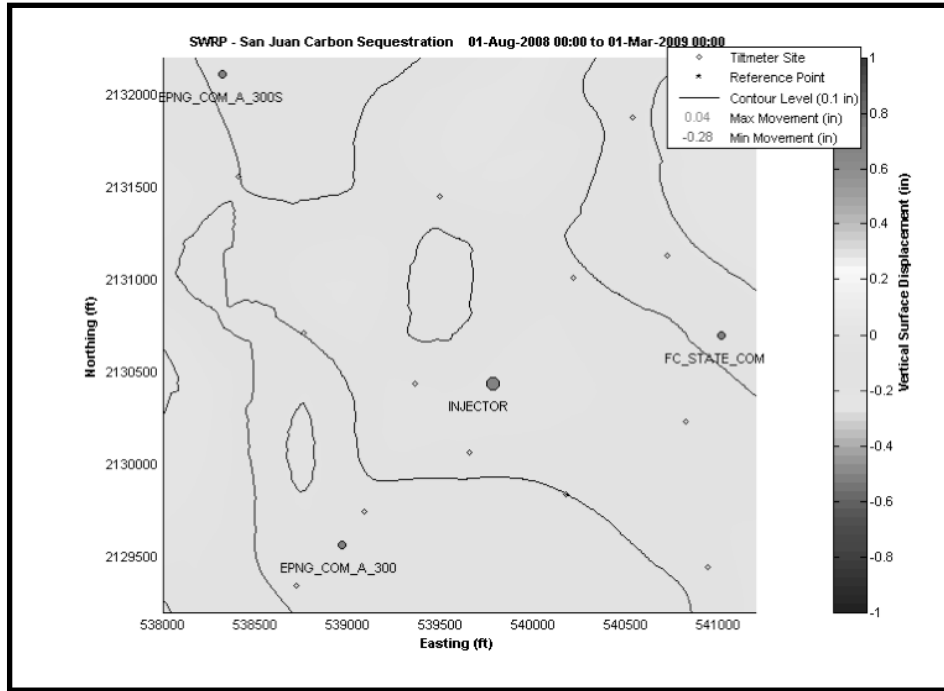


Figure 54: Cumulative Surface Deformation for Period August 01, 2008 to March 01, 2009

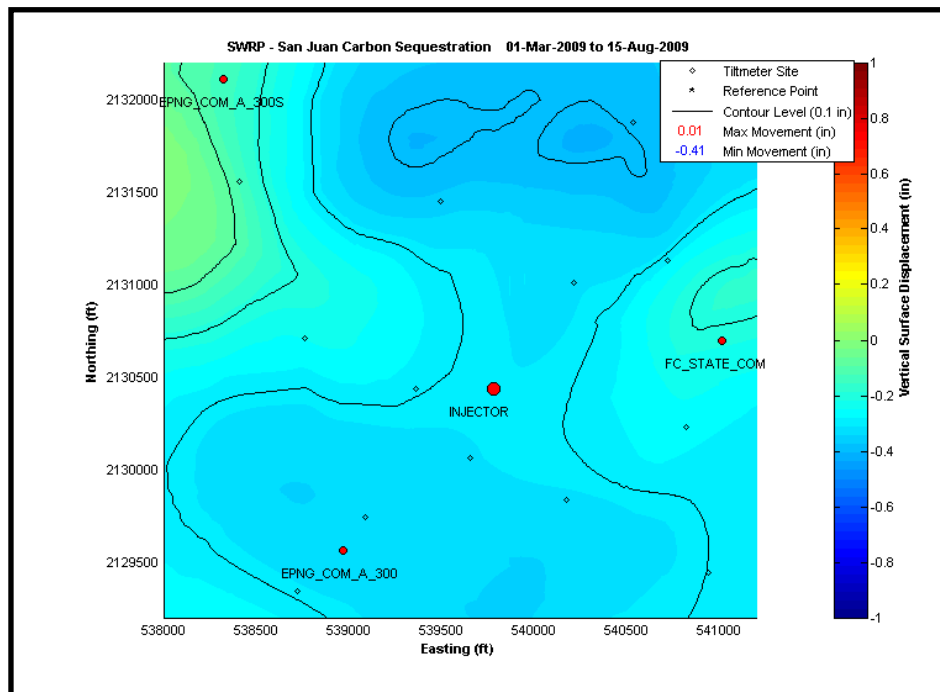


Figure 55: Cumulative Surface Deformation for Period March 01, 2009 to August 15, 2009

Figures 54 and 55 show that prior to March 01, 2009 there is minimal uplift near the injector and at the northern section of the array. The magnitude of the uplift is extremely small (0.04 inch) and within the uncertainty of the computed surface elevation. Post-March 01, 2009, there is predominantly subsidence over the whole array. The slight uplift at the western edge in both images can be discounted as it is due to the reference site being to the immediate west of that region. The deformation image post injection is shown in Figure 56, (i.e. from August 15, 2009 to November 17, 2009).

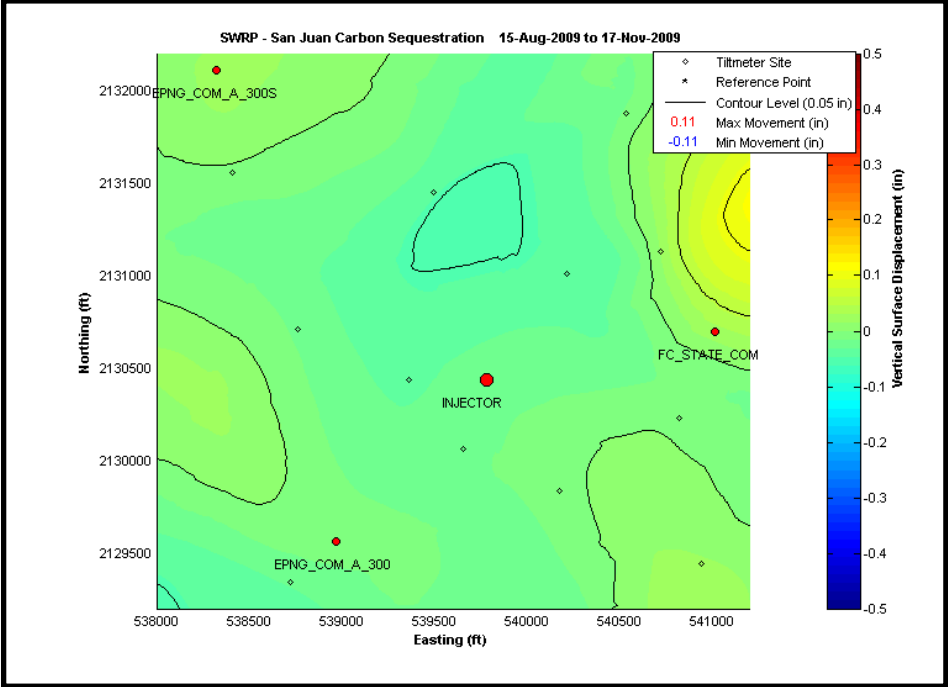


Figure 56: Cumulative Surface Deformation for Period August 15, 2009 to November 17, 2009

In Figure 56 above, note that there is some uplift post-injection primarily concentrated near the periphery of the array. The reason for this uplift is not clear at this time. However, on analyzing the post injection tiltmeter data it is seen that subsidence continued up to approximately October 01, 2009 (Figure 57). The bulk of the uplift seen in the above image (Figure 56) occurred between October 01, 2009 and November 17, 2009.

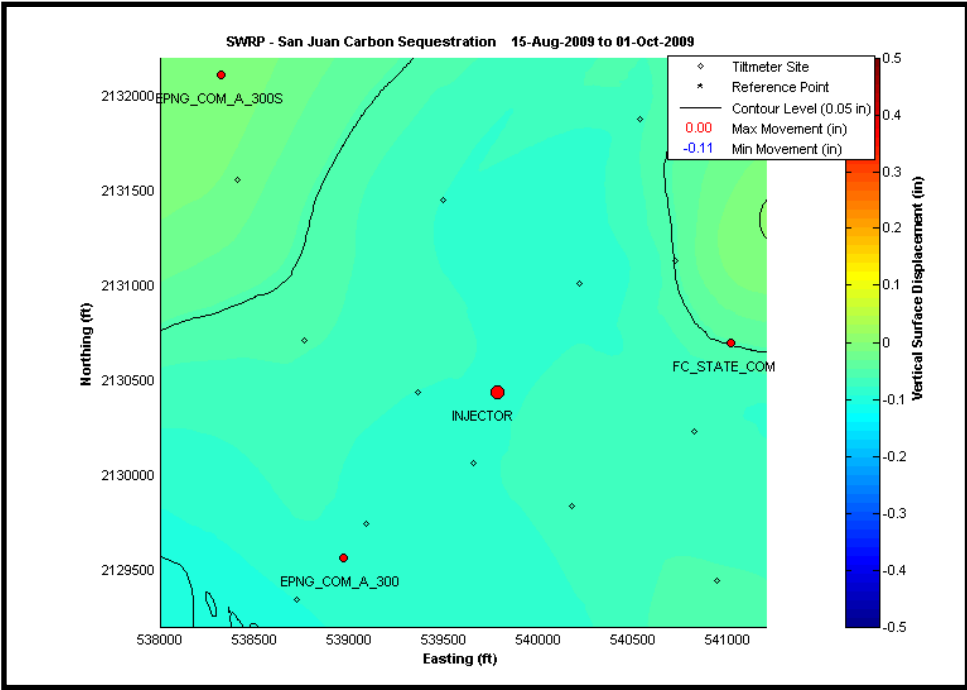


Figure 57: Cumulative Surface Deformation for Period August 15, 2009 to October 01, 2009. Period for Approximately 1.5 Months Post-Injection

5.3.2 GPS Elevation Profile

A differential GPS system was also set-up and consisted of one remote and one base station. The base station was located at the far NW section of the tiltmeter array (**Figure 5**), and the remote station is located approximately 400 ft to the west of the injector (**Figure 58**).

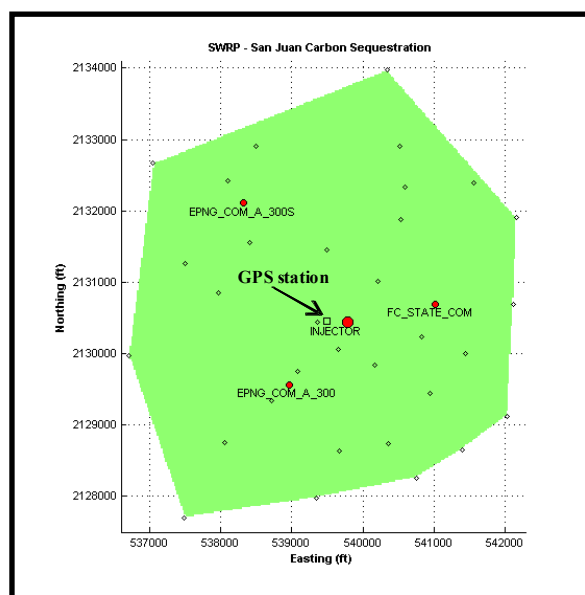


Figure 58: Array and Well Layout Showing the Location of the Remote GPS Station

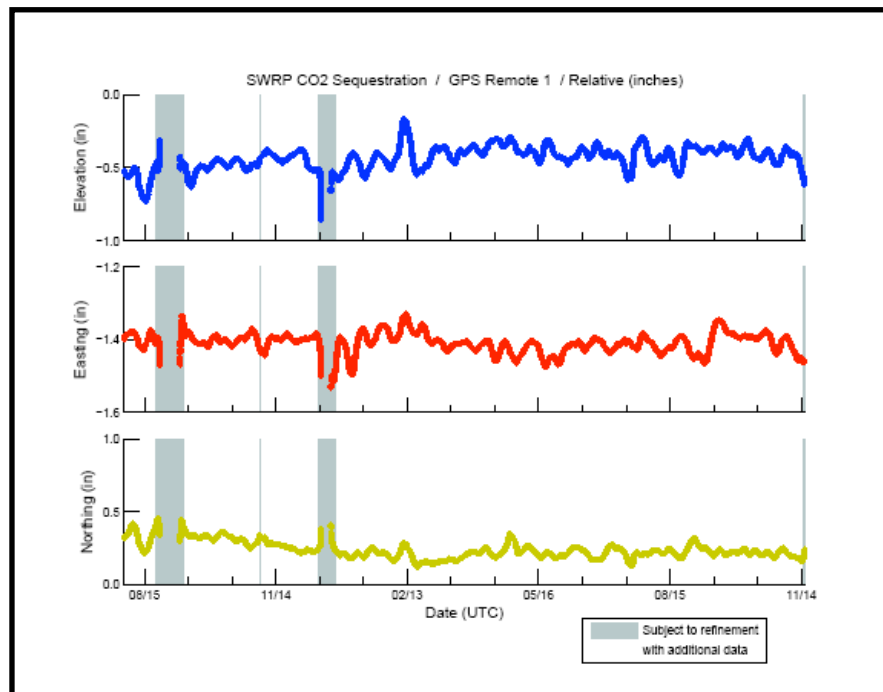


Figure 59: GPS elevation Profile for Period from August 01, 2008 through November 17, 2009. Data Processed Using a 240 hr Filter, Both Pre and Post Data Point

The GPS elevation profile from August 01, 2008 to November 17, 2009 (**Figure 59**) shows that there is no significant cumulative elevation change during this period. There are minor fluctuations inherent with any “natural” data. There was also a period of some unusual uplift during the February 10-13 time frame, but that uplift was recovered subsequently. The

lack of cumulative elevation change in the GPS elevation profile serves as independent verification of the overall surface deformation behavior, (i.e. lack of significant elevation change) seen in the surface tilt.

The GPS system was installed in early June 2008. The initial two months of data were discarded due to initial settling, and lack of reliable data. Sufficient data is required both prior to, and after, the relevant data point being processed for reliable elevation computation. For this project a 240-hr (10-day) filter interval (both pre and post data point) was chosen to obtain elevation data. Initial data is shown in **Figure 60**.

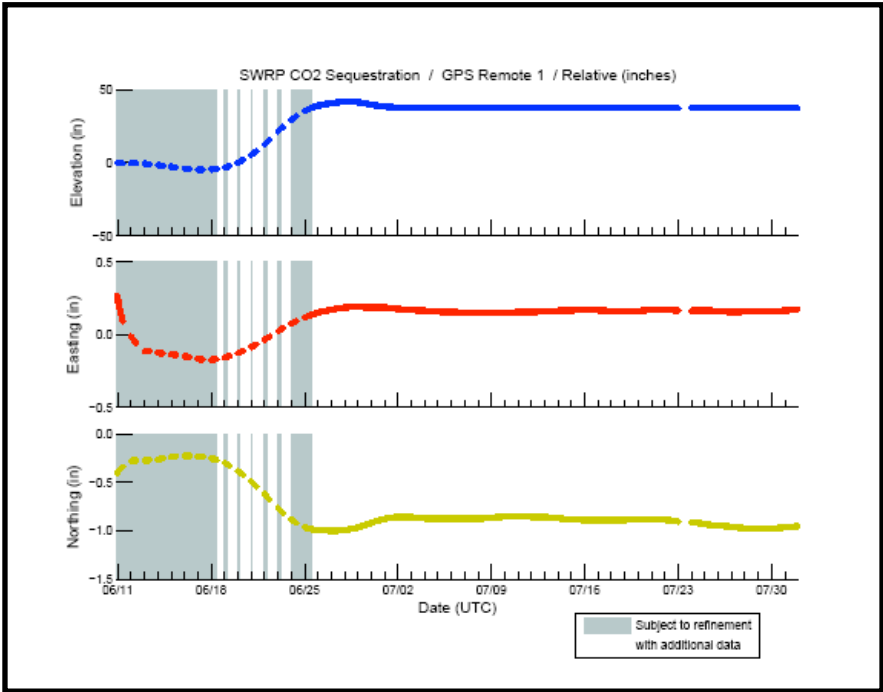


Figure 60: GPS Elevation Profile from Early June 2008 to July 31, 2008. Data Discarded Due to Initial Settling and Insufficient Data.

5.3.3 Reservoir Strain Computation

The surface tilt measurements were also used to compute volumetric strain at the reservoir level. The “reservoir” is divided into blocks of 200 ft x 200 feet with a thickness of 60 feet and a depth to center of 3,000 feet. Surface tilt measurements for a certain time period (i.e.

extracted tilt) are then used to invert for the strain at reservoir depth (Segal, Du). Regularization parameters such as a smoothness constraint and/or a volumetric constraint need to be chosen for the inversion. For the chosen time periods, the tilt signals need to be coherent (i.e. the tilt vectors should form a recognizable pattern suggestive of reservoir level strain). For this project, we were unable to identify any periods of significant tilt-coherence due to the small magnitudes. Nevertheless two representative periods, one pre-March 01, 2009 and the other post-March 01, 2009, were chosen for demonstration.

For both of these periods a 28-day time interval, the first one from January 06, 2009 to February 03, 2009 and the second one from August 25, 2009 to September 22, 2009, were selected. The inversion using pre-March data was performed using only a smoothness constraint. There was no volumetric constraint, (i.e. the strain was free to be positive or negative). The results for this inversion are presented in **Figure 61**.

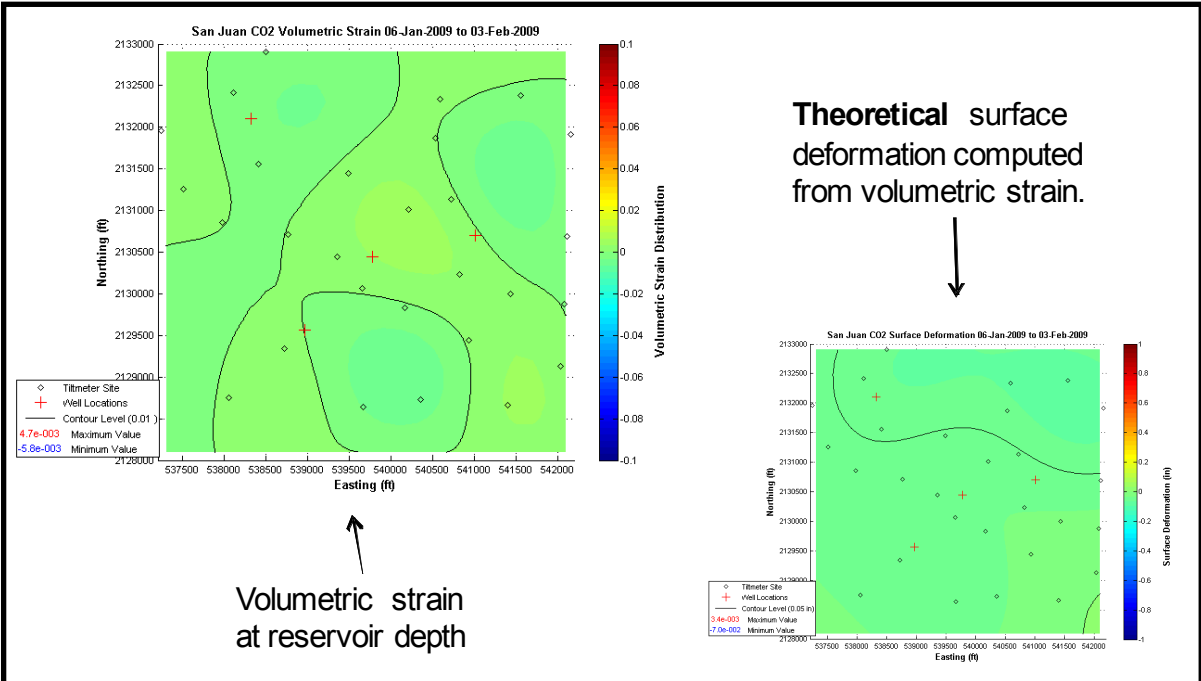


Figure 61: Reservoir Strain Computation Results for Period January 06, 2009 to February 03, 2009 Performed Using Volumetrically Unconstrained Inversion. Volumetric Strain at Reservoir Depth (Dimensionless) is shown in the Image at the Left while Theoretical Deformation at Surface (Inches) is shown in the Image to the Right.

In the inversion results (**Figure 61**), both the volumetric strain at reservoir depth, and the theoretical surface deformation computed from the reservoir strain, are presented. The surface deformation shown here is not computed by direct integration of surface tilt as shown in the previous figures but is computed from the calculated reservoir strain using the forward model of the inversion (Segal, Du). It is seen that the surface deformation computed from the forward model shows reasonable similarity to the surface computed by direct integration of surface tilt. In **Figure 61**, the image of volumetric strain at reservoir depth (left side) indicates that there is some positive strain located just north of the injector; however, the magnitudes are extremely small and lie within uncertainty limits of computed strain.

Inversion to compute volumetric strain was also performed for the second time-period chosen (August 25, 2009 to September 22, 2009). As this period was post-injection, it was not expected that there would be any positive strain (expansion) at reservoir depth. Therefore, in addition to a smoothness constraint, a volumetric constraint (negative constraint) was also chosen. Thus, the strain was free to be only zero or negative (contraction). The results for this inversion are presented in **Figure 62**.

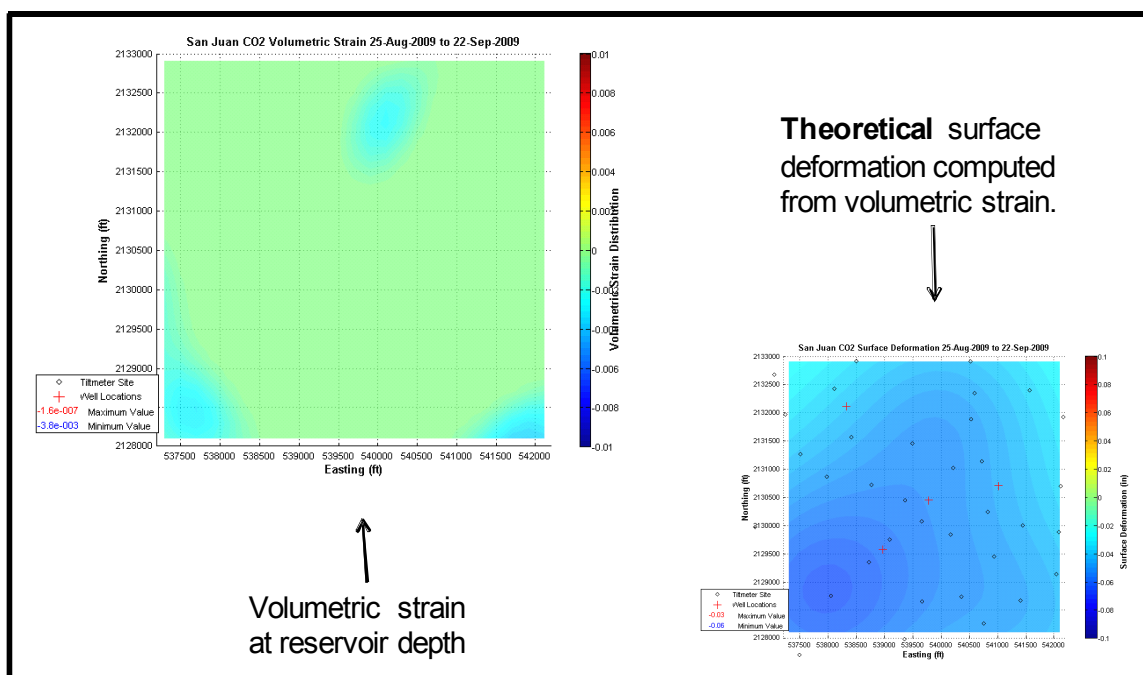


Figure 62: Reservoir Strain Computation Results from August 25, 2009 to September 22, 2009 Performed using Volumetrically Negatively Constrained Inversion. Volumetric Strain at Reservoir Depth (Dimensionless) is shown in the Image at the Left While Theoretical Deformation at Surface (Inches) is shown in the Image to the Right.

In the inversion results (**Figure 62**), we see that the bulk of the volumetric strain is zero with some negative strain located some distance to the north of the injector. The strain at the SW and SE edges is on the periphery and could be due to edge effects. The theoretical surface deformation (image on the right) computed from the reservoir strain bears good resemblance to that obtained by direct integration of surface tilt.

The above two cases demonstrate the possibility of using surface tilt measurements with appropriate regularization parameters (smoothness/volumetric/compactness constraints) to obtain volumetric strain at reservoir depth.

5.3.4 Conclusions

There has not been any significant cumulative surface uplift due to CO₂ injection observed. This behavior has been independently verified by the lack of cumulative elevation change in the GPS elevation profile computed at a point 400 feet to the west of injector. The

possible reason for this could be insufficient CO₂ injection into the formation. At cessation of injection on August 12, 2009, and accounting for production from only the three producers in section 32 Fruitland coal there was a 1:1 injection/production ratio (i.e. equal injected and produced volumes). In addition to this production there was also production from the Mesaverde formation at 5,500 ft depth in Section 32 and significant production from a ring of wells surrounding Section 32. Accounting for production from approximately half of these surrounding wells, there is a production/injection mismatch of approximately three times support the resultant overall surface deformation behavior computed from surface tilt measurements to have been subsidence.

5.4 Soil Gas and Tracers

The following section is describing the results from the injected tracers and soil gas analysis to monitor the CO₂ migration.

As discussed in Section 3.8, there were a total of 46 soil gas monitoring stations and 36 tracer monitoring stations. Samplings for these parameters began in September 2008. The breakthrough of tracer at the east and southwest off set wells is shown to occur in mid-December, 2008 and June 2009 (**Figures 63 and 64**) from the results of PFC tracer monitors placed directly in front of vents that are releasing a split stream of produced gas from these wells. CO₂ measurements to date have given no indication of breakthrough, but the conservative tracer breakthrough seems likely to precede CO₂ breakthrough. It is important to note that the breakthrough of tracer occurs at the same locations where the increase in nitrogen has been noticed and at equivalent timings (November 2008 for the FC State Com 1 east well and February 2009 for the EPNG Com A 300 southwest well).

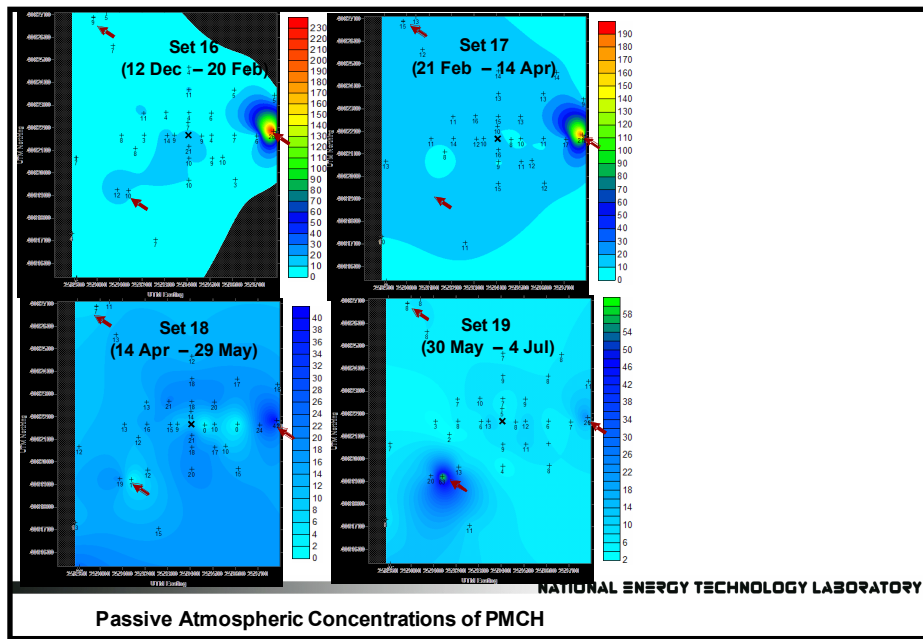


Figure 63: Breakthrough of Tracers at the Offset Well Split Stream Gas Vents

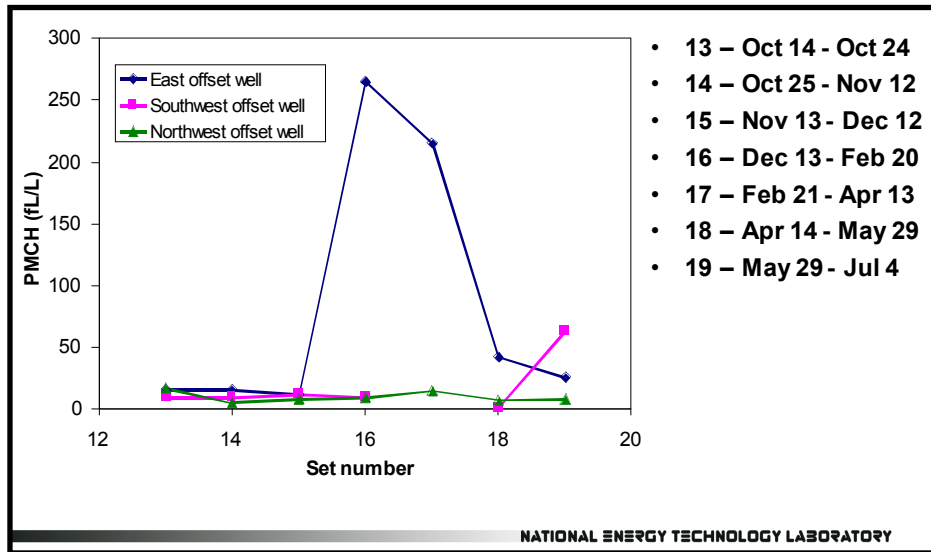


Figure 64: PMCH Tracer Signal from the Offset Wells – San Juan Basin Site

Soil-gas tracer depth profiles are shown in **Figures 65 to 67** for Sites 36 and 51. These two locations were the only sites to show amounts of PFC tracers beyond background levels and are located near the injection well and to the south and west of the injection well. There is a current effort underway by Carnegie Mellon University, in collaboration with NETL, to apply a Bayesian Belief Network Analysis to all near-surface results at the San Juan Basin to determine the statistical significance of the results and the techniques employed. Prior to the completion of

this analysis, the general rule-of-thumb is that significant leakage should be suspected from PFC tracer levels more than 2 orders of magnitude beyond background level. The results shown in **Figures 65 to 67** are below this level, but are none-the-less consistent between sets and between tracers.

Evidence that the minute levels of tracer detection for sets 18 and 19 might be coming from depth rather than an atmospheric tracer plume reaching the monitors via barometric pumping into the soil include:

1. the generally increasing or level tracer concentrations with depth at site 36 (**Figures 65 and 66**)
2. the lack of any evidence of an atmospheric tracer plume release after tracer injection (**Figure 68**)
3. geophysical measurements (conductivity and lineament analysis) indicating that areas to the south and west of the injection well show at least the potential for near surface expression of migration pathways (**Figure 69**). Site 36 also shows a hydrocarbon anomaly (**Figure 16**).

It is also interesting to note that Set 18 (14 April – 29 May, 2009) reveals an increase in soil-gas tracer above that of Set 17 at both soil-gas arrays and for all tracers. There is also an indication of tracers arriving at sites to the south and to the west of the injection well in Set 18, 1 meter passive grid (**Figure 70**, bottom left graphic.) There is no known activity at the injection well that would correlate to the time frame of Set 18.

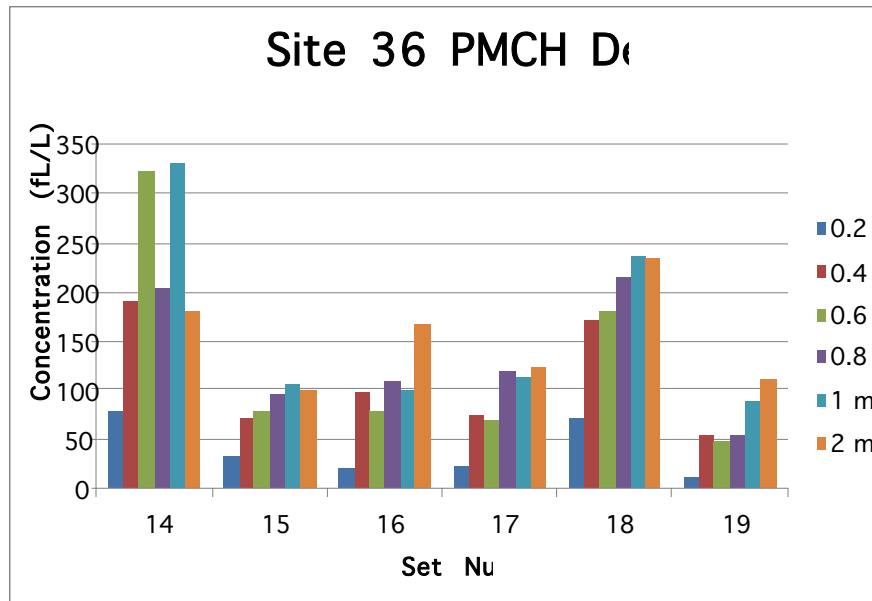


Figure 65: PMCH Soil-Gas Depth Profile at Site 36, San Juan Basin Site

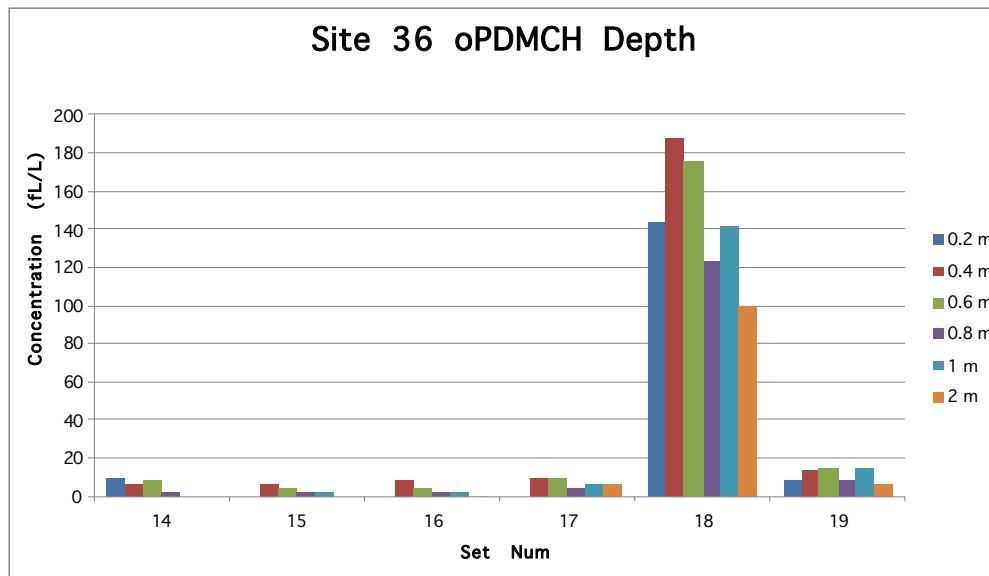


Figure 66: PDCH Soil-Gas Depth Profile at Site 36, San Juan Basin Site

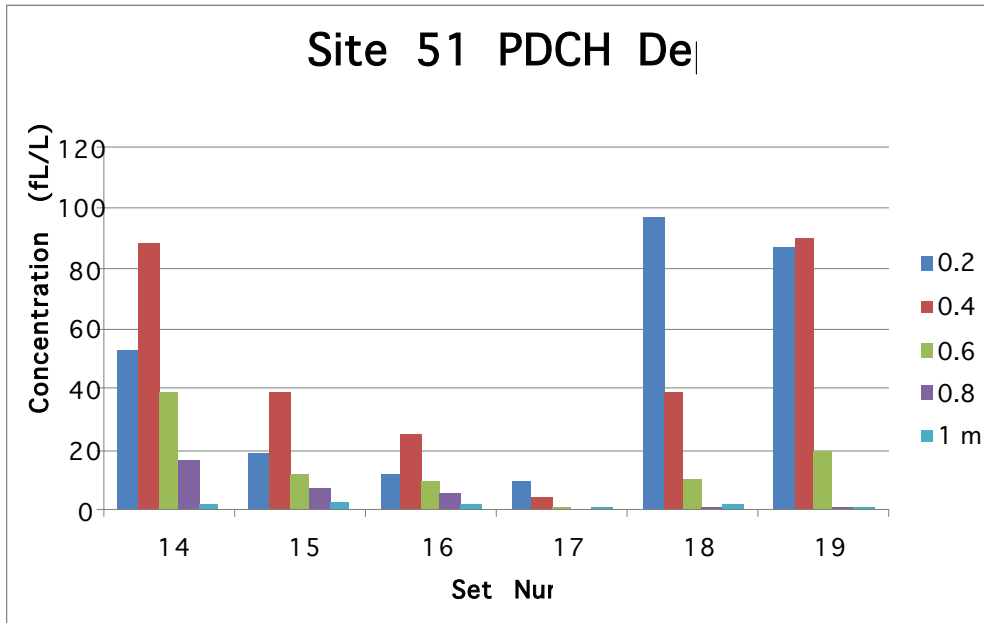


Figure 67: PDCH Soil-Gas Depth Profile at Site 51, San Juan Basin Site

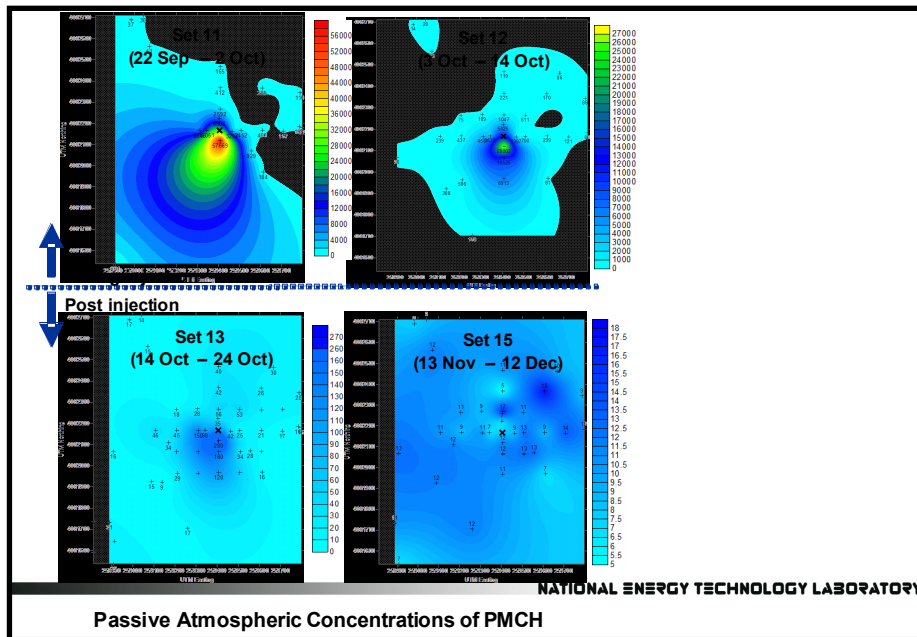


Figure 68: Atmospheric Tracer Plumes Monitored at the San Juan Basin Site

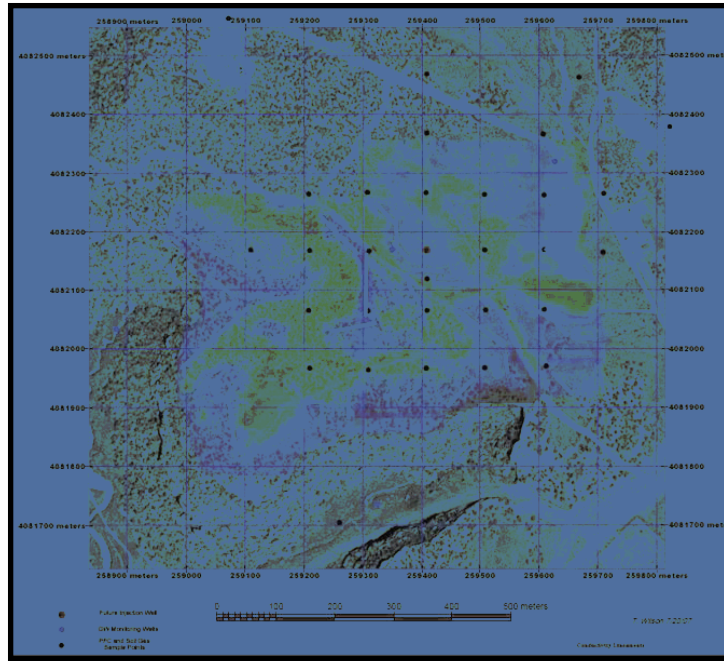


Figure 69: Conductivity Survey and Lineament Evaluation at the San Juan Basin Site

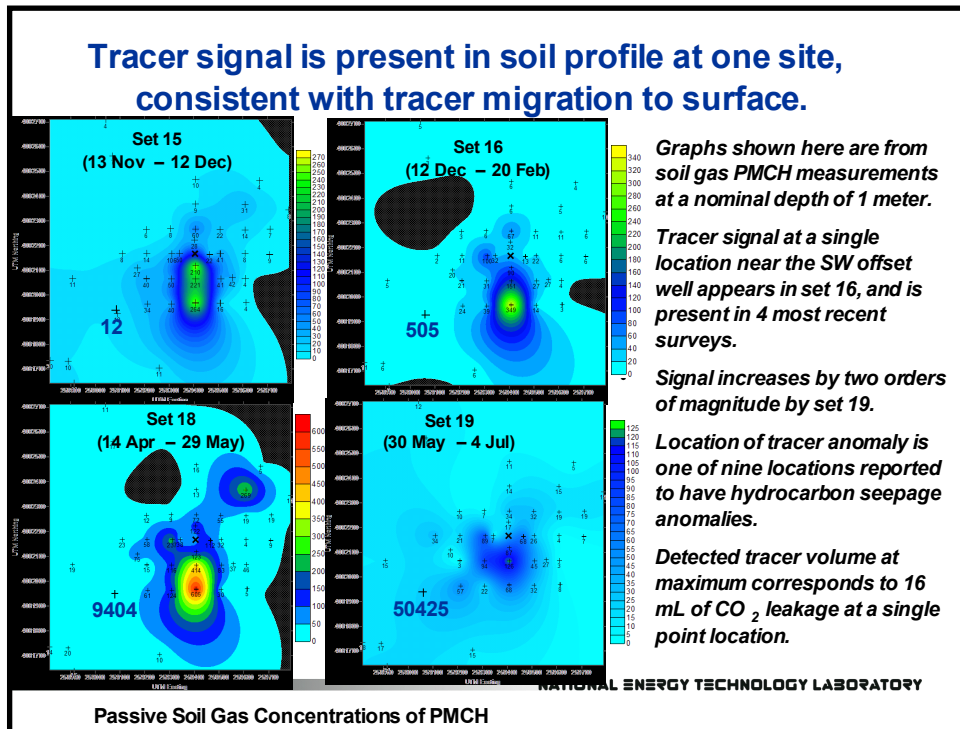


Figure 70: PMCH Tracer in Soil-Gas at the San Juan Basin Site

Any potential detection indicated from the results shown here would be exceedingly small. Post injection CO₂, isotope, and hydrocarbon measurements at site 36 did not indicate any significant changes from the pre-injection baseline surveys. Modeling for subsurface and near surface migration pathways for injected CO₂/tracer will be conducted in the upcoming year and should aid in evaluating the near surface data collected at the San Juan Basin Site.

Near surface monitoring at the San Juan Basin Site is expected to continue for at least one year following the completion of CO₂ injection.

5.5 *Water Analysis*

The following section is describing the results from the analysis of the produced water samples collected at nine producing wells at the site. The water sampling started on August 8, 2007.

5.5.1 Analysis Methods and Produced Water Chemistry

5.5.1.1 Ion Concentration

The ion concentration of the produced water was analyzed by ion chromatography (Dionex DX-120). The Six-Cation-II and Five anion standard solutions were used for preparation of the calibration curve. The produced water samples were filtrated with a 0.22 μm filter to remove large particulates and suspensions before ion analysis. All produced water samples were diluted to desirable concentrations (~50 mg/L Na⁺) for ion analysis.

5.5.1.2 Trace Metal Ion Analysis

The trace metals of the produced water were characterized with inductively coupled plasma-mass spectrometry (ICP, ELAN). Water samples were diluted to the desired concentration and introduced into the central channel of the spectrophotometer. As a droplet of nebulized sample enters the central channel of the ICP, it evaporates and any solids that were

dissolved in the liquid will vaporize and then break down into atoms. At the temperatures prevailing in the plasma, a significant proportion of the atoms of many chemical elements are ionized and then detected by the spectrophotometer.

Ion species that were monitored in the produced water include: August, Al, Ba, Be, Cd, Cr, Cu, Fe, Mn, Mo, Ni, Ni, C, Sb, Se, SiO₂, Sn, Sr, Th, Tl, V.

5.5.1.3 Carbon Isotope Analysis

In a natural geological system, an isotopic equilibrium is established between gas, water and formation rock. As CO₂ is injected into a coalbed formation, the original equilibrium is broken because the injected CO₂ has a carbon isotopic composition ($\delta^{13}\text{C}$) different from that of formation water. Measuring $\delta^{13}\text{C}_{\text{CO}_2}$ values in produced water and tracking the isotope change gives an important indication of the front line of CO₂ movement during geological sequestration. In addition, a chemical reaction between the injected fluid and formation water or precipitation may result in changes in the carbon isotope, so isotope analysis will give indications of CO₂ movement and its kinetic reaction with formation water as well as with rocks.

5.5.1.4 Dissolved Organics

During CO₂ injection, dissolution of CO₂ into the formation water reduces its pH dramatically. As a result, the dissolved organics in produced water from the formation will decline correspondingly, due to the diminished solubility of low molecular hydrocarbon at lower pH. Therefore, the organic composition can be tracked throughout the CO₂ injection process. A Shimadzu TOC-5000A analyzer was used to measure the dissolved organic composition of produced water samples. The analysis was carried out by using combustion at 680°C. The accuracy of measured values for TOC was estimated at around 5%.

5.5.2 Results and Discussion

The water samples were collected from wells closest to the injection well. Specifically, the water composition from well EPNG Com A 300 is closely monitored for detection of potential early breakthrough along the cleat orientation. The purpose of the water chemistry analysis is to identify potential early CO₂ breakthrough and to adjust the original injection plan, including sealing off the basal coal formation and reducing injection pressure.

5.5.2.1 Baseline Measurement of Chemical Composition of Produced Water

The chemical composition of the produced water, including ion species and concentration, total organic carbon, and trace metal ions, was analyzed for a baseline measurement.

The chemistry of formation water from the nearby producing well was studied by ion chromatography (IC). The results are summarized in **Table 4**.

Table 4: Summary of the Composition of Formation Water from the Nearby Offset Wells

Elements	Ion Concentration, mg/L						
	COM #1	Howell A 301S	Howell A #300	Howell D350S	Howell D #351	Howell G300	EPNG A #300S
CO ₃ ²⁻	475.1	312.5	175.9	348.3	150.3	393.7	508.5
HCO ₃ ⁻	8112.9	6956.6	5870.3	7215	7309.5	8155	10534.2
Cl ⁻	2520.9	3104.9	2389.5	2919.7	3092.3	3211.6	2837.7
F ⁻	33.2	16.4	28.8	19.6	39.0	18.9	22.9
Na ⁺	5164.0	5148.5	4169.3	5235.8	4774.1	5727.8	5784
K ⁺	22.1	18.0	35.0	20.0	55.5	28.0	25
Mg ²⁺	21.2	23.0	19.0	19.0	22.0	23.0	19
Ca ²⁺	14.0	7.3	11.0	9.8	9.1	17.0	7.4
TDS	16363.5	15587.3	12698.8	15787.2	15451.9	17575.0	19738.7

5.5.2.2 Water Chemistry after Injection

The water chemistry of CBM produced waters from nearby offset wells was analyzed. **Figures 71 to 79** give the ion concentration of produced water obtained from the offset wells over a period of two years. Ion species were also monitored during the whole CO₂ injection process. It was observed that the ion concentration varied over the production period. Several spikes of ion concentration in produced water were found to be influenced by the presence of H₂S. Presence of acid gas (i.e. H₂S) in produced water interferes drastically with the detection of CO₂ movement; this mechanism needs to be further investigated.

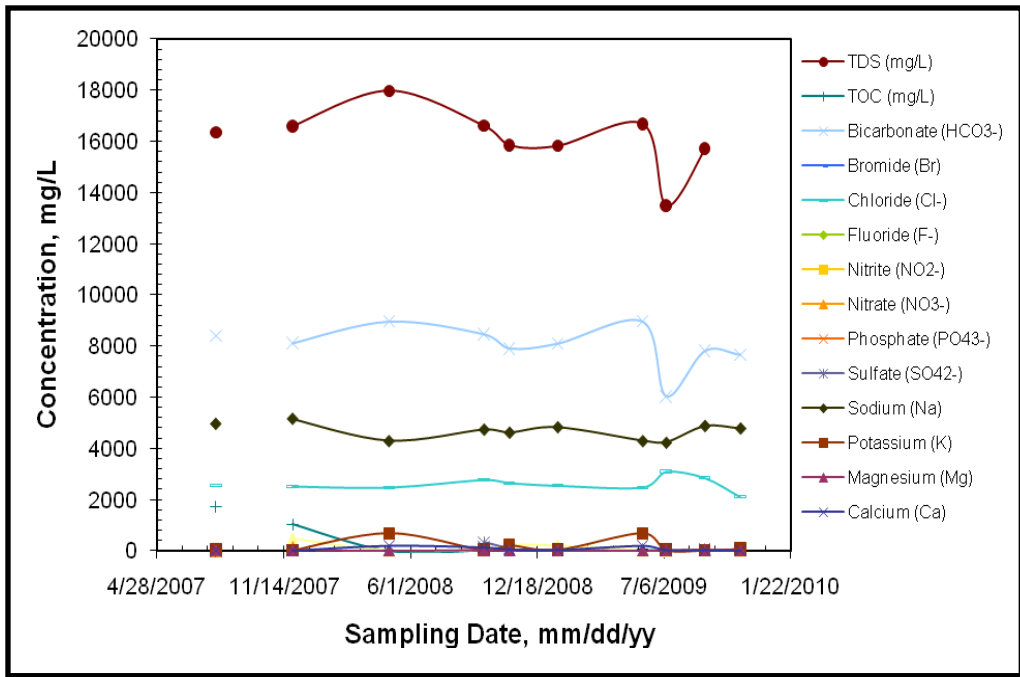


Figure 71: Water Chemistry of Well FC State COM #1

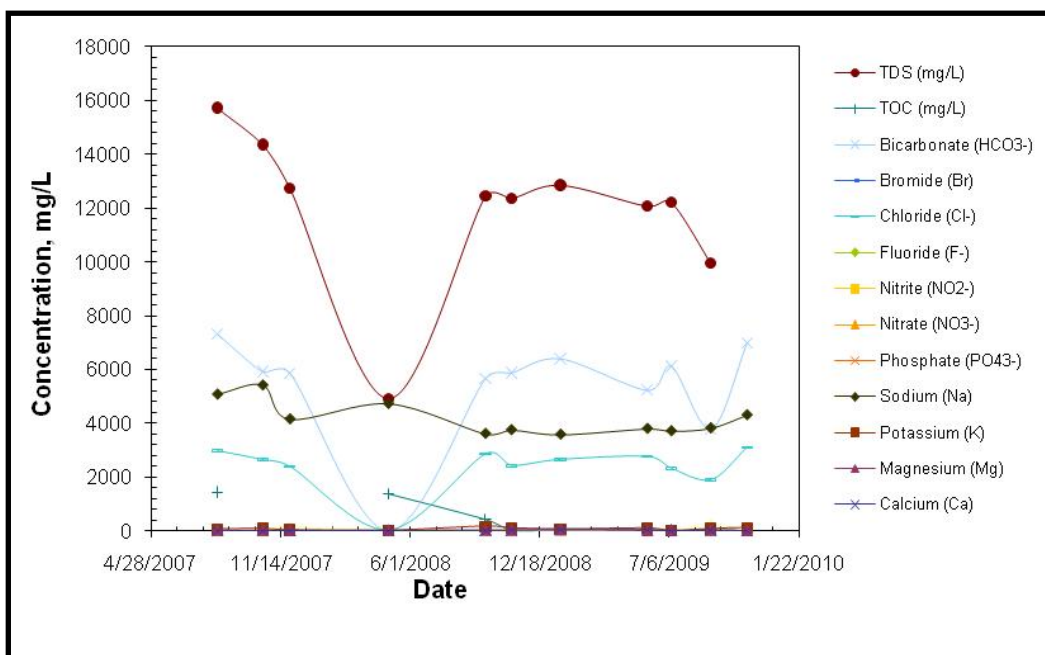


Figure 72: Water Chemistry of Well Howell A #300

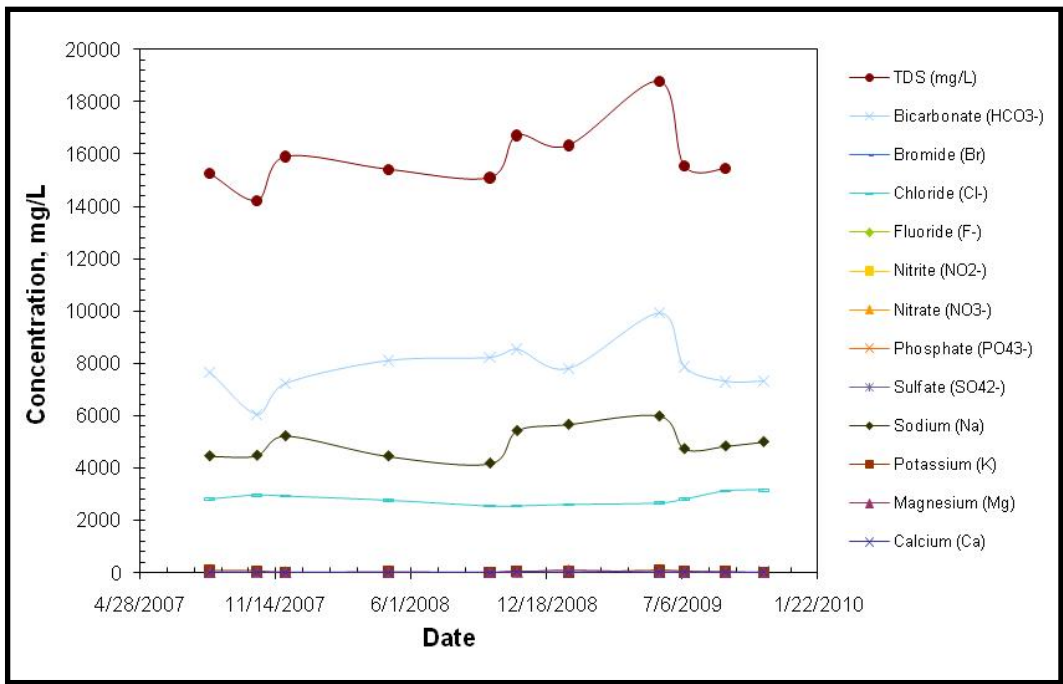


Figure 73: Water Chemistry of Well Howell D350S

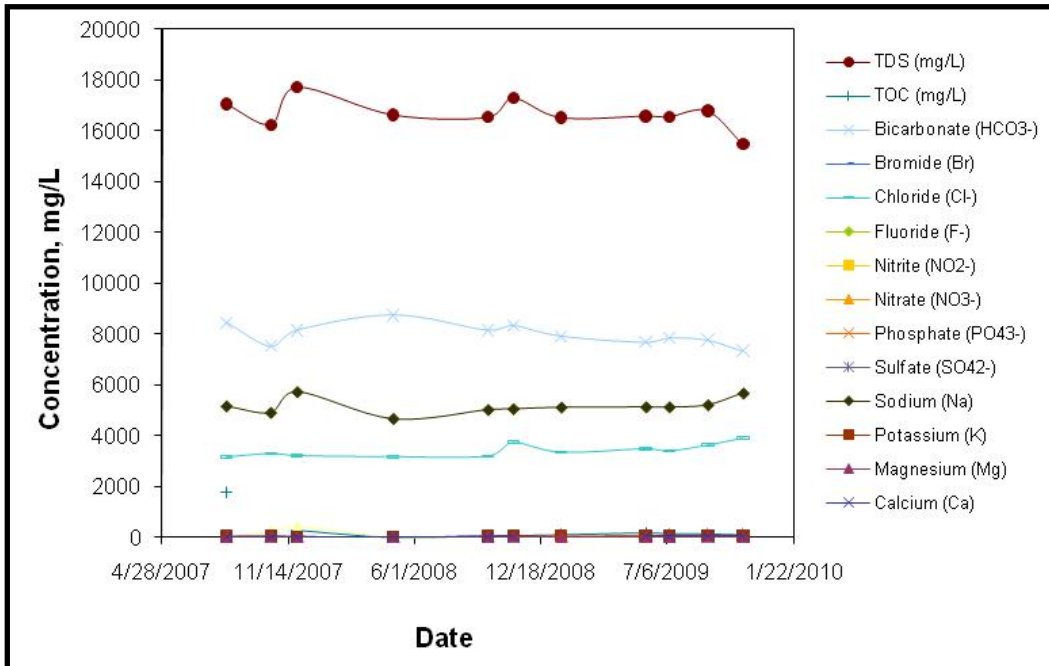
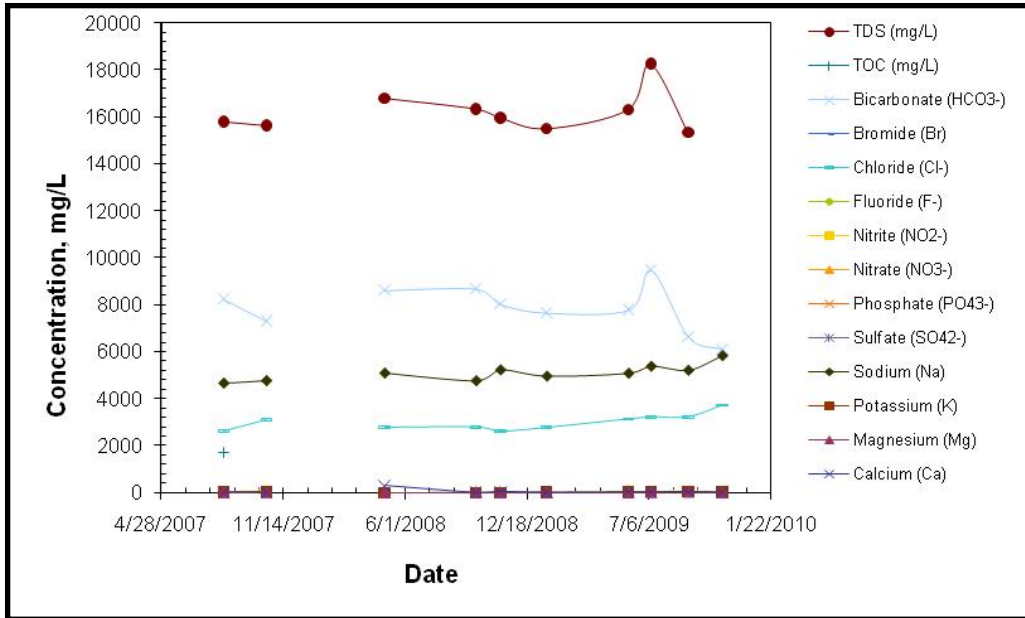


Figure 74: Water Chemistry of Well Howell D351

Figure 75: Water Chemistry of Well Howell G300

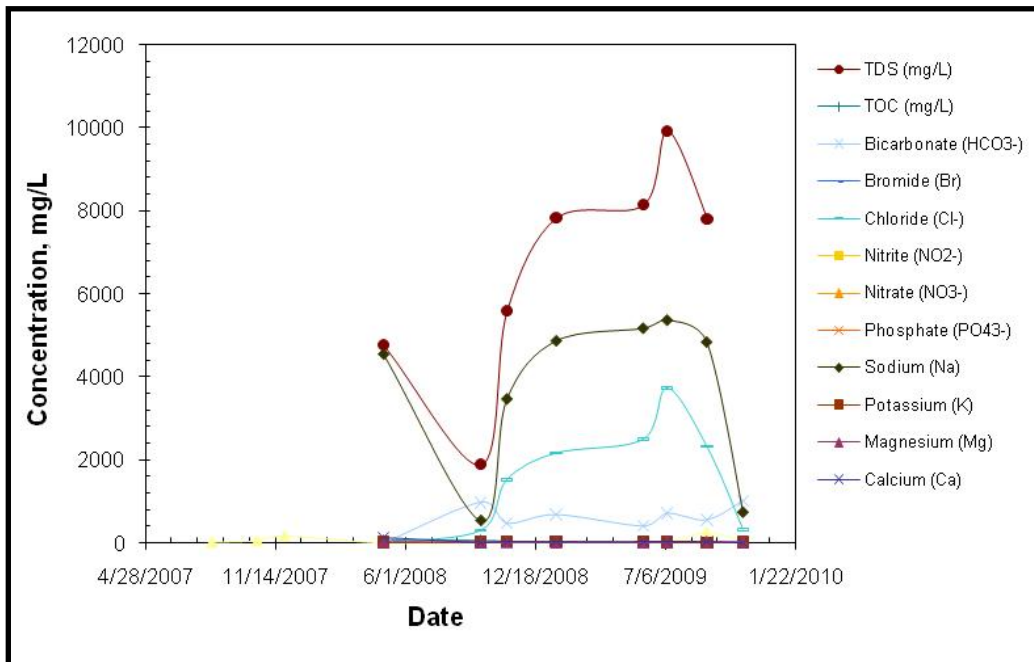
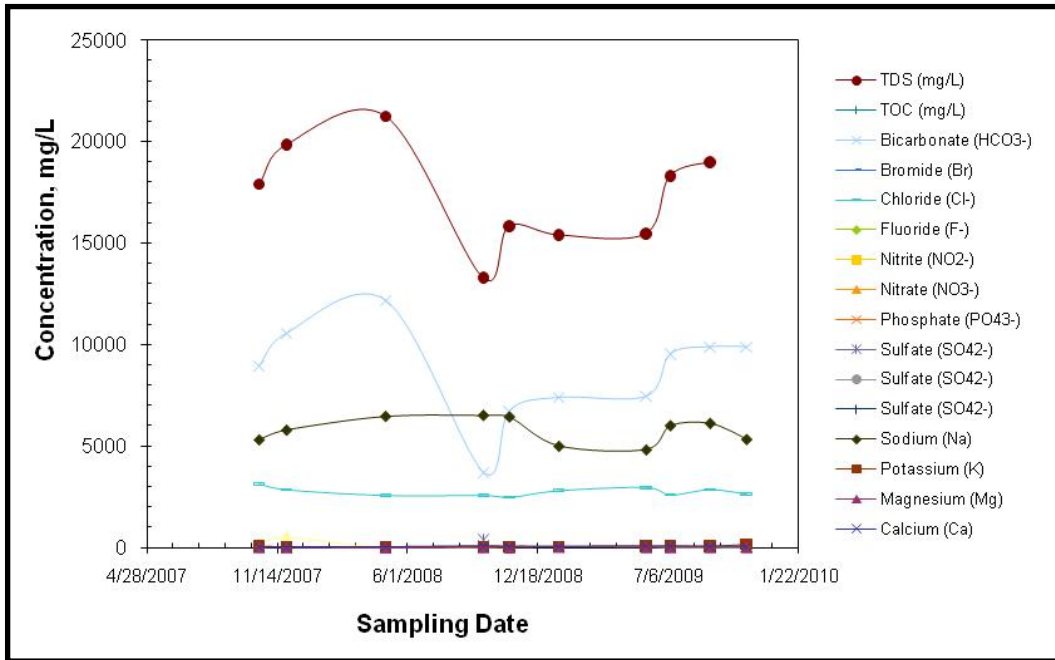


Figure 76: Water Cchemistry ofW EPNG COM A300s

Figure 77: Water Chemistry of Well EPNG COM A300

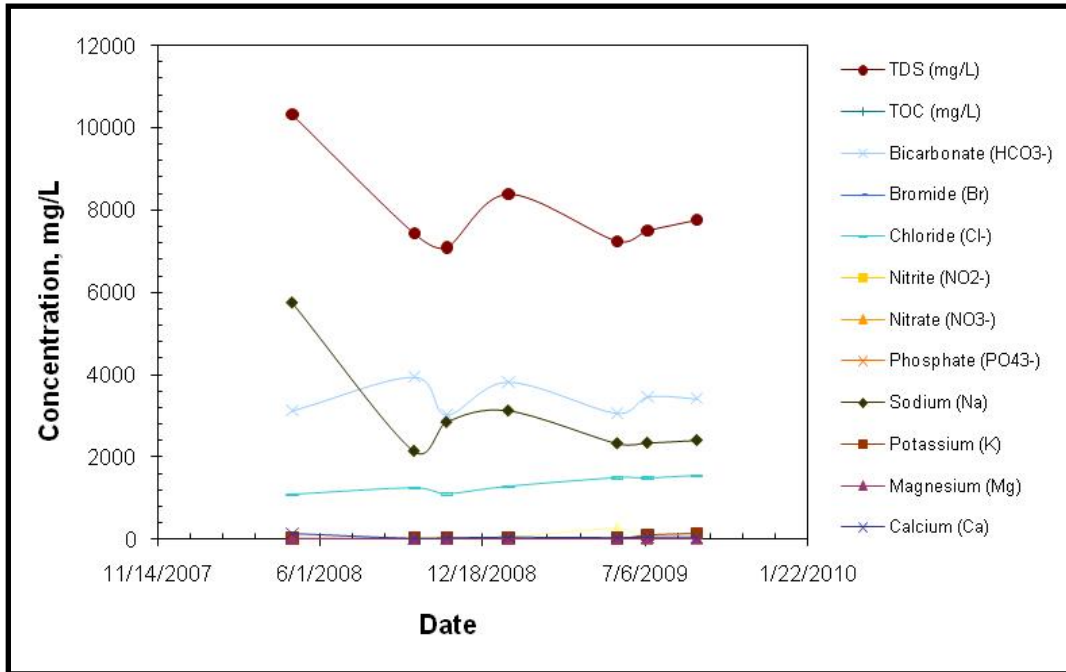


Figure 78: Water Chemistry of Well Howell D353

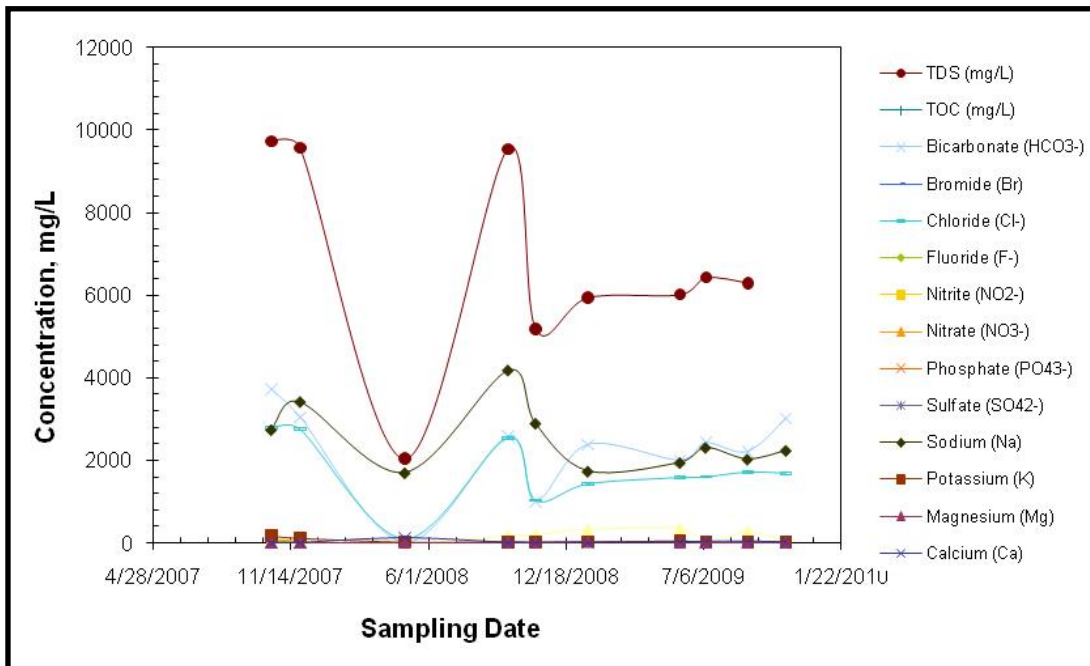


Figure 79: Water Chemistry of Well Howell D352S

Figure 80 gives the pH of produced water from the nearby offset wells. The pH of the solutions stabilized at around 8.0, with variations ranging from 7.0 to 9.0. The spike in pH in June 2008 is attributed to a high concentration of H₂S in the produced water. The carbonate and bicarbonate ion concentration could be an important indicator of the front line of the CO₂ plume and thus are carefully monitored during CO₂ injection. **Figure 81** gives the HCO₃⁻ concentration of the produced water and **Figures 82 and 83** give the strontium and barium ion concentration of the produced water. So far, no dramatic change in water chemistry was observed from offset wells during the testing period. Since early breakthrough is expected to occur at the EPNG COM A300 and FC State COM 1, water chemistry and pH values from these two wells were closely monitored.

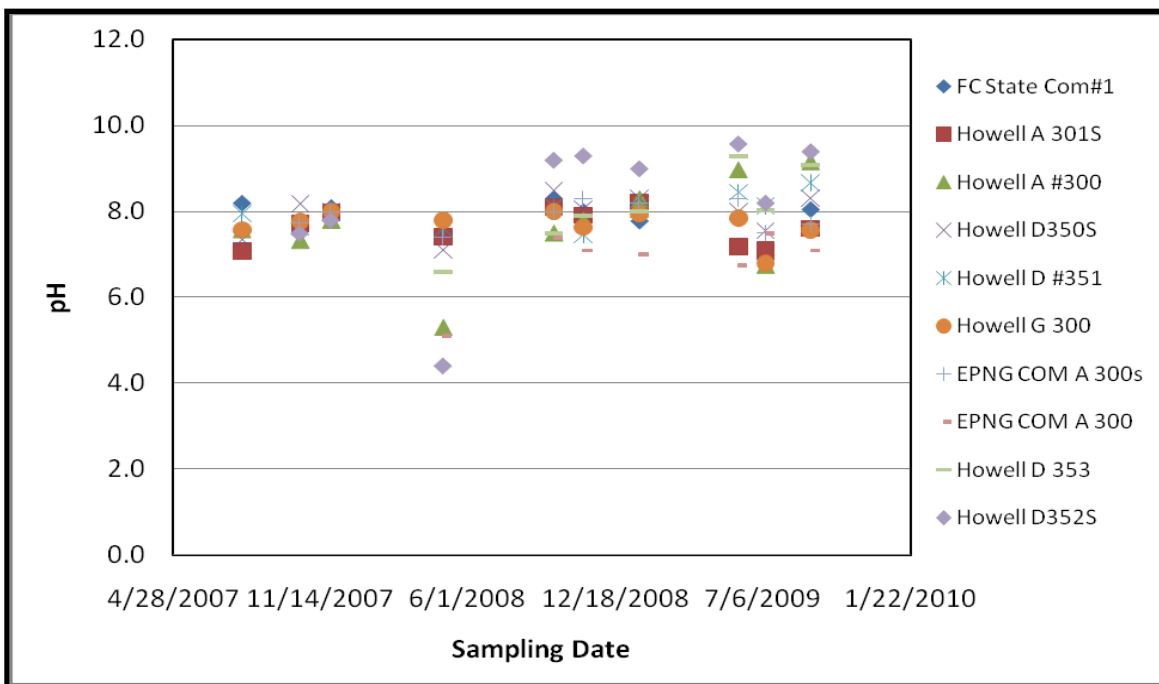


Figure 80: pH of Produced Water from Offset Wells

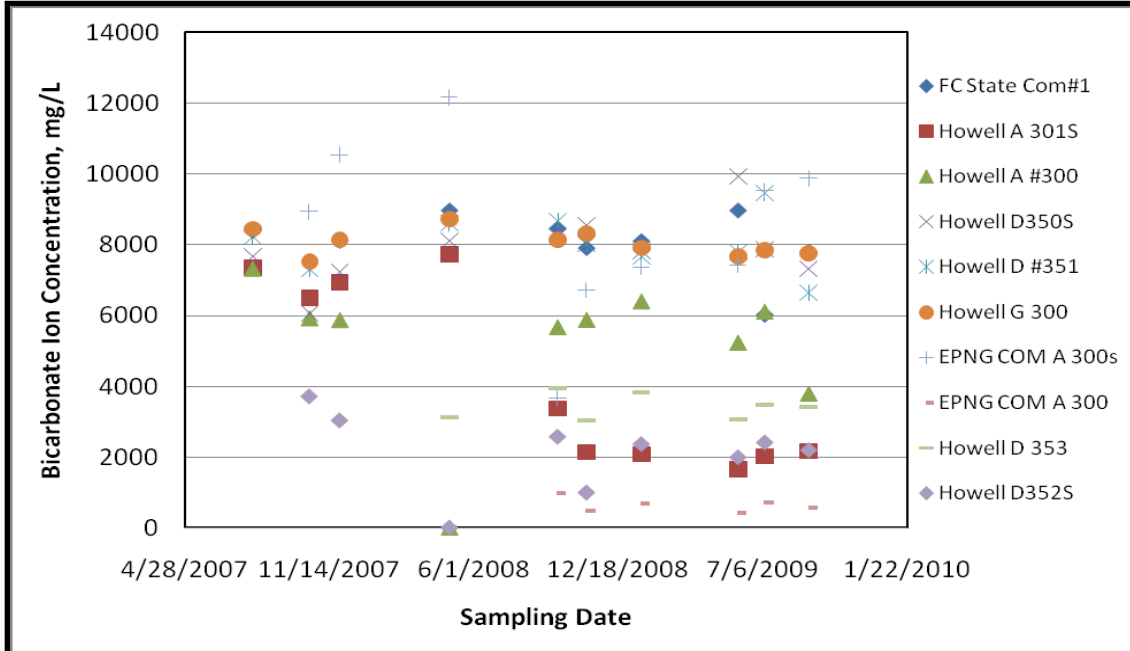


Figure 81: Concentration of Bicarbonate Ion Species in the Produced Fluid from Offset Wells

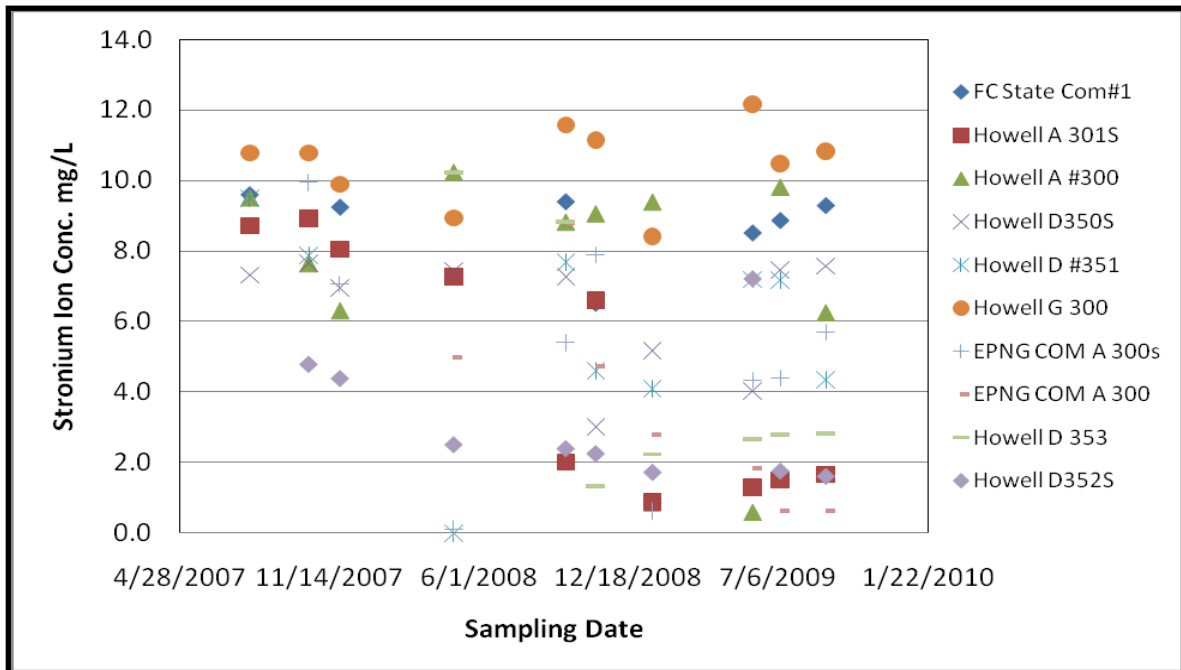


Figure 82: Strontium Ion Concentration in the Produced Water from Offset Wells

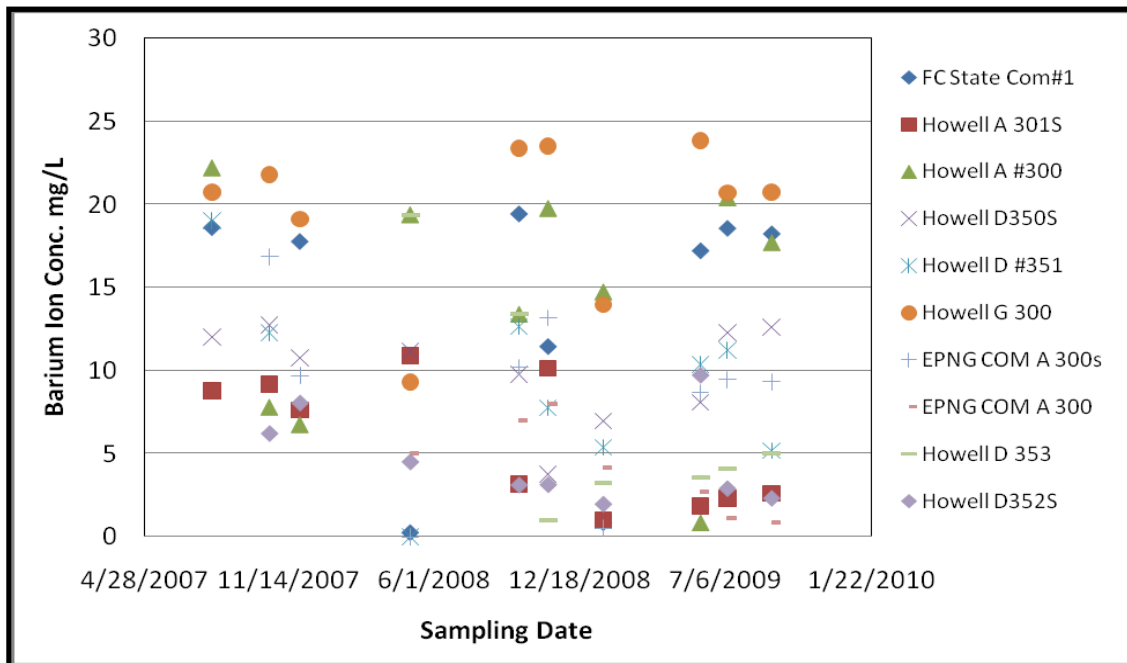


Figure 83: Concentration of Barium Ion in the Produced Water from Offset Wells

5.5.3 Conclusions and Recommendations

About 40 water samples were collected for baseline measurement and over 70 water samples were collected after CO₂ injection for monitoring the movement of CO₂ as well as its impact on the receiving environment. Comprehensive analysis of water chemistry, including ion composition and concentration, dissolved organics, trace metal ion species, carbon isotope, oxygen isotope, and pH values, was carried out and the observations are summarized as:

- (1) Presence of other acid gases, such as H₂S, shows a dramatic impact on the water chemistry analysis. The fluctuation of H₂S in produced water was not fully understood.
- (2) Early breakthrough was expected to occur at EPNG COM A300 and FC State COM 1. So far, there has no conclusive indication of water chemistry change as a result of CO₂ breakthrough.

- (3) A high concentration of bicarbonate ions was detected in the coalbed methane produced water. Since large fluctuations occurred in the pH value of the original produced water and subsequent variations in bicarbonate ions, bicarbonate ion concentration and pH might not be an ideal indicator of the front line of the CO₂ plume in coalbed methane formations.

6.0 Reservoir Characterization

6.1 Database Development

The Pump Canyon Geodatabase was designed to contain individual feature classes for each type of MVA activity, simulation study, or other testing. These features are all represented on a consistent projection (NAD 83) and allow comparisons to be readily made between activities on a project scale.

Features include location of tiltmeters, shallow monitor wells, gas and water sample wells, CO₂ sensor sample wells, soil flux samples, CO₂ pipeline and desalination project.

To complement the Pump Canyon Geodatabase and to provide a context for assessing/integrating MVA, modeling, and risk assessment, the geodatabase also includes basin-scale features that are critical to a larger-scale analysis should commercial application of CCS technology be considered for the San Juan Basin, such as state and county boundaries, townships and ranges, wilderness preservation areas, native Indian lands, federal lands, cities and towns, depositional limits for Lewis Shale, Pictured Cliffs Sandstone, Fruitland formation and CBM Fairway.

In addition, well NEBU 77 has been designated as the type well and is very close to the Pump Canyon project area. Regional dip and strike cross sections have been constructed; dip sections align NE-SW in the basin and strike sections align NW-SE. The focus for the geologic map is the Ojo Alamo Sandstone to the Huerfanito Bentonite within the Lewis Shale. Of particular importance is the relationship of the Ojo Alamo Sandstone to the Fruitland as there is an erosional unconformity that removes the Kirtland Shale caprock along the eastern side of the basin.

The six-township area centered on the Pump Canyon Pilot (Township 30-31 North and Range 7-9 West) is the primary focus of cross-section development. A total of 20 cross sections

consisting of 68 wells with raster images were developed. Of these, four cross sections are oriented in the northeast-southwest direction, which parallels depositional dip and eight cross sections parallel depositional strike. An additional seven cross sections were used to ensure all wells with raster images tied correctly with the main dip and strike cross sections.

Where raster log coverage is available, the correlations that are being developed include: (1) the basin wide Huerfanito Bentonite, (2) a fairly consistent high conductivity response within the Lewis Shale, (3) the top of the Lewis Shale, (4) the top of the Pictured Cliffs Sandstone, (5) the upper Pictured Cliffs tongues within the basal Fruitland, designated UP1, UP2, and UP3, (6) the top of the Fruitland formation, (7) the top of the Kirtland Shale, and (8) the top of the Ojo Alamo Sandstone.

The correlations being utilized in this geologic model are well described in the *Geologic Evaluation of Critical Production Parameters for Coalbed Methane Resources, Part 1, San Juan Basin, Annual Report (August 1988 – July 1989), GRI-90/0014.1* and the *Geology and Fuel Resources of the Fruitland formation and Kirtland Shale of the San Juan Basin, New Mexico and Colorado, U.S. Geological Survey Professional Paper 676* by J.E. Fassett and J.S. Hinds. **Figures 84 and 85** are an example of top and isopach maps that were generated for the Fruitland formation and the Kirtland Shale.

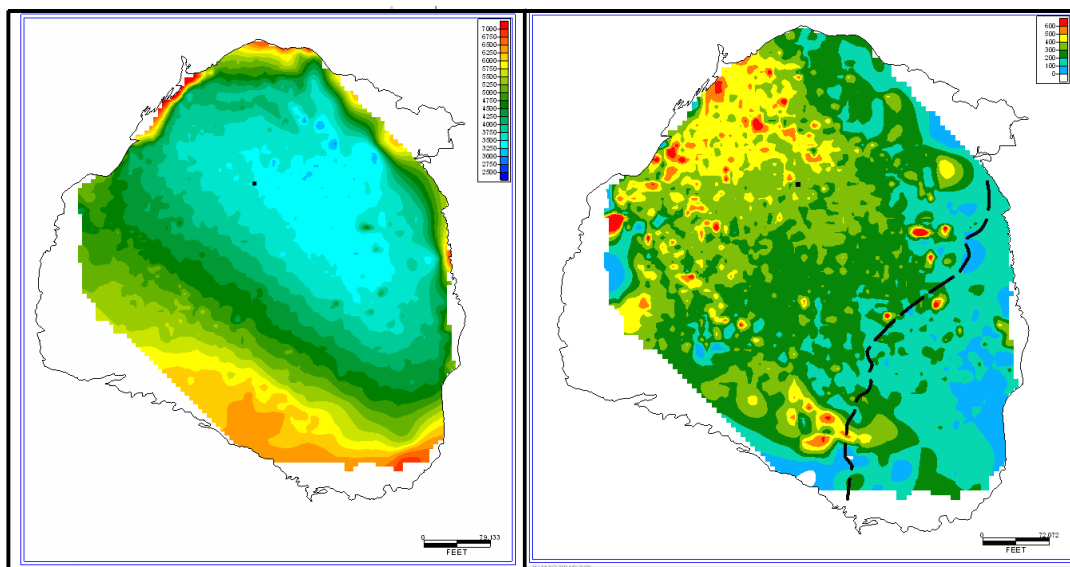


Figure 84: Top and Isopach of the Fruitland Formation

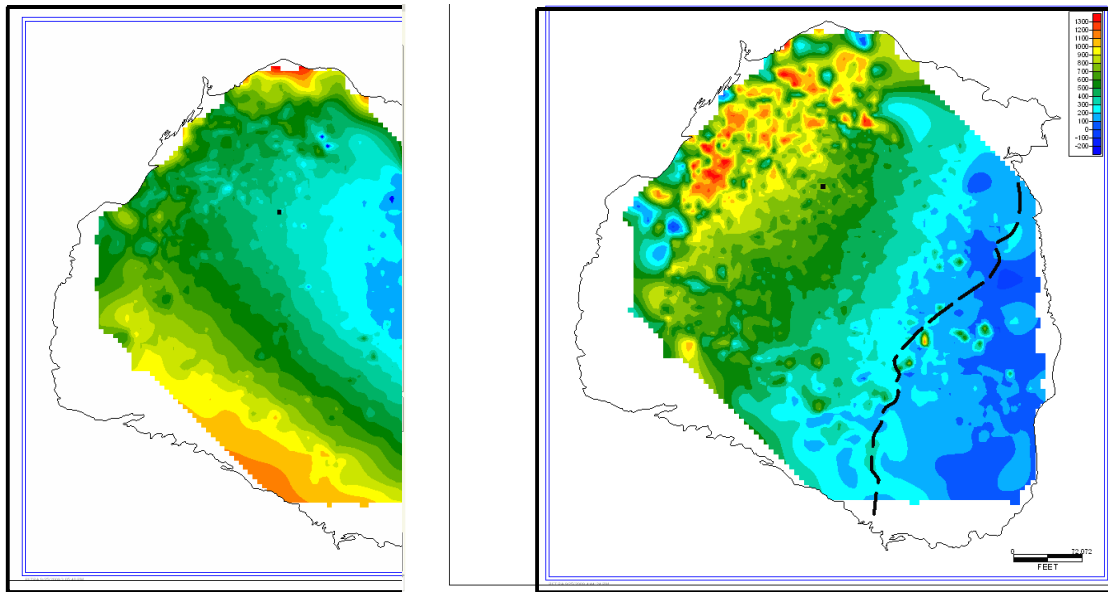


Figure 85: Top and Isopach of the Kirtland Shale

6.2 Core Analysis

This section will be provided as an independent topical report, and is mentioned here for completeness.

6.3 Analysis of Bottomhole Pressure Data

On September 8, 2008, two bottomhole memory readout (MRO) gauges were installed within the EPNG Com A Inj #1 well at a depth of 2,865 feet. The gauges were pre-programmed to record high data density pressure and temperature information, which was collected during the injection of carbon dioxide into the Fruitland coal seams.

Following the termination of injection and in preparation for well abandonment, the MRO gauges were retrieved from the well and the data was downloaded. **Figure 86** depicts the raw pressure and temperature data collected from the well. Regrettably, the high-density collection of data stopped on February 17, 2009 due to a full MRO data bank. Nevertheless, sufficient data existed to perform pressure transient analysis on this data set.

In reviewing **Figure 86**, one can clearly identify the periods of injection that are denoted by pressures exceeding 2,000 psia, bottomhole, as well as those periods of interrupted injection

where the pressure declines in some cases to 100 psia, bottomhole. It is these pressure falloff periods (PFO) that we will investigate further.

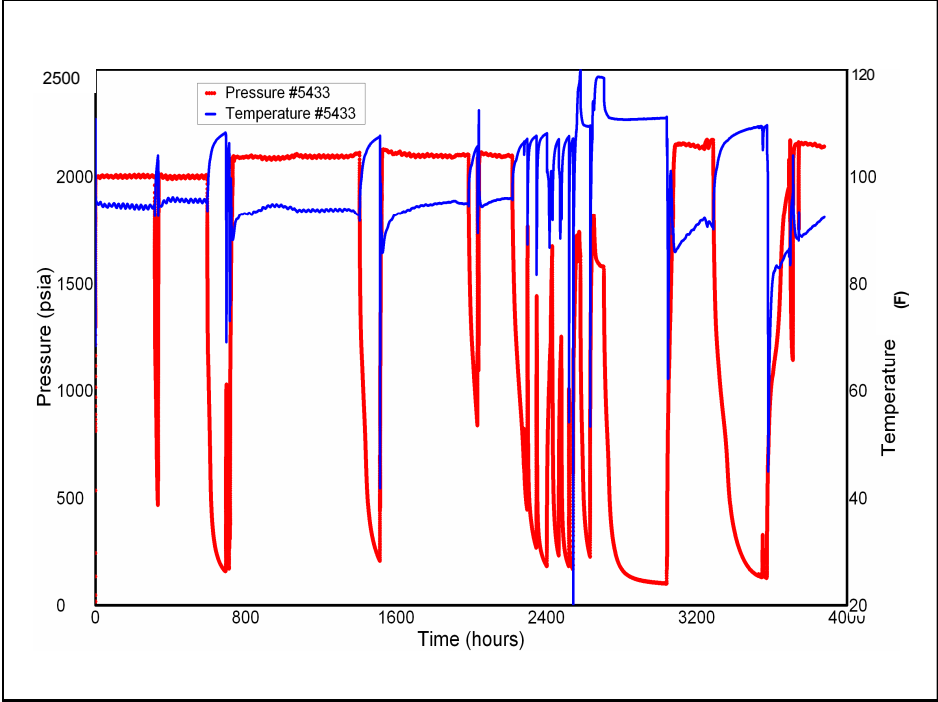


Figure 86: Raw Pressure and Temperature Gauge Data

For the nearly 4,000 hours of collected data, **Figure 87** overlays the six PFO periods and the cumulative injection data at each PFO on a plot of pressure and injection rate (note: sign convention is negative for injection). **Table 5** depicts the primary input parameters for the well test analysis package. It is important to note that well test software, unlike reservoir simulation software, models the injection reservoir as one discrete formation and not three discrete members of the formation. Thus, the results represent the accumulated formation thickness and are not representative of the discrete coals.

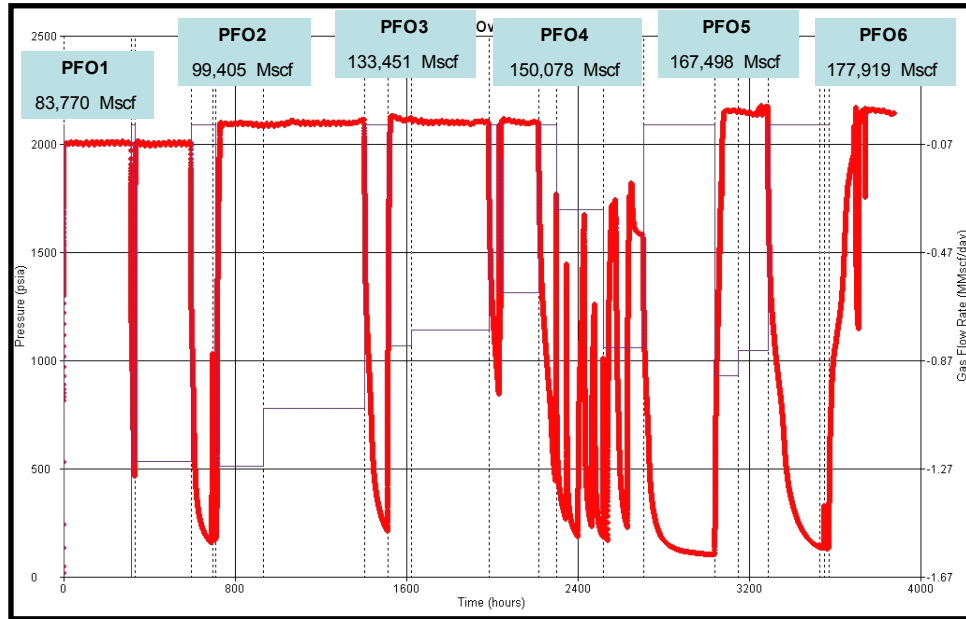


Figure 87: Pressure and Injection Rate

Table 5: Well Tests Primary Input Parameters

Parameter	Value	Unit
Thickness	60	ft
Porosity	0.5	%
Total Compressibility	2.70E-02	1/psi
Wellbore Radius	0.375	ft

Figure 88 shows an overlay of each of the six PFOs on the traditional log-log diagnostic plot. An upward shift of the pressure curves from PFO 1 to PFO 6 indicates decreasing permeability, which one might expect to see permeability continue to decline due to coal swelling in the presence of continued CO₂ injection. Interestingly enough, five of the six pressure derivative curves decline rapidly, but at successively longer equivalent times.

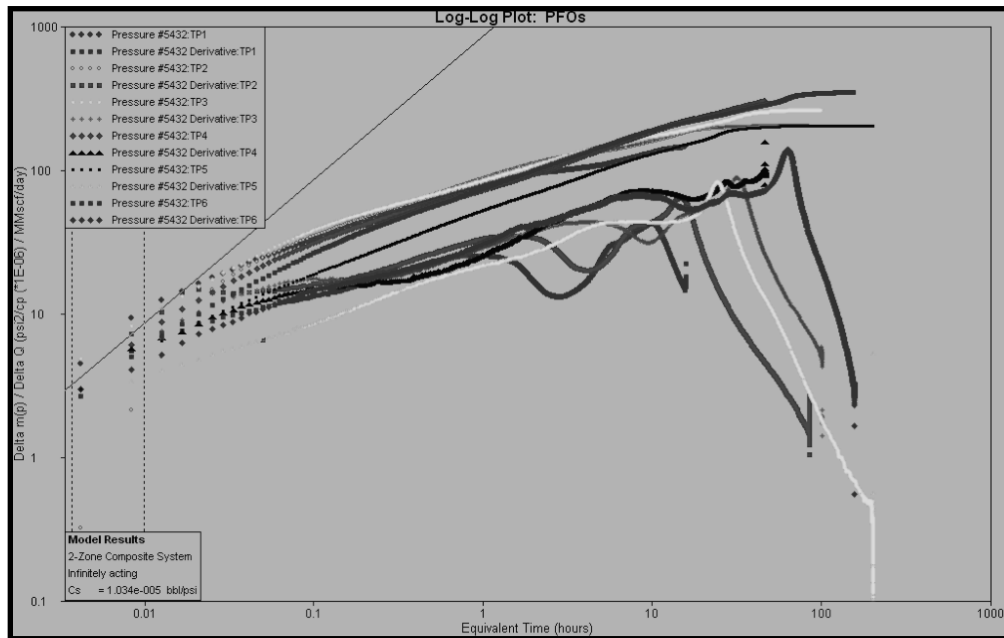


Figure 88: PFOs Overlay

Based on these observations, it was theorized that a radial composite solution may be the most proper way to model this data set. What this model represents is an inner radius of very low permeability (k on the subsequent plots) and skin factor (s) out to a radius (RI_2). Outside of this radius, the permeability (K_2) increases to a baseline value that is nearly infinite as compared to the inner permeability value. While this has been modeled as 5,000 md, it should be noted that there is little sensitivity in this value above 250 md. As such, this value was fixed and this “increasing” permeability away from the well is believed to be the cause of a steeply declining derivative curve as it attempts to stabilize in radial flow and/or the intersection of highly depleted portions of the Fruitland as the transient approaches the offset production wells.

Unfortunately, the log-log plots do not reveal the classic radial flow period (a flattening of the derivative curve that allows the analyst to clearly define permeability and skin factor) in any of the six diagnostic plots (**Figures 89 through 94**). Fortunately, reasonable best-fit matches were generated that fit the perceived expectation of results for this transient data set. That is, an ever decreasing permeability, near-wellbore, that continues to grow outward as

additional CO₂ is injected into the Fruitland coal seams. The results of this analysis are listed in **Table 6**.

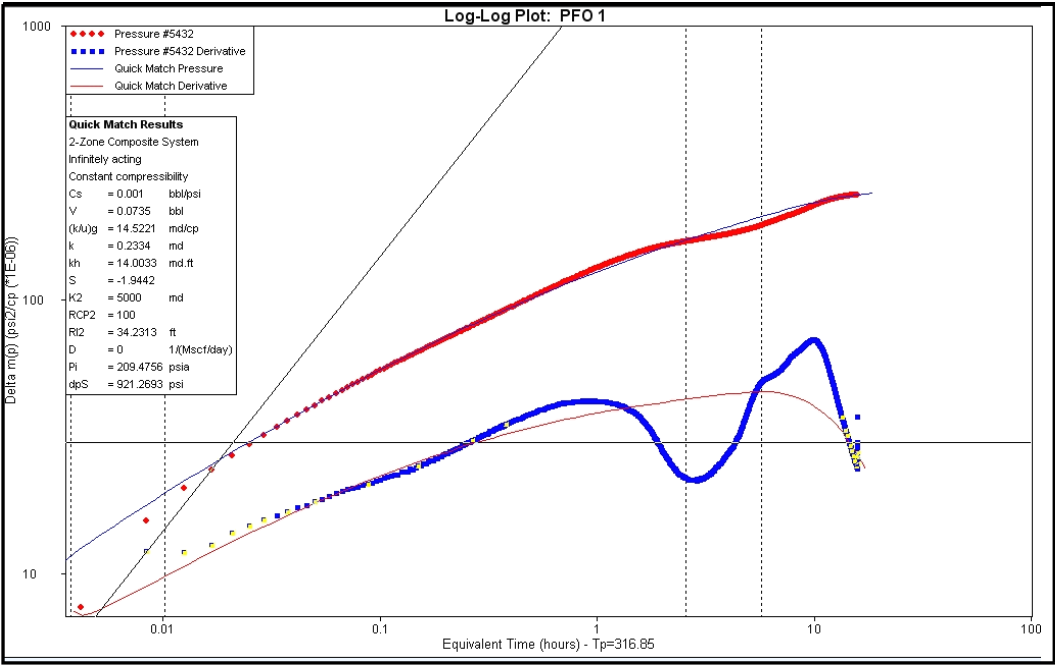


Figure 89: PFO1 Log-Log Plot

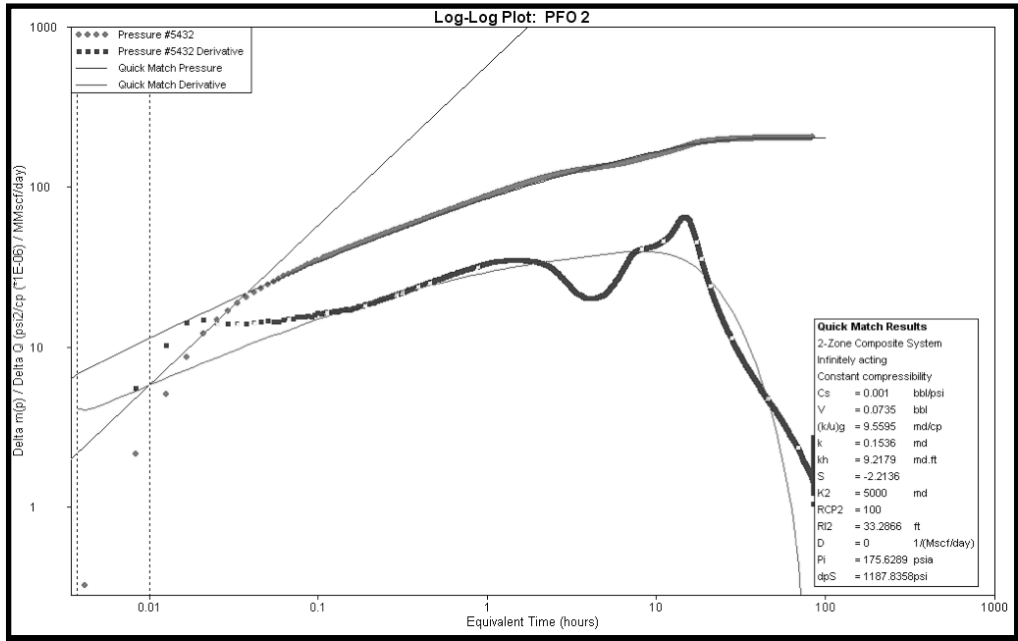


Figure 90: PFO2 Log-Log Plot

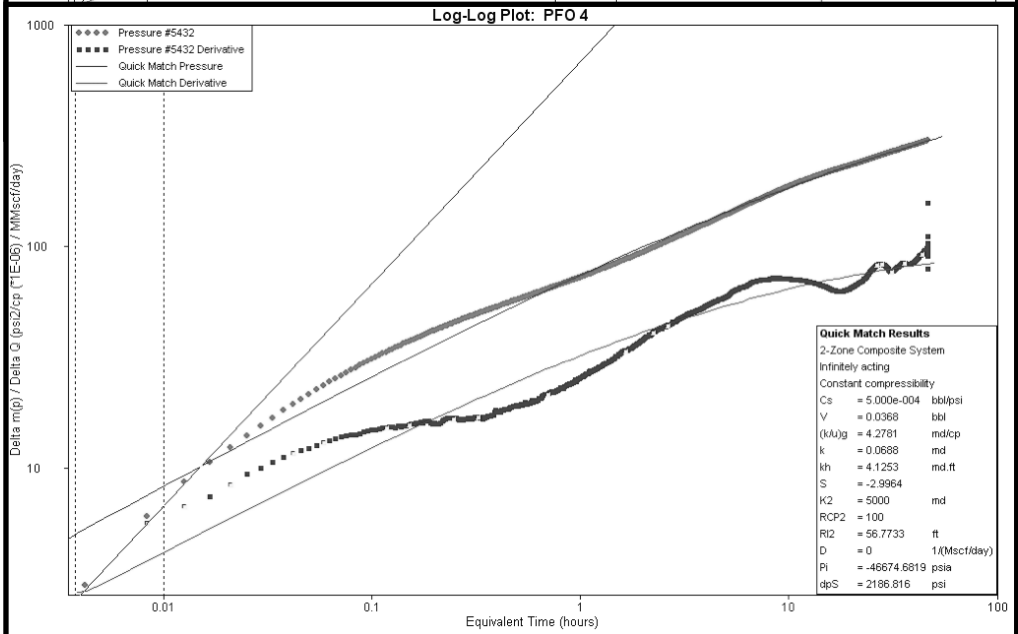
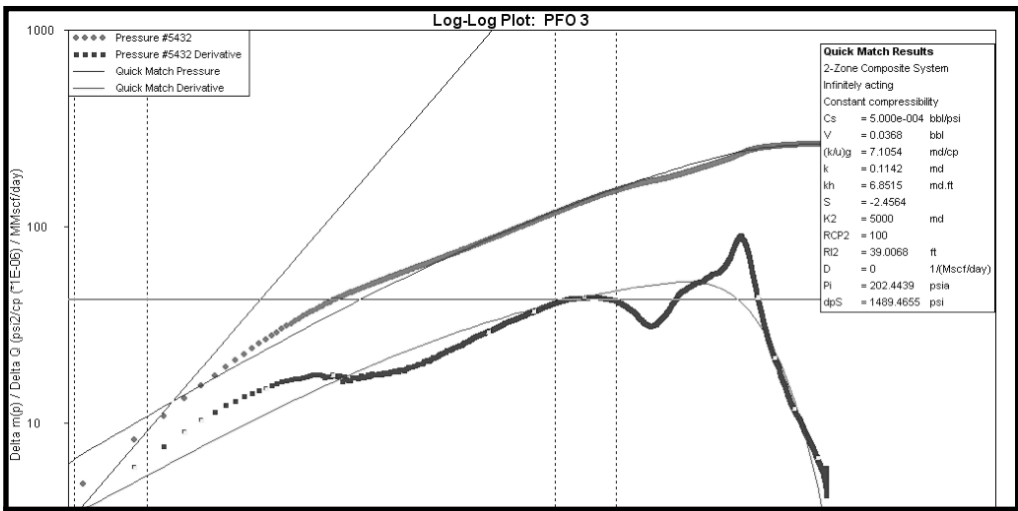


Figure
PFO3
Log

91:
Log-
Plot

Figure 92: PFO4 Log-Log Plot

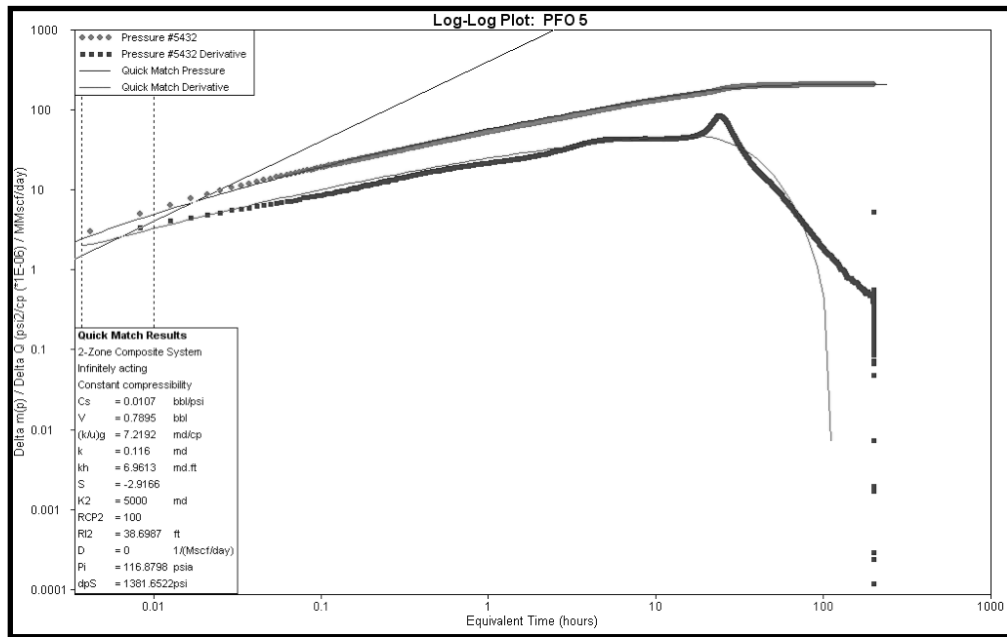


Figure 93: PFO5 Log-Log Plot

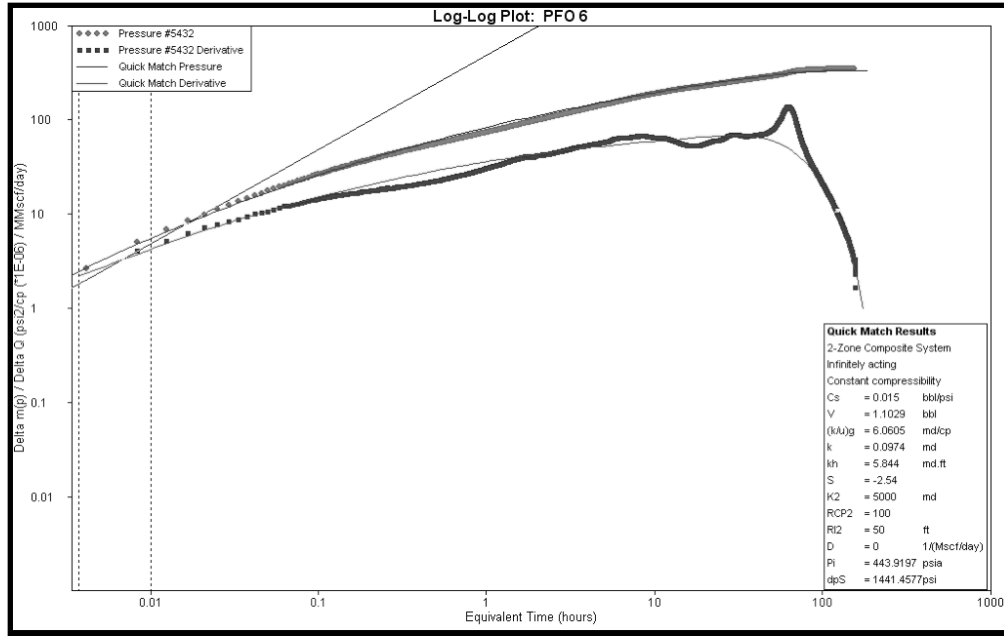


Figure 94: PFO6 Log-Log Plot

Table 6: Analysis Results

PFO	Cum CO ₂ Injected (Mscf)	Perm (mD)	RI (ft)	Skin	Perm 2 (mD)
1	83,770	0.23	34	-1.9	5,000
2	99,405	0.15	33	-2.2	5,000
3	133,451	0.11	39	-2.5	5,000
4	150,078	0.07	57	-3.0	5,000
5	167,498	0.12	39	-2.9	5,000
6	177,919	0.10	50	-2.5	5,000

A plot (**Figure 95**) of the near-well permeability (k) and its radius of influence (RI2) against cumulative CO₂ injection clearly shows these two behaviors – an increasing radius of influence as permeability declines. Interestingly enough, while a linear fit is suitable for the increasing radius, a power law fit is superior for the permeability decline.

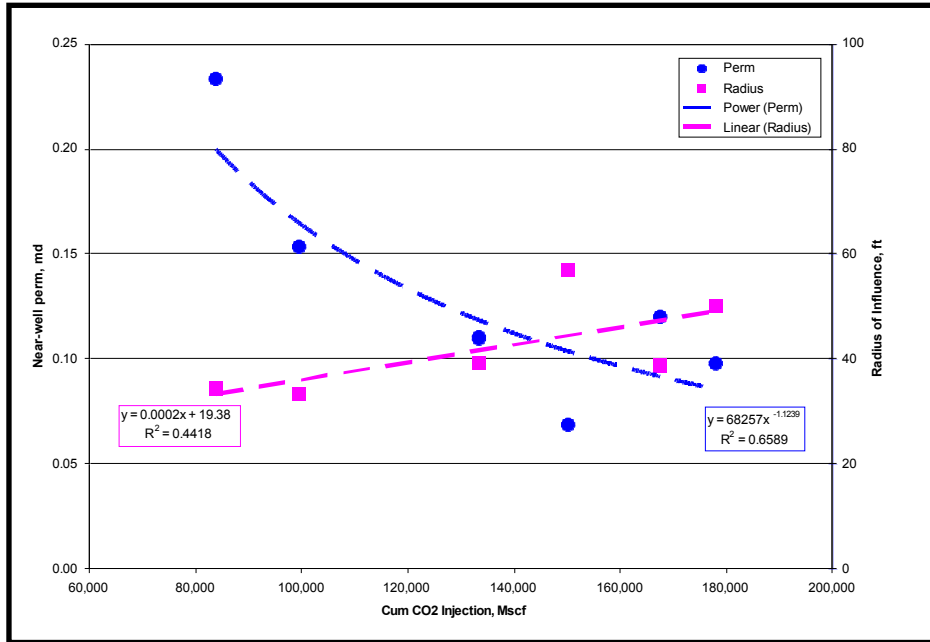


Figure 95: Near-Well Permeability and Radius of Influence Versus Cumulative Injected CO₂

When reviewing these trends, as well as the pressure transient data, itself, it is clear that PFO 4 does not behave like the remaining five PFOs (see **Figure 92**) as there is no steeply declining pressure derivative curve. It is unclear, based on available data why this is the case and as a result, this period should be removed as an outlier. Similarly, there is several hundred hours of erratic injection activity following PFO 4 and preceding PFO 5 (**Figure 87**). Pressure never reaches maximum injection pressure during this time and it is believed that injectivity data or pattern depletion has impacted this PFO period. As such, **Figure 96** shows greatly improved correlations without PFO 4 and 5, supporting the basic understanding of coal swelling.

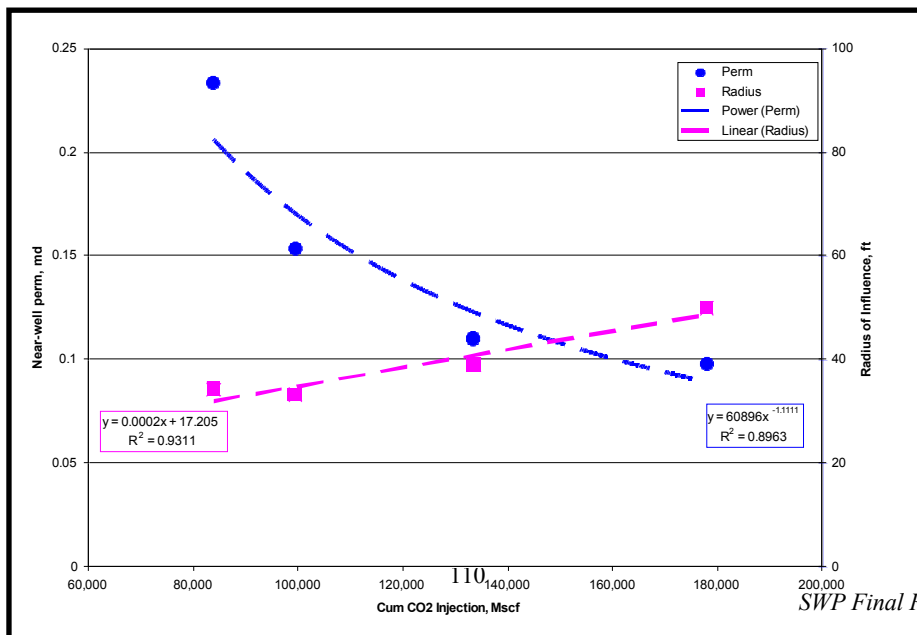


Figure 96: Near-well Permeability and Radius of Influence Versus Cumulative Injected CO₂ (without PFO4 and PFO5)

Since most of the injection is believed to have entered the basal coal, we can generally say that each of the permeability values may in fact be approximately twice as large, while the radius of influence would be approximately 1.4 times as large (the square root of two), due to the injection impacting half of the thickness.

7.0 Reservoir Modeling

The modeling efforts focused on Section 32 (as the CO₂ plume is not expected to go far due to its adsorption in the coal), which included the injector as well as the three immediate offset wells.

7.1 Reservoir Description

7.1.1 Structure and Isopach

Structure and isopach maps of each coal were constructed based on ConocoPhillips log data. The maps were generated using available data from 21 wells. An example structure map for the upper coal is presented in **Figure 97**, and the total net coal isopach is presented in **Figure 98**.

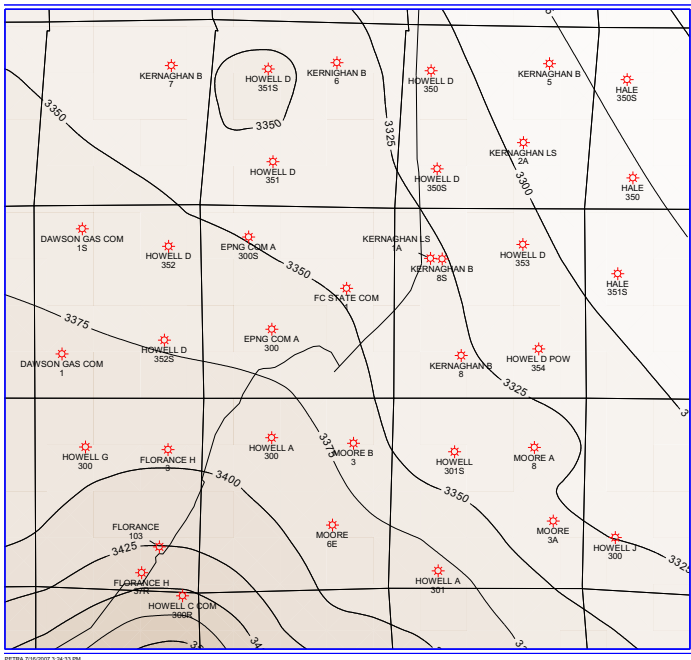


Figure 97: Structure Map, Upper Coal (Units in Feet Above Sea Level)

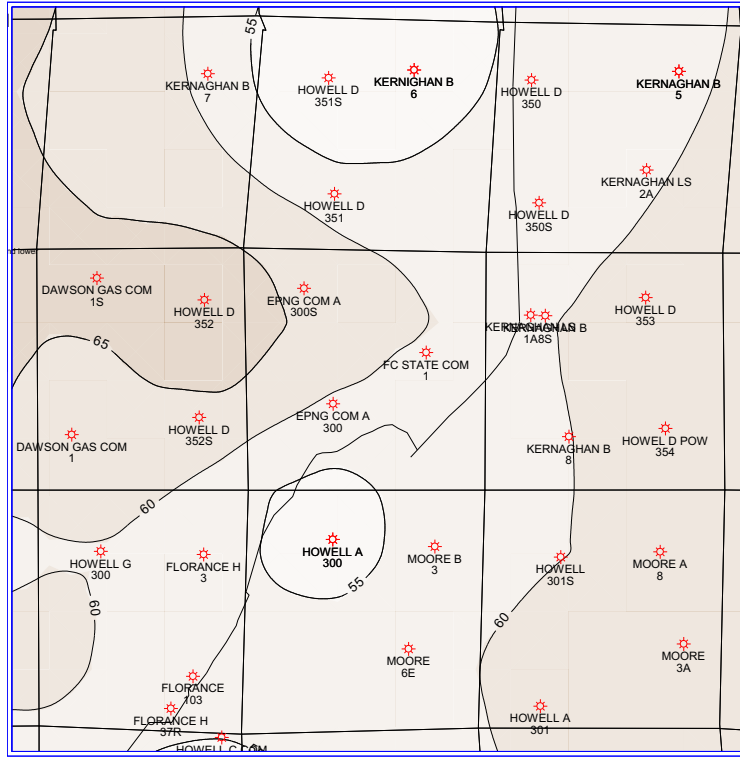


Figure 98: Total Net Coal Isopach (units in feet)

7.1.2 Isotherms

Sorption isotherms for both CH₄ and CO₂ were available from five wells in the vicinity of the demonstration. In four wells, two methane isotherms were available for the upper coal, four for the middle coal and four for the basal coal. In two wells, one carbon dioxide isotherm was available for the middle coal and two for the basal coal. These isotherms are illustrated in **Figure 99** and the Langmuir constants summarized in **Table 7**.

Due to the lack of information for a carbon dioxide isotherm for the upper coal, estimations were made based on CH₄/CO₂ Langmuir ratios for the middle and basal coals. These data were then converted from a dry, ash-free basis into in-situ conditions and appropriate units (using coal density) for use in the reservoir simulator, **Table 8**. As no data were available for nitrogen, CH₄/N₂ Langmuir volume ratios from the Tiffany Unit N₂-ECBM pilot were used to

compute nitrogen Langmuir volume from the Pump Canyon CH₄ isotherm data. **Table 9** summarizes the data used in the simulator.

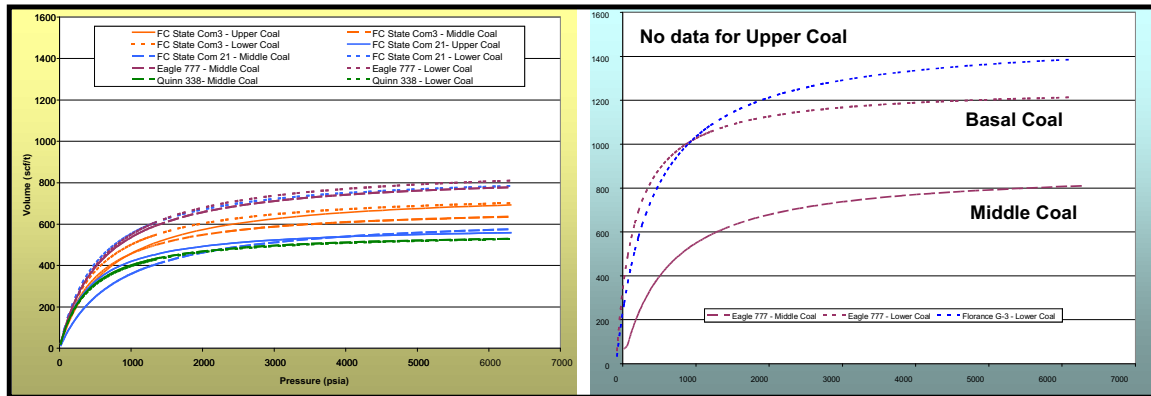


Figure 99: Isotherm Data

Table 7: Langmuir Isotherm Constants

Coal	Methane*		Carbon Dioxide*	
	V _L (scf/ton)	P _L (psia)	V _L (scf/ton)	P _L (psia)
Upper	596-766	420-672	1234 ⁺	317 ⁺
Middle	563-851	404-807	1244	260
Lower	562-890	418-621	1274-1506	253-490

*dry, ash-free basis

+ computed based upon CO₂/CH₄ Langmuir constant ratios for middle and lower coals

Table 8: Langmuir Isotherm Constants at In-Situ Conditions

Coal	Average Density ¹ (g/cc)	Moisture ² (%)	Ash Content ³ (%)	Methane		Carbon Dioxide	
				V _L In-Situ (scf/ton)	V _L In-Situ (scf/ft ³)	V _L In-Situ (scf/ton)	V _L In-Situ (scf/ft ³)
Upper	1.51	3.4	31.1	390-503	18-24	809	38
Middle	1.54	3.4	34.6	347-524	17-25	766	37
Lower	1.44	3.4	22.4	419-664	19-30	950-1126	43-50

¹ over nine-section area

² average of isotherm samples

³ using ρ_{coal}=1.3 g/cc and ρ_{ash}=2.5 g/cc

Table 9: Model Isotherms Inputs

Coal	Methane*		Carbon Dioxide*		Nitrogen	
	V _L In-Situ (scf/ft ³)	P _L (psia)	V _L In-Situ (scf/ft ³)	P _L (psia)	V _L In-Situ (scf/ft ³)	P _L (psia)
Upper	21	546	38	317	12.1	1429
Middle	21	605.5	37	260	12.3	1429
Lower	24.5	519.5	46.5	372	11.5	1429

7.1.3 Pressure Data

Initial reservoir pressure data measured in the late 1980's were available for four wells in the demonstration area. This data, summarized in **Table 10**, indicated an over-pressured reservoir, with an estimated initial pressure gradient in the 0.50-0.57 psig/ft range.

Table 10: Reservoir Pressure Measurements

Well Number	Date	Depth (ft)	Pressure (psi)	Pressure Gradient (psi/ft)
Howell D 352	Jun-88	3,150	1,584	0.50
EPNG Com A 300	May-89	3,075	1,604	0.57
Howell G Com 300	Apr-89	2,800	1,604	0.57
Howell A 300	Jun-88	3,070	1,613	0.53

7.1.4 Cleat Orientation

Cleat orientation was measured in the Northeast Blanco Unit #403 well, approximately seven miles to the east of the demonstration site. These data indicated a face-cleat orientation of N35E, as shown in **Figure 100**. The simulation grid was oriented in order to respect a higher permeability in that direction.

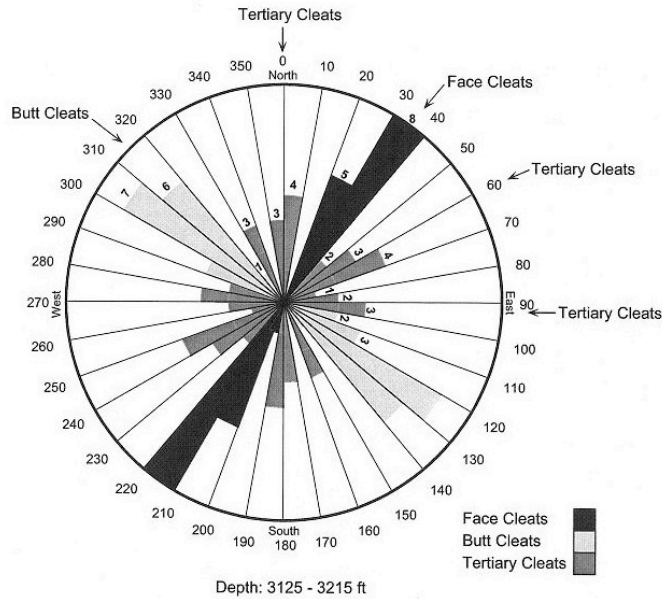


Figure 100: Cleat Orientation

7.1.5 Permeability and Porosity

Based on experience in the area (ConocoPhillips) and the review of available logs, the basal coal seems to be of better quality as compared to the upper and middle coals. Based on this information, permeability was allowed to be higher in the basal coal as compared to the middle and upper coals during the history-match process.

Porosity was assumed to be correlated with permeability. According to Schwerer and Pavone⁵, permeability can be related to porosity in a fracture through **Equation (1)** where k and ϕ are permeability and porosity with the exponent n typically 3.0.

$$\frac{k}{k_i} = \left(\frac{\phi}{\phi_i} \right)^n \quad (1)$$

Using this equation, porosity was correlated with permeability using **Equation (2)** where the factor 'a' was allowed to vary during the history-matching process.

$$\phi = a * k^{0.3333} \quad (2)$$

7.2 Model Construction

The reservoir simulator used for the study was the *COMET3* (binary isotherm – CH₄ and CO₂) model. Details on the model theory are provided in the references^{6,7}.

Initially, a three-layer (upper, middle and basal), nine-section (Section 32 plus the eight surrounding sections) model was constructed to perform the simulation study. The coal structure and thickness information for each layer was directly input from geologic maps. The simulation grid was oriented in order to respect the face-cleat orientation of N35E. Matching the full-field, nine-section area proved difficult and requiring extensive modeling time. It was then decided to focus on the middle section, primarily. The area considered is shown on **Figure 101** (in blue) and was determined taking into account the interference with surrounding wells (it should be noted that well Kernaghan 1A is not producing, explaining its close location to the simulated area).

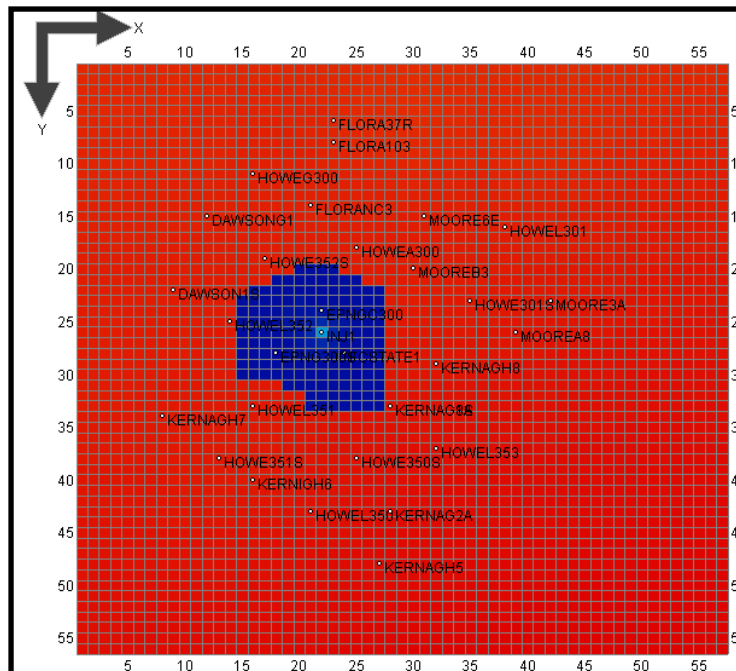


Figure 101: Simulation Model Base Map

A 3D view of the model is also shown on **Figure 102**. A multiplication factor of 20 between the vertical axis and the horizontal axis was used to ease the view of the model.

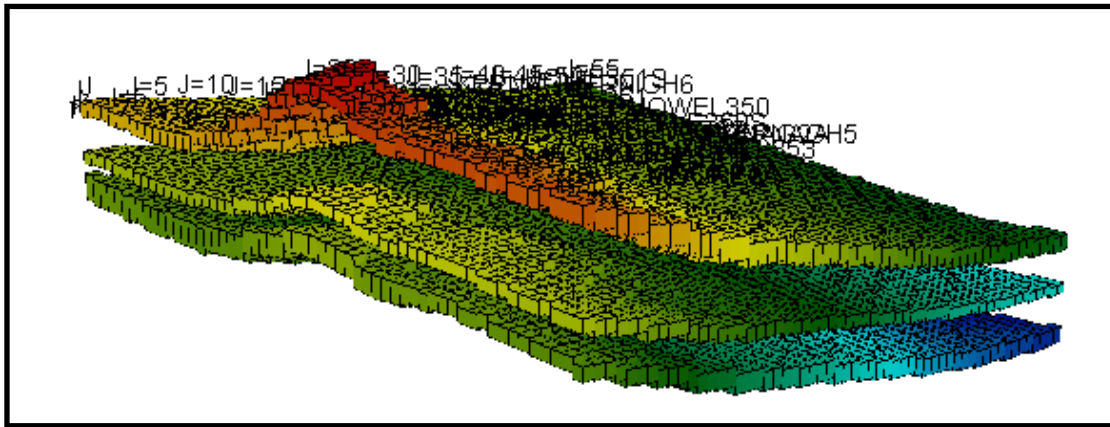


Figure 102: Model 3D View

7.3 History Matching

7.3.1 Procedure

A computer-assisted procedure was used to facilitate the history-match of the Pump Canyon demonstration site. This procedure is an iterative technique utilizing two software programs: a global optimizer (*ClearVu*) and a fractured reservoir simulator (*COMET3*). Before the optimization process is started, a base case is defined and possible ranges for uncertain input parameters, as well as the total number of simulations to be run and the number of simulations per batch (also referred to as an iteration), are also selected. The workflow of the process is outlined in **Figure 103**.

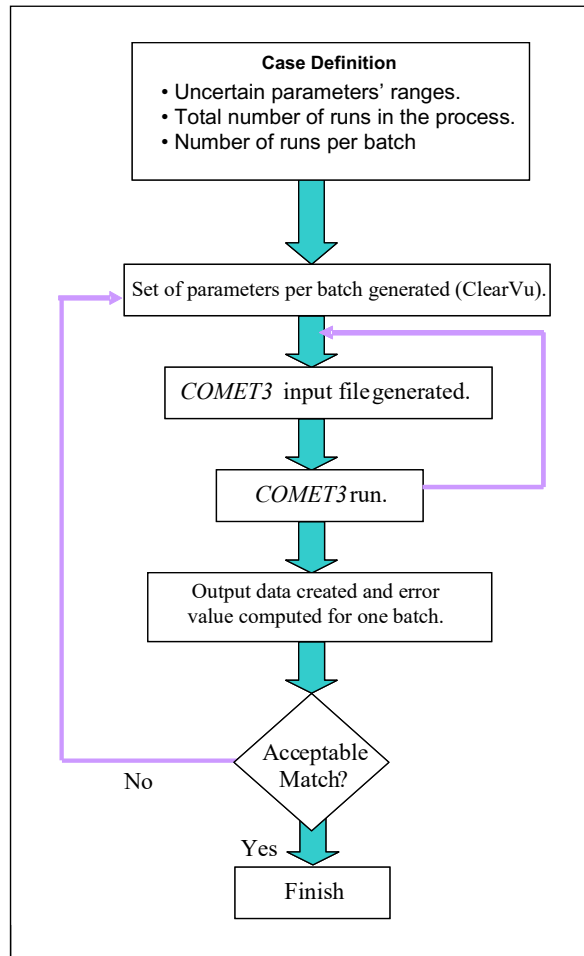


Figure 103: Optimization Workflow

As illustrated in **Figure 103**, simulations are executed one after another and at the end of each iteration, the output data from each simulation is saved and compared to historical data. The corresponding error value is computed using **Equations 3 to 5**. **Equation 3**, weighted sum of squares of the difference between actual data and simulation data, is used most frequently and recognizes the goodness-of-fit measure for optimization purposes.

$$ErrorValue = \frac{\sum \left(\frac{(SimData - ActualData)^2}{2 * Variance} \right)}{NumberOfData} \quad (3)$$

With

$$Variance = \frac{\sum (ActualData - Mean)^2}{NumberofData} \quad (4)$$

And

$$Mean = \frac{\sum ActualData}{NumberofData} \quad (5)$$

These computed error values serve as objective (goodness-of-fit) function values and are evaluated by the optimizer, which produces a new set of input parameters. The next iteration can then be initialized. When several output parameters are to be matched, the objective function is computed separately for each parameter with the final error value being the sum (or some other combination) of the independent values. The process completes when the objective function stabilizes at a minimum value.

7.3.2 History-Match

During the history-matching process, the simulations were run with the wells producing on gas rate, while matching gas rate, gas composition and bottomhole pressure (when available). Water data believed to be unreliable was not matched. The injector was controlled using wellhead pressure while matching gas injection rate (composition of 98.5% CO₂ and 1.5% N₂). The history-match was run until August 2009, corresponding to the end of the injection. **Tables 11 and 12**, show the list of the parameters that were kept constant during the simulation and the list of the parameters that were varied, respectively, as well as their ranges.

Table 11: History-Match Fixed Parameters

Parameters	Units	Value
Formation Properties		
Vertical Permeability	mD	0.0001
In-situ CH4 Langmuir Volume, Layer 1	scf/ton	447
In-situ CH4 Langmuir Volume, Layer 2	scf/ton	436
In-situ CH4 Langmuir Volume, Layer 3	scf/ton	542
CH4 Langmuir Pressure, Layer 1	psi	546
CH4 Langmuir Pressure, Layer 2	psi	606
CH4 Langmuir Pressure, Layer 3	psi	520
Sorption Time, CH4	days	1
In-situ CO2 Langmuir Volume, Layer 1	scf/ton	809
In-situ CO2 Langmuir Volume, Layer 2	scf/ton	766
In-situ CO2 Langmuir Volume, Layer 3	scf/ton	1038
CO2 Langmuir Pressure, Layer 1	psi	317
CO2 Langmuir Pressure, Layer 2	psi	260
CO2 Langmuir Pressure, Layer 3	psi	372
Sorption Time, CO2	days	1
In-situ N2 Langmuir Volume, Layer 1	scf/ton	258
In-situ N2 Langmuir Volume, Layer 2	scf/ton	255
In-situ N2 Langmuir Volume, Layer 3	scf/ton	257
N2 Langmuir Pressure, Layers 1, 2 & 3	psi	1429
Sorption Time, N2	days	1
Temperature	°F	126
Relative Permeability Relationships		
Maximum Krw	-	1
Irreducible Gas Saturation	-	0
Water Properties		
Density	lbm/ft ³	62.4
Viscosity	cp	0.6

Table 12: History-Match Variables and Ranges

Parameters	Units	Min	Max
Formation Properties			
Porosity Layer 3	-	0.005	0.03
Initial Water Saturation	fraction	0.75	1
Absolute Permeability Layer 3	mD	10	1000
Permeability Anisotropy	fraction	1	5
Pore Compressibility	1/psi	5.00E-05	6.00E-04
Matrix Compressibility	1/psi	5.00E-07	5.00E-06
Permeability Exponent	-	2	4
Differential Swelling Factor	-	1	3
Initial CO ₂ Content	fraction	0.01	0.25
Relative Permeability Relationships			
Irreducible Water Saturation	-	0.05	0.4
Maximum Krg	-	0.65	0.95
Krw Exponent	-	1	3
Krg Exponent	-	1	3
Well Parameters			
Producer Initial Skin	-	-1	2
Producer Stimulated Skin	-	-5	0

Note that Corey relative permeability functions were among the variable parameters. No capillary pressure effects were considered.

Figures 104 and 105 show the total error function reduction during the optimization process and the evolution and convergence of one of the variables (absolute permeability in Layer 3).

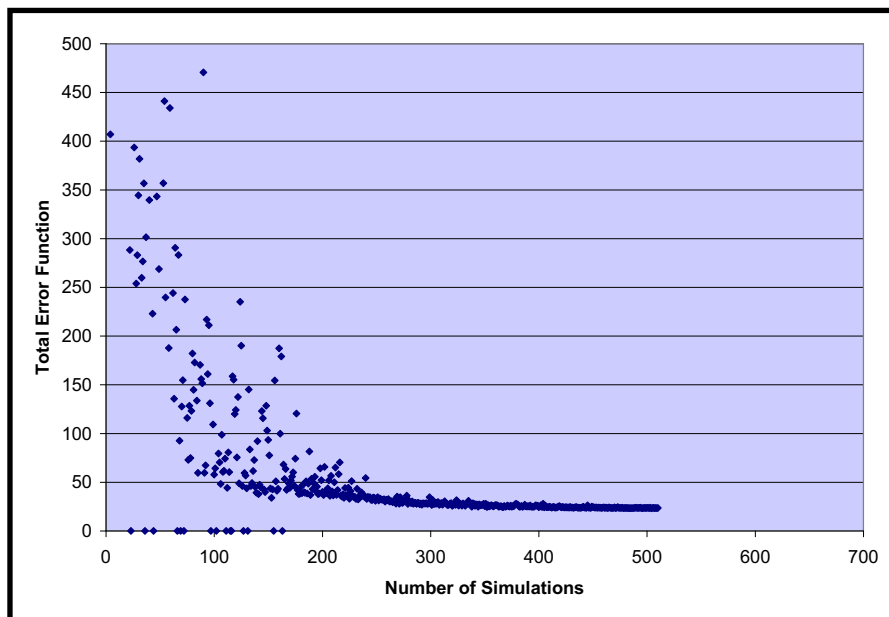


Figure 104: Error Function Reduction

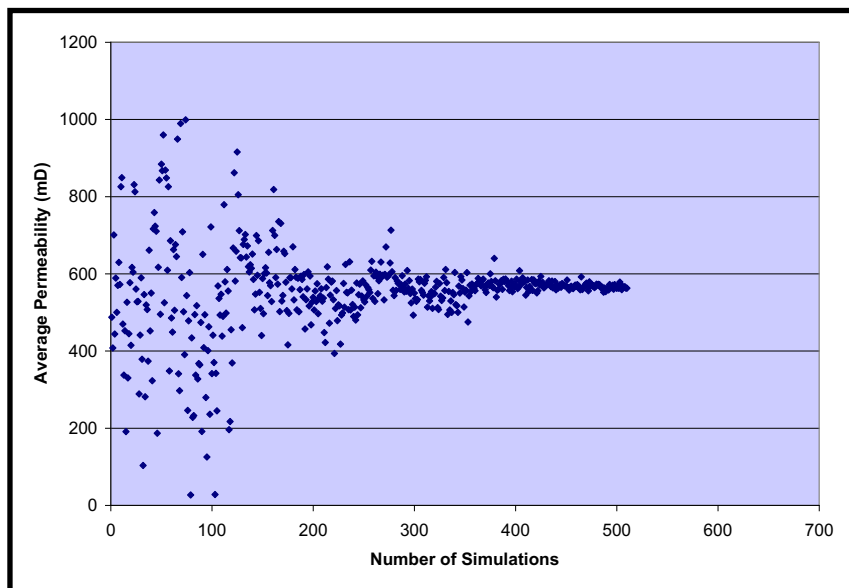


Figure 105: Permeability Optimization

Figures 106 to 108 illustrate the history match results for the three offset wells (Section 32), EPNG Com A 300, EPNG Com A 300S and FC State Com 1. In general, the results were quite good. The gas rate in late time could not be perfectly reproduced for the EPNG Com A 300S and the FC State Com 1. The nitrogen content increase noticed in the gas samples could be fairly well replicated except for the EPNG Com A 300S well where an increase in nitrogen content is noticed in the simulation and not in the field.

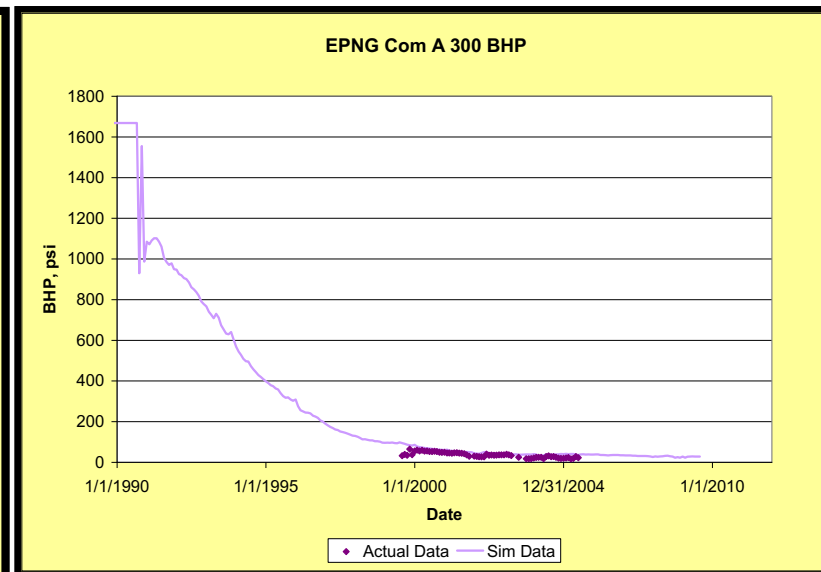
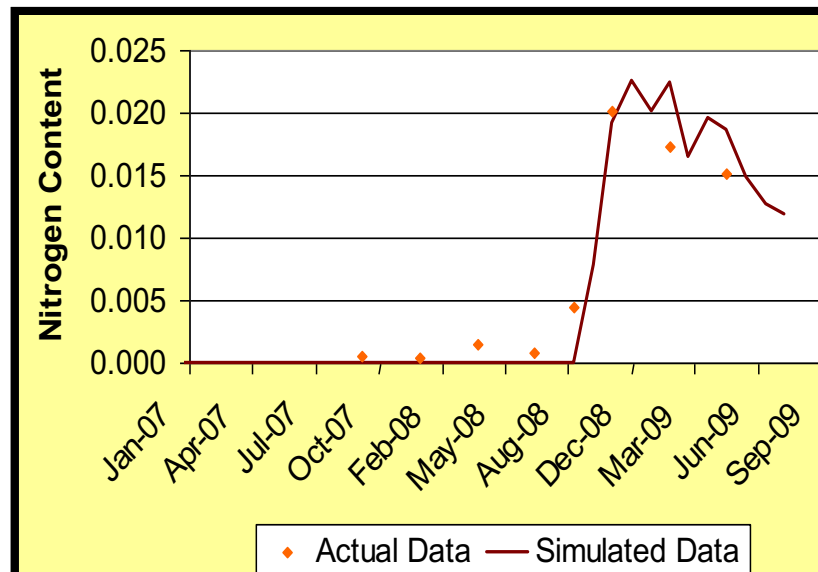
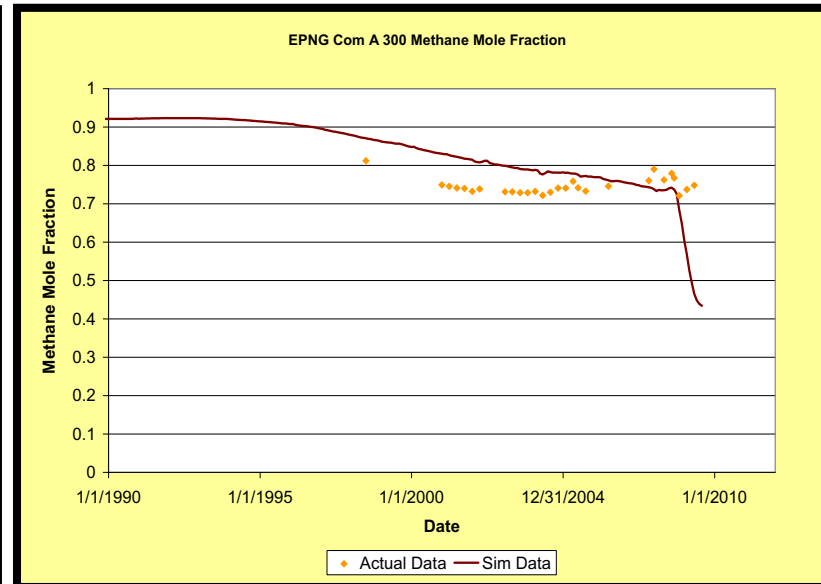
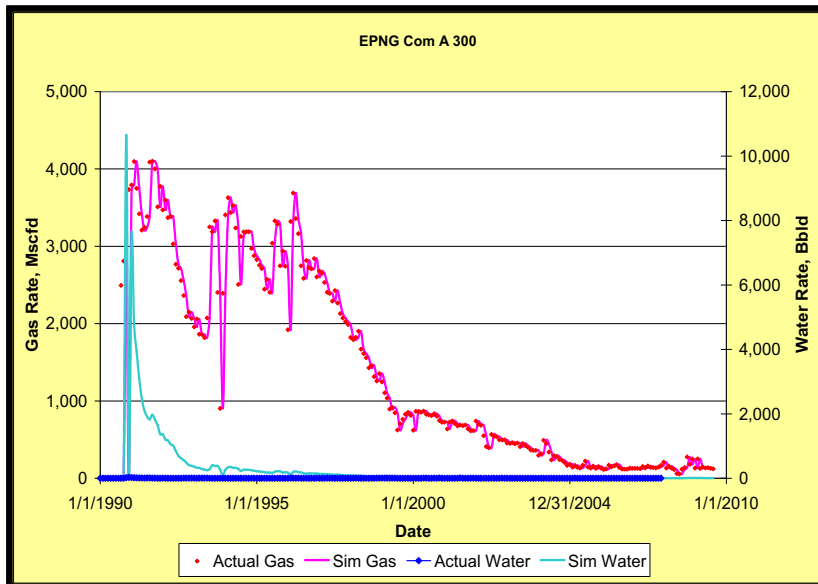


Figure 106: Well EPNG Com A 300 History-Match Results

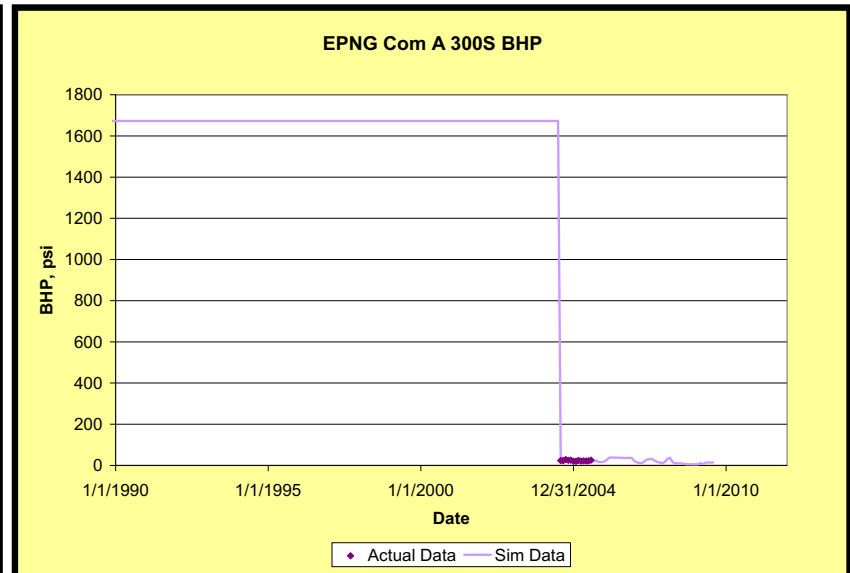
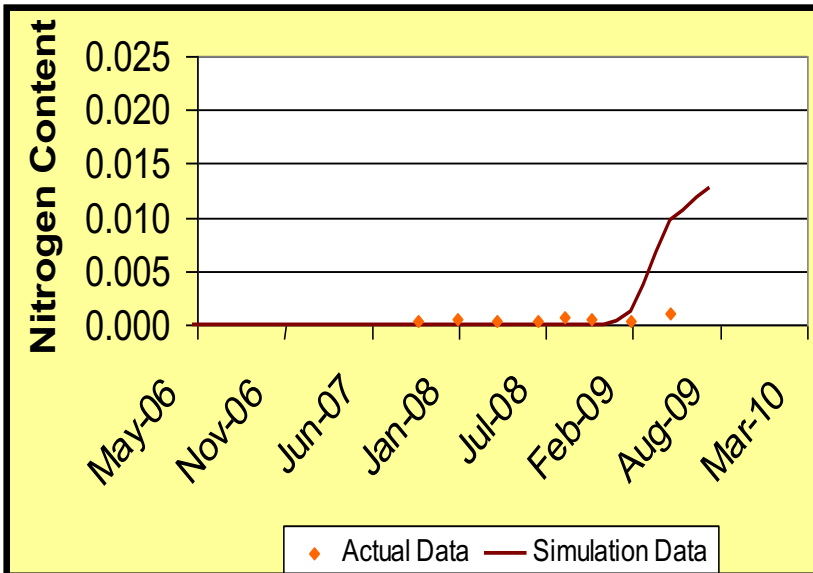
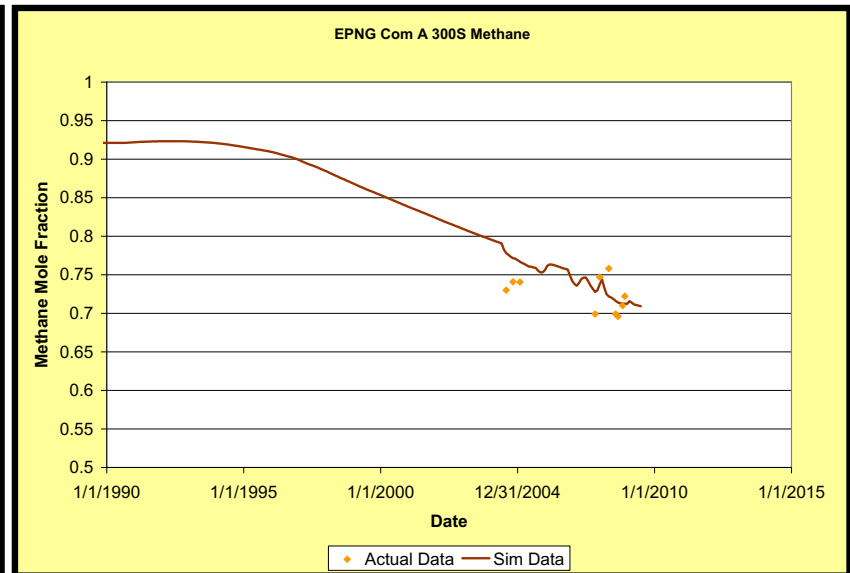
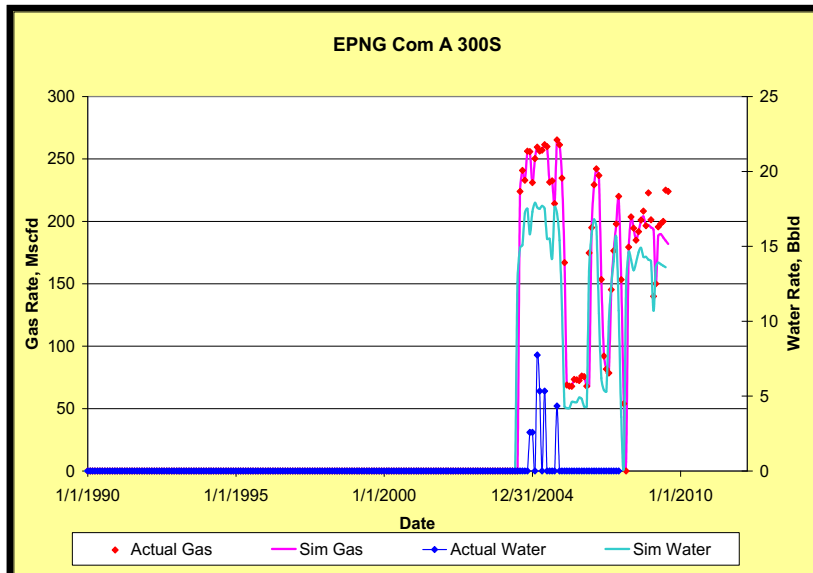


Figure 107: Well EPNG Com A 300S History-Match Results

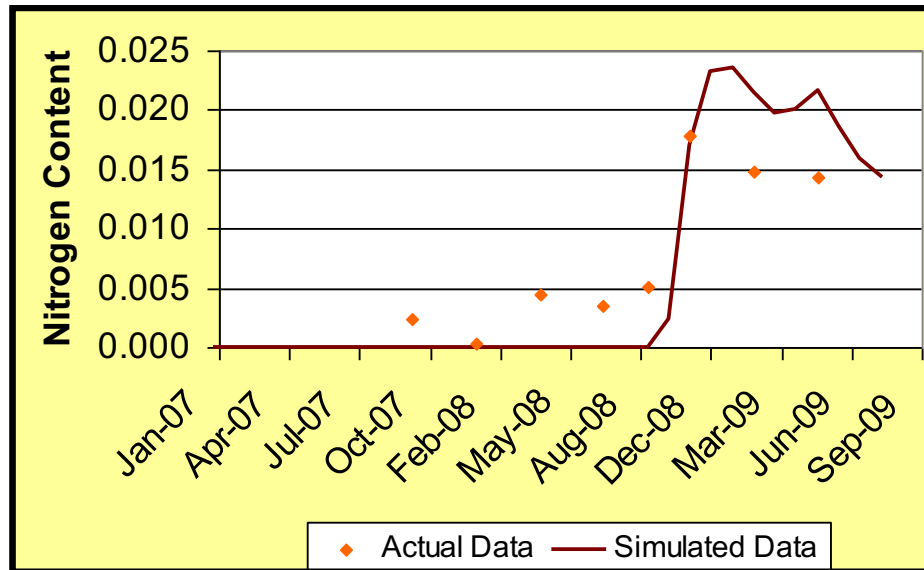
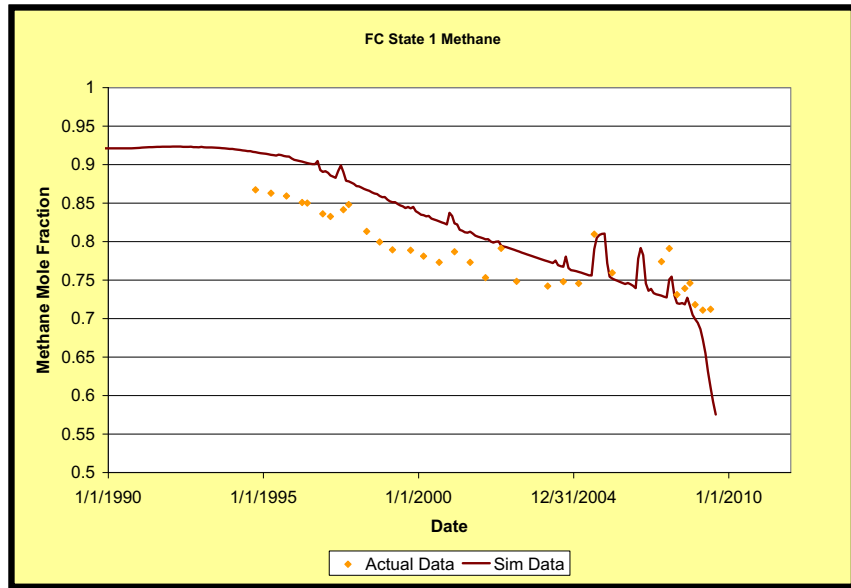
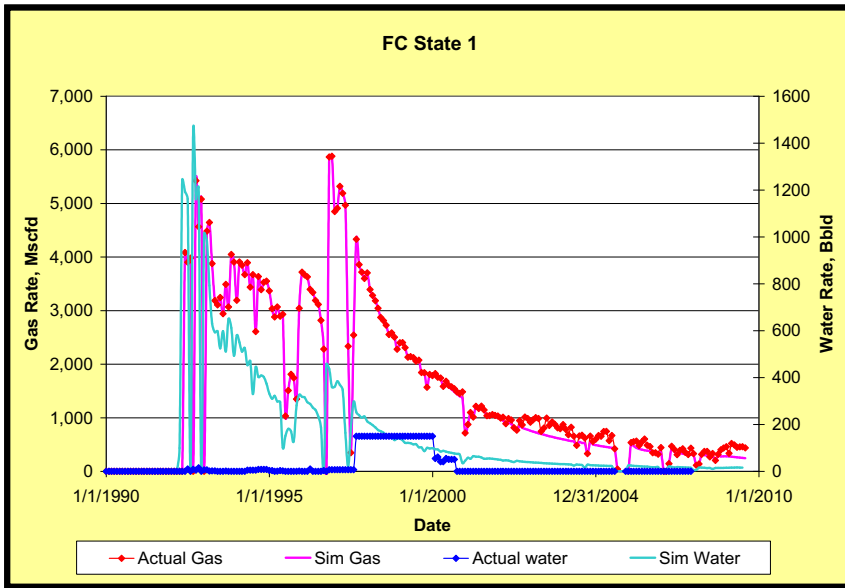


Figure 108: Well FC State Com 1 History-Match Results

Figure 109 illustrates the match of both injection rate as well as the injection wellhead pressure. The skin was allowed to vary with time, positive at the beginning to reflect damage/plugging caused during the drilling and improving as the well was being cleaned-up during injection. The match is quite good, except for a peak in February 2009, which could not be reduced and as a consequence overestimates the quantity of injected CO₂. Data consistency is currently under review to ascertain if this was the cause.

It is important to note that some pressure/rate actual data are inconsistent and could not be replicated in the model. Looking carefully at the first month of injection for example, as pressure increases by steps, the rate should increase by peaks whereas it is progressively increasing. Similarly, when the injector is reopened in February 2009, it is believed the rate should have been a larger peak than it actually was.

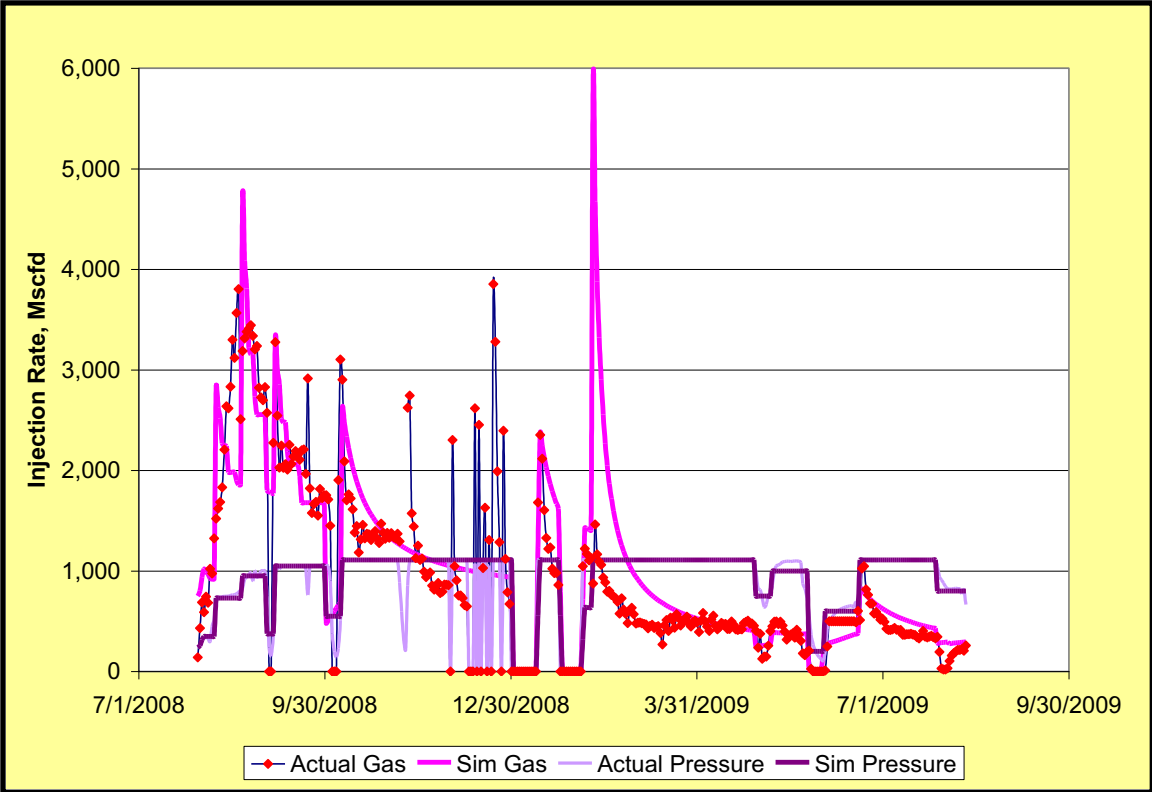


Figure 109: Injector History-Match Results

Table 13 provides the optimized parameters from the history-match. It should be noted that an average permeability value of 582 mD was found for the better quality basal coal, corresponding to a permeability of 146 mD for the upper and middle coals (a 4:1 ratio was applied between the basal layer and the upper/middle layers). Respective porosities were 2.3% in the basal coal and 1.4% in the upper and middle coals. Using these optimized permeability values, the injection rate could not be perfectly matched (too much CO₂ was being injected).

According to an injectivity profile test conducted during the injection period, more than 80% of the injected CO₂ is shown to be going into the basal coal. To replicate this finding, the permeability of the upper and middle coals were altered around the injector and reduced to 10 mD.

Table 13: History-Match Optimized Parameters

Parameters	Units	Min	Max	Optimized
Formation Properties				
Porosity Layer 3	-	0.005	0.03	0.023
Initial Water Saturation	fraction	0.75	1	0.99
Absolute Permeability Layer 3	mD	10	1000	582
Permeability Anisotropy	fraction	1	5	1.0
Pore Compressibility	1/psi	5.00E-05	6.00E-04	2.85E-04
Matrix Compressibility	1/psi	5.00E-07	5.00E-06	4.70E-06
Permeability Exponent	-	2	4	3.7
Differential Swelling Factor	-	1	3	2.5
Initial CO ₂ Content	fraction	0.01	0.25	0.059
Relative Permeability Relationships				
Irreducible Water Saturation	-	0.05	0.4	0.15
Maximum Krg	-	0.65	0.95	0.85
Krw Exponent	-	1	3	1.6
Krg Exponent	-	1	3	1.9
Well Parameters				
Producer Initial Skin	-	-1	2	1.9
Producer Stimulated Skin	-	-5	0	-3.5

7.3.3 Discussion

It can be noticed that simulated CO₂ breakthrough is occurring for wells EPNG Com A 300 and then FC State Com 1. This is consistent with the gas samples results (increase in N₂ content is a sign of upcoming CO₂ breakthrough) and tracer data. However, breakthrough hasn't occurred at the site yet (even though breakthrough might be occurring at the FC State Com 1 well according to the CO₂ sensors results 3% CO₂ gain). This might be due to an overestimated permeability around the injector or the fact that, in the simulation, too much CO₂ is being injected (mainly due to the peak and following period in February 2009), thereby accelerating the breakthrough. Nevertheless, it is believed breakthrough of the CO₂ may have been imminent for the project, based on the modeling results.

7.3.4 Enhanced Coalbed Methane

In order to assess if additional production was recovered due to the CO₂ injection, a “no injection” case was modeled. The results are summarized in **Table 14**. **Figures 110 to 112** show the difference in methane production rate for the injection case versus the non-injection case for the three offset wells.

Table 14: Cumulative Methane Recovery Comparison

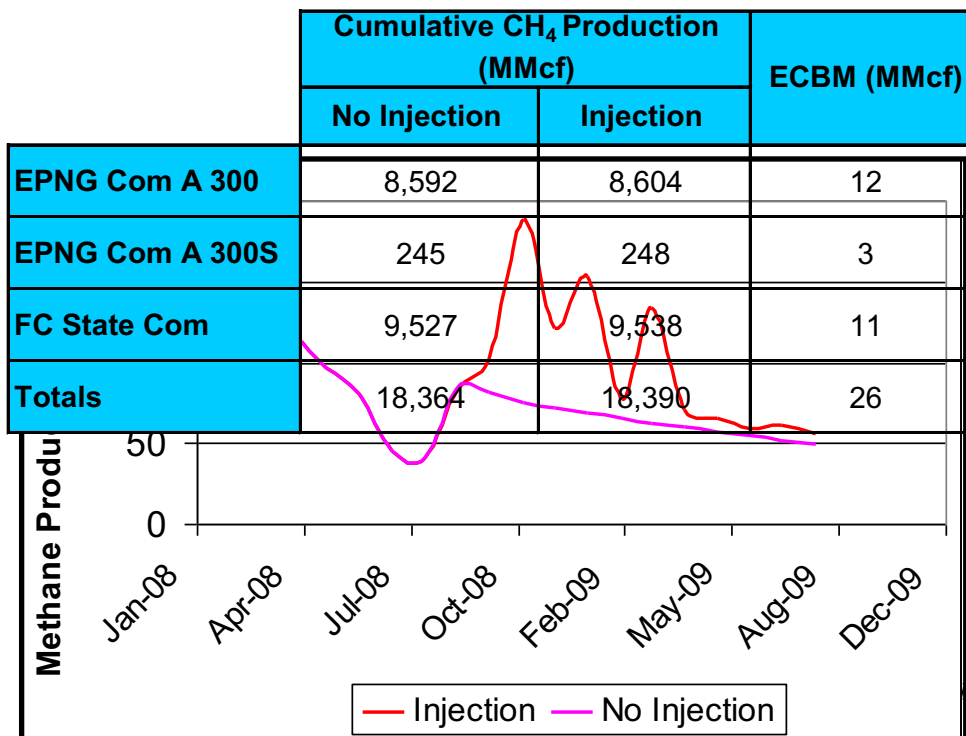


Figure 110: Well EPNG Com A 300 Methane Production Rate – Injection Versus No Injection Comparison

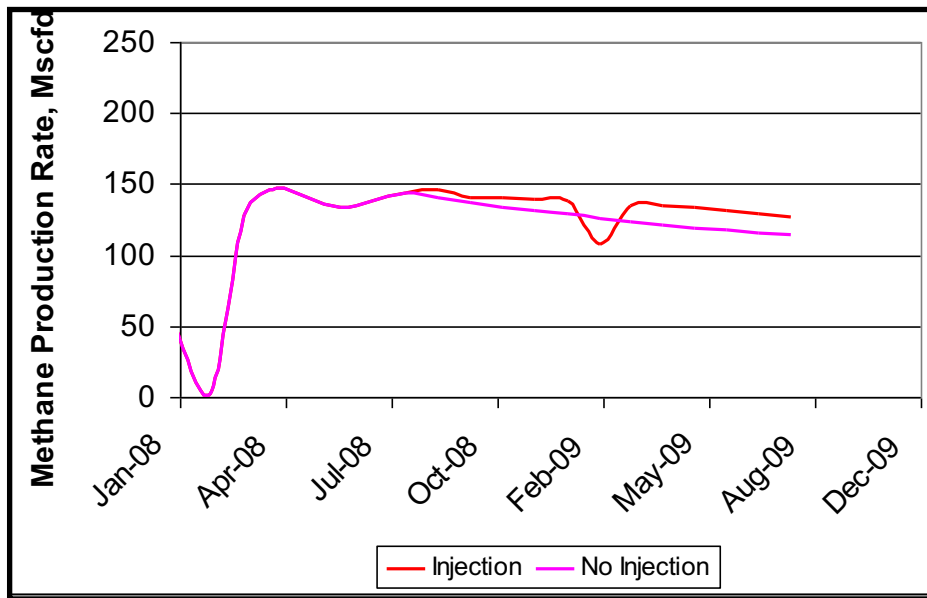


Figure 111: Well EPNG Com A 300S Methane Production Rate – Injection versus No Injection Comparison

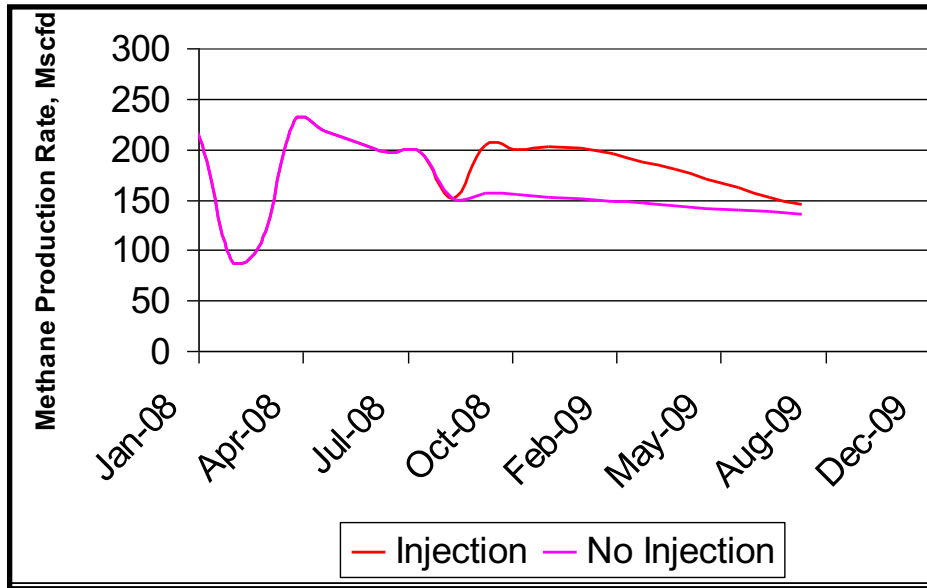


Figure 112: Well FC State Com 1 Methane Production Rate – Injection versus No Injection Comparison

The simulation comparison reveals 26 MMscf of incremental gas recovery (ECBM) may be attributable to CO₂ injection, which appears to be significant for two of the three wells.

7.3.5 What-if Scenarios

In order to gain some insight as to how CO₂ injectivity could have been improved, and perhaps maximize ECBM recovery, several additional simulations were run. For all cases, the well was considered to be stimulated (while the actual injection well was not).

- Case 1: continuous CO₂ injection (permeability reduction, near well)
- Case 2: continuous CO₂ injection with homogenous permeability (no permeability reduction removed)
- Case 3: continuous injection with doubled permeability (to simulate cavitation)
- Case 4: continuous injection within a 2,000 ft long horizontal well, completed in the three coals (incomplete)

Figures 113 to 116 show the different cumulative injection profiles as well as the production profiles for each of the three offset wells (total gas and CO₂). Figures 117 to 119 show the cumulative CH₄ produced for each well. The cumulative injection numbers should be compared to the actual cumulative injection of 255,000 Mscf.

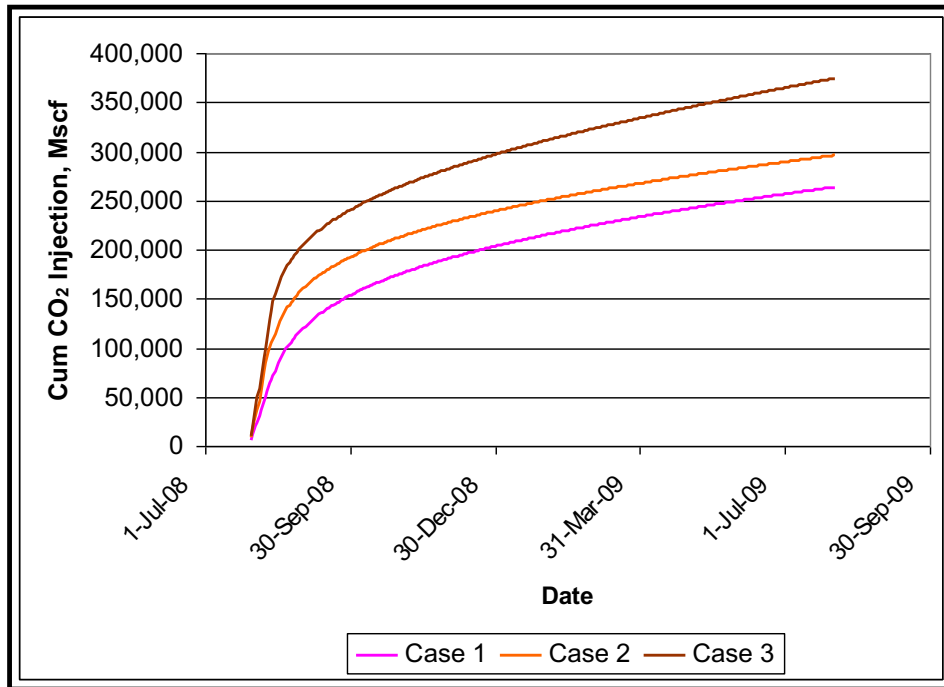


Figure 113: Cumulative CO₂ Injection

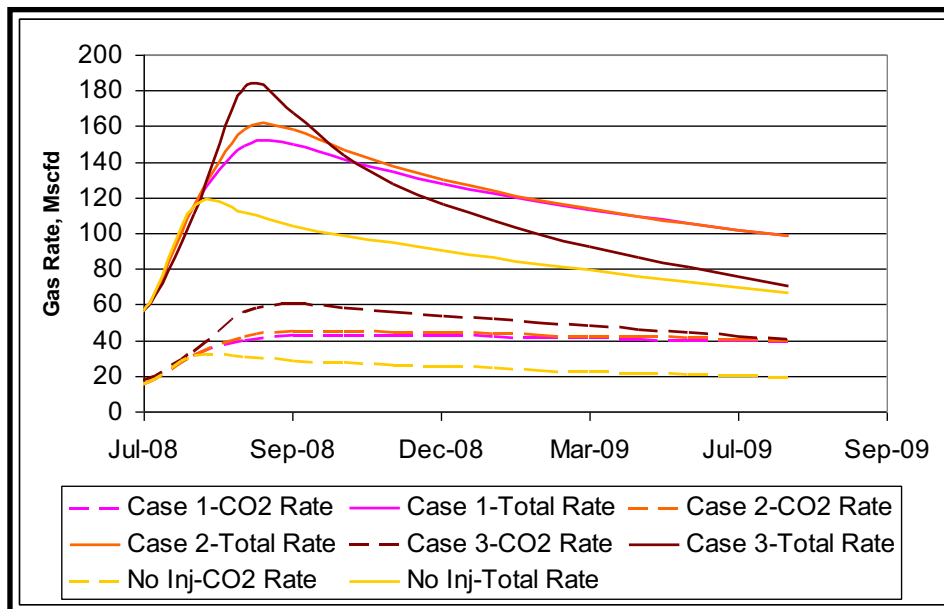


Figure 114: EPNG Com A 300 Total and CO₂ Rate

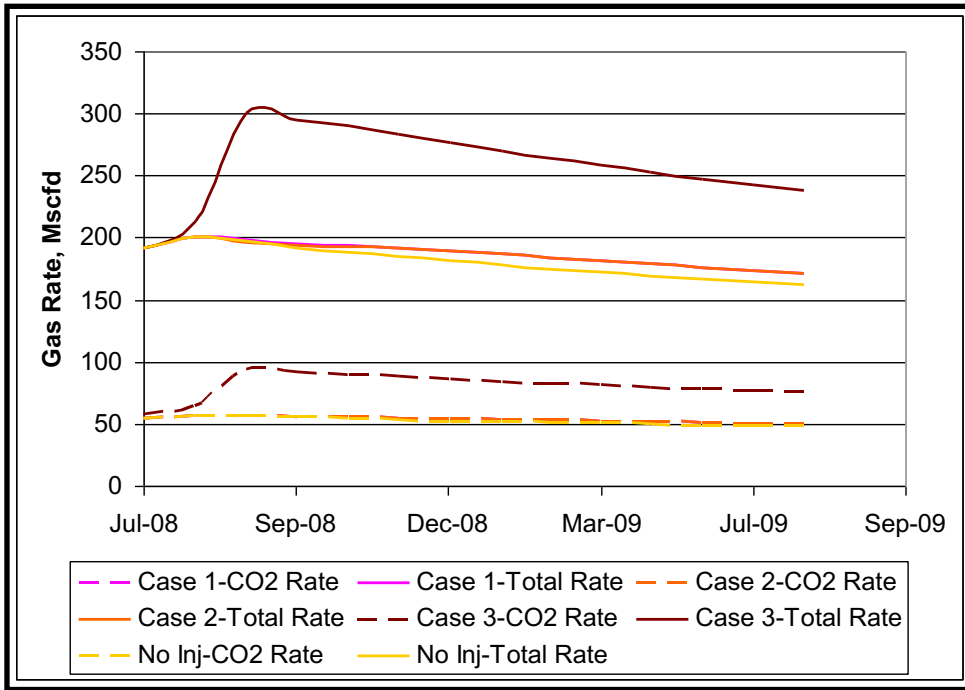


Figure 115: EPNG Com A 300S Total and CO₂ Rate

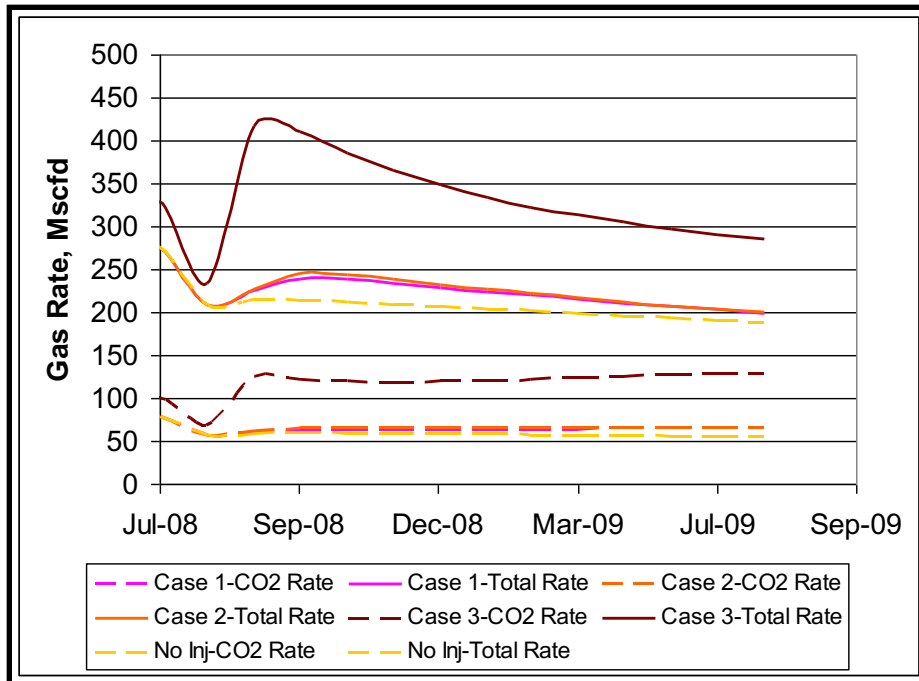


Figure 116: FC State Com 1 Total and CO₂ Rate

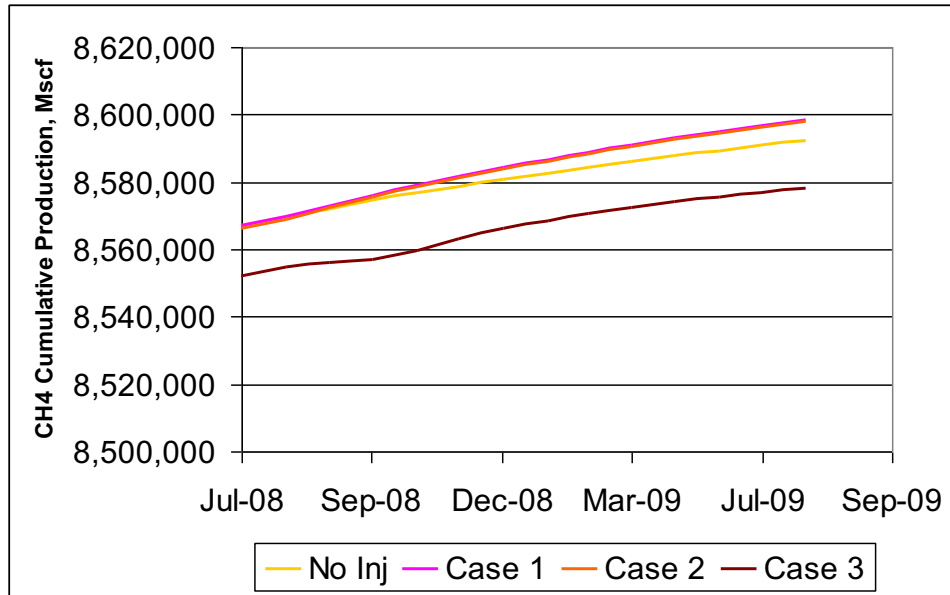


Figure 117: EPNG Com A 300 Cumulative CH₄ Production

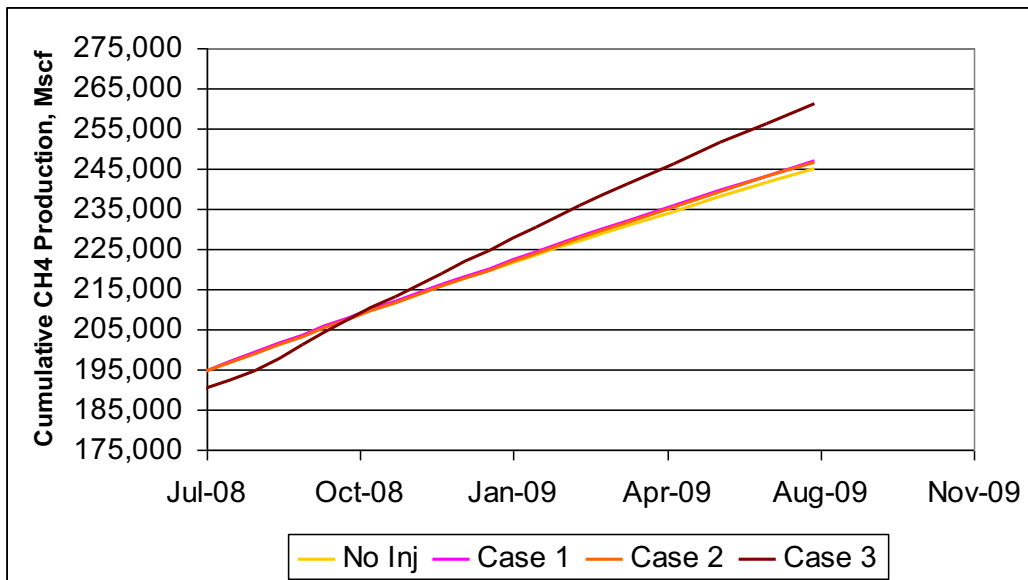


Figure 118: EPNG Com A 300S Cumulative CH₄ Production

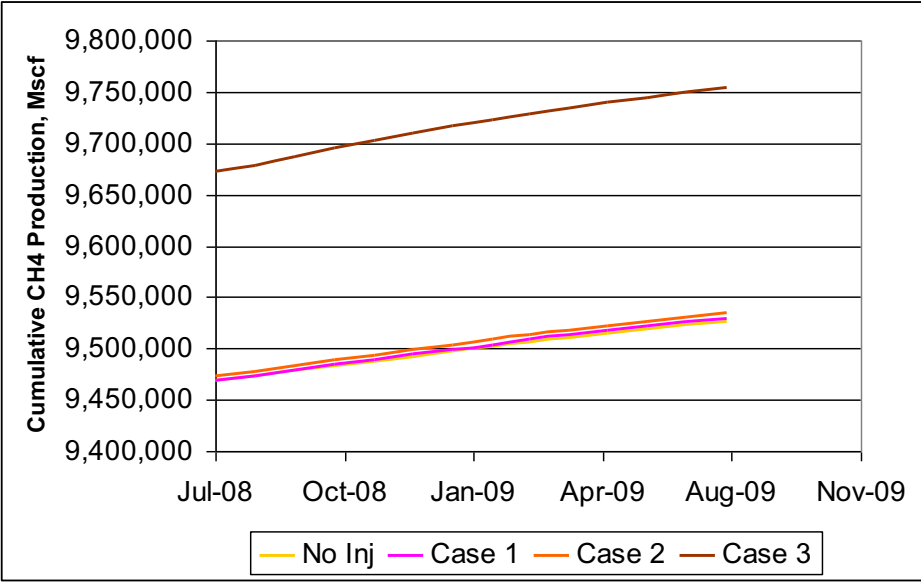


Figure 119: FC State Com 1 Cumulative CH₄ Production

These different scenarios show that ECBM could have been improved if the injection well had been cavitated (even though well EPGN Com A 300 would have to be shut in due to CO₂ breakthrough).

8.0 Conclusions

The CO₂-ECBM/sequestration pilot project at Pump Canyon is an injection success. A total of 256 MMscf of CO₂ (or 14,885 tons) was injected over a 12-month period (July 30st, 2008 to August 12, 2009); primarily due to a highly permeable coal. However, the CO₂ injectivity dramatically decreased over the injection period due to matrix swelling and permeability reduction as a result of the CO₂ being adsorbed onto the coal while displacing methane and increasing reservoir pressure (porefilling).

A number of MVA techniques were employed to track the CO₂ plume inside and outside the reservoir. The CO₂ sensors installed at the three immediate offset wells, as well as gas sampling (at the three immediate offset wells as well as an additional ring of surrounding wells), suggest that no CO₂ breakthrough has occurred at the site. However, a steady increase in the CO₂ content at one of the offset wells, the FC State Com 1, might be a sign of imminent breakthrough. The CO₂ monitoring system has been left in place and the data will be regularly updated to access CO₂ flowback.

Perfluorocarbon tracers injected in the CO₂ stream showed up a few months after their injection at the two closest offset wells, the FC State Com 1 followed by the EPNG Com A 300 (where breakthrough was expected to occur first due to its alignment with the face cleats). Teamed with the observed nitrogen increases in these wells, this information indicates the preferential breakthrough path.

The different ground monitoring techniques used (Tiltmeters, GPS and InSar) all suggest the same conclusion: no ground deformation is seen even though their effectiveness was probably limited due to the small amount of CO₂ injected.

In order to assess the integrity of the site, a thorough seismic interpretation of approximately nine square miles of 3D seismic data, centered around the injection well, was conducted and reveals a considerable stratigraphic complexity in the Fruitland formation

depositional system. Post-stack processing of the 3D seismic suggests the presence of fracturing and minor faulting within the Kirtland Shale caprock, whereas indicators for extensive fracturing and faulting within the Fruitland sequence are much less apparent. However, interpreted faults and fracture zones have limited vertical extent and major penetrative faults have not been observed at the site, reinforcing the idea that no leakage should occur. Baseline and post injection monitor vertical seismic profiles (VSP) were collected at zero offset and three non-zero offsets but the preliminary processing is still in progress. A detailed study of the integrity of the Kirtland Shale caprock is provided in an independent report.

The simulation work was able to replicate the production/injection profile of the injector and the three immediate offset production wells. The model is also indicating that methane production was enhanced due to the CO₂ injection (26 MMscf). While the match is not perfect and predicts breakthrough a bit early, the model was able to tie the MVA results to the well performance (production).

9.0 References

- (1) Druckenmiller, M.L., M. M. Maroto-Valer, “Carbon Sequestration Using Brine of Adjusted pH to Form Mineral Carbonates,” *Fuel Processing Technology*, 86, 1599-1614, 2005.
- (2) Johnson, G., et al., “Tracing the Fate of Injected CO₂ During Enhanced Oil Recovery Using Stable Isotope Techniques,” *CSPG CWLS Conversion*, 118-122, 2008.
- (3) Kharaka, Y.K., D.R. Cole, S.D. Hovorka, W.D. Gunter, K.G. Knauss, and B.M. Freifeld, “Gas-Water-Rock Interactions in Frio Formation Following CO₂ Injection: Implication for the Storage of Greenhouse Gases in Sedimentary Basins,” *Geology*, July, 577-580, 2006.
- (4) Raistrick, M., B. Mayer, M. Shevalier, R.J. Perez, I. Hutcheon, E. Perkins, and B. Gunter, “Using Chemical and Isotopic Data to Quantify Ionic Trapping of Injected Carbon Dioxide in Oilfield Brines,” *Environ. Sci. Technol.* 40, 6744-6749, 2006.
- (5) Schwerer, F. C., and Pavone, A. M.; “Effect of Pressure-Dependent Permeability on Well-Test Analyses and Long-Term Production of Methane From Coal Seams”, paper SPE/DOE/GRI 12857 presented at Unconventional Gas Recovery Symposium, Pittsburgh, PA, May 13-15, 1984.
- (6) Sawyer, W. K., Paul, G. W., and Schraufnagel, R. A.; “Development and Application of a 3D Coalbed Simulator,” *CIM/SPE* 90-119, presented at the 1990 CIM/SPE International Technical Conference, Calgary, June 10-13, 1990.
- (7) Paul, G. W., Sawyer, W. K., and Dean, R. H., “Validation 3D Coalbed Simulators”, *SPE* 20733, presented at SPE Annual Technical Conference and Exhibition, Houston, TX, September 23-26, 1990.